CWRF SUMMER PRECIPITATION PREDICTION OVER THE UNITED STATES LAND AND COASTAL OCEANS: EFFECTS OF ENSEMBLE CUMULUS PARAMETERIZATION CLOSURES

BY

FENGXUE QIAO

DISSERTATION

Submitted in partial fulfillment of the requirements
for the degree of Doctor of Philosophy in Atmospheric Sciences
in the Graduate College of the
University of Illinois at Urbana-Champaign, 2013

Urbana, Illinois

Doctoral Committee:

Professor Xin-Zhong Liang, Chair
Professor Donald J. Wuebbles
Professor Greg McFarquhar
Professor Praveen Kumar

ABSTRACT

A long-standing problem in climate modeling is the accurate prediction of precipitation with respect to three key characteristics: geographic variation of total amount, frequency and intensity, and the diurnal cycle. In particular, coarse-resolution climate models have low predictive skills at regional scales, while the higher-resolution regional climate/weather models show improved downscaling skill but still exhibit biases and are highly sensitive to cumulus parameterization (CUP) especially during the summer. Most current models also tend to predict rainfall too early in the daytime and too frequently at the light intensity over both land and oceans. These problems have been identified with model deficiencies in CUP. As the core problem of CUP, cumulus closure assumptions fundamentally determine the location, frequency and intensity of convective rainfall. Numerous closures have been proposed, but there is no consensus with respect to their relative performance.

This study uses the CWRF model which incorporates an Ensemble Cumulus Parameterization (ECP) scheme to evaluate the performance of different widely-used closures for summer precipitation prediction regarding the above three key features. The ECP includes five major groups of closure assumptions with 16 different algorithms: the Arakawa-Schubert quasi-equilibrium (AS), the vertical velocity (W), the moisture convergence (MC), the total instability adjustment (KF), and the instability tendency (TD). Extensive experiments are conducted by implementing these closures separately over the continental U.S. and adjacent coastal oceans. Results show that cumulus closures significantly affect U.S. precipitation patterns, heavy rainfall occurrence, and the diurnal cycle, with strong regional dependence differing between land and coastal oceans.

Over the U.S. coastal oceans, two closure algorithms using the average vertical velocity at the cloud base (W_2) and moisture convergence (MC_3) complementarily reproduce the summer precipitation patterns and amount, and both skillfully capture the frequency of heavy rainfall events. However, the instability tendency closures are superior in capturing the diurnal phase but with much larger amount deficits. This suggests that cloud base vertical velocity and moisture convergence primarily determine seasonal mean and daily precipitation variability, but the instability tendency plays a critical role in regulating precipitation sub-daily variation.

Over the continental U.S., the MC closure most realistically reproduces Central U.S. summer rainfall amount, daily precipitation variation and frequency distribution, but produces wet biases over the North American Monsoon (NAM) region and Southeast U.S. which can be significantly reduced by using the W closure. Further skill enhancement can be made using an optimized ensemble of the MC and W closures. The TD and KF closures show advantages in capturing the diurnal signals over the Central U.S. and NAM, respectively. This reasonably explains the systematic behaviors of several major CUP schemes.

This research further compares the performance of CWRF using the ECP with other 11 CUP schemes in predicting the Central U.S. summer floods. The ECP scheme with the MC and W_2 closures separately over the land and oceans shows advantages over other schemes in simulating the Central U.S. flood amount, daily rainfall frequency and intensity. The Grell scheme shows superiority in reproducing Central U.S. nocturnal rainfall maxima, but other schemes generally fail. This advantage of the Grell scheme is primarily due to the instability tendency closure assumption. Future studies will attempt to incorporate this instability tendency assumption as a trigger function in the ECP scheme to improve the Central U.S. rainfall diurnal simulations.

Dedicated to My Parents

ACKNOWLEDGEMENTS

I give my deepest thanks to my advisor, Professor Xin-Zhong Liang, for his great inspiration, insightful guidance, and continuous encouragement throughout my Ph.D. research. He sets a good example for me as a professional scientist with his strong motivation, everlasting enthusiasm, and academic rigor toward the research work. I will carry all of these forward and they will benefit my future research and life.

I would like to thank Professor Donald Wuebbles, Greg McFarquhar and Praveen Kumar for serving on my thesis committee and providing thoughtful discussion, invaluable comments, and advice on my thesis. Many thanks go to my group members and friends, especially Min Xu, Tiejun Ling, Shenjian Su and Ligang Chen for their tremendous help in model setup and code development. I also thank Shuyan Liu, Feng Zhang, Yuxiang He, Ibraheem Khan, Chao Sun, David New, and Professor Zhuo Wang for their help and encouragement. Special thanks are extended to Professor Bob Rauber for his help in my curricular practical training and job applications. Thanks also go to my classmates, especially Wenjing Jia, Hang Lei, Catrin Mills, Alexandra Jones, Joseph Ching and Rahul Barman for their companionship and joyful friendship. Finally, but most importantly, I wish to thank my parents and husband for their endless supports and love.

I acknowledge the financial support from the NOAA Education Partnership Program (EPP) COM Howard University and Climate Prediction Program for the Americas (CPPA) NA11OAR4310194 and NA11ORA4310195. Any opinions and findings expressed in this research are those of the authors and do not necessarily reflect the views of the sponsor.

TABLE OF CONTENTS

CHAPTER 1: INTRODUCTION

1.1. Motivations

Precipitation plays an important role in the hydrological cycle at the global and regional scales, primarily by transferring water vapor from the atmosphere to the surface and distributing it across the time and space. Over land, it is considered to be the immediate source of fresh water which is essential for all living creatures. Any sizable anomaly of precipitation can have considerable consequences on human activity by affecting the agriculture growth, hydrological process, and water resources. On the other hand, the latent heat released from precipitation systems is the major driver of the dynamic coupling between atmosphere, land and ocean (Koster and Suarez 1995), and thus affects the large-scale circulations and climate systems. Over certain key regions such as the northern Atlantic Ocean, precipitation and its variability can also modulate the water salinity and change the heat transport and ocean currents, leading to vastly different thermohaline circulation, which can have prolonged impacts on the Northern Hemisphere climate (Velligna and Wood 2002). As climate changes, the largest impacts in the future will most likely be from precipitation variability (Dai 2006). Therefore, it is vital for current models to realistically simulate the observed precipitation over both land and oceans in order to make credible future projections.

However, it is still a great challenge for general circulation models (GCMs) and regional climate models (RCMs) to accurately predict three precipitation key characteristics that are crucial for practical applications and impacts assessments: geographic variation of total/mean amount, precipitation frequency and intensity, and the rainfall diurnal cycle (e.g., Trenberth et al. 2003; Dai 2006). The difficulty arises from the complexity of representing precipitation physical

processes, including cumulus convection, cloud microphysics, planetary boundary layer, land/ocean surface processes, and radiative forcing (Trenberth et al. 2003; Dai 2006). Among these processes, cumulus convection plays a central role in regulating the precipitation geographic distribution and temporal variations, especially in summer (Arakawa 2004). Numerous modeling studies have demonstrated that summer rainfall simulation is significantly sensitive to the representation of subgrid-scale cumulus convection through the cumulus parameterization (CUP), and important model biases have been identified with the CUP deficiencies.

1) *Geographic variation of total precipitation:* Most previous studies have focused on analyzing or improving model simulations in spatial patterns of total precipitation amounts (e.g., Delworth et al. 2002; Covey et al. 2003; Liang et al. 2004a, b; Dai 2006; Lin 2007; Liang et al. 2007, 2012). Despite the fact that GCMs can well capture broad patterns of mean precipitation over large areas, they generally have little predictive ability at regional scales because of their coarse resolutions and model formulation deficiencies with topography effects, eddy processes and other subgrid phenomena (Wehner et al. 2010). One commonly noted problem in the coupled GCMs without flux corrections is the tendency to produce the doubled Intertropical Convergence Zone (ITCZ) rainbands (Wu and Zhang 2003). The spurious rainband in the south of the Equator has been suggested to result from warm bias of sea surface temperature (SST) due to insufficient low clouds in the models (Ma et al. 1996; Dai et al. 2003) and unrealistically strong coupling of SST to the atmosphere through CUPs (Lin 2007; Takayabu et al. 2010). As RCMs better resolve the terrestrial hydrology and land-sea contrasts with finer resolutions, they have shown higher predictive skill than most GCMs on seasonal-interannual precipitation prediction (Liang et al. 2012). However, there still exist important biases and uncertainties that

are not fully understood. Particularly for summer, a majority of studies have documented that precipitation patterns simulated by RCMs are very sensitive to the choice of CUPs and have large controversies in their regional dependence (e.g., Giorgi and Shields 1999; Gochis et al. 2002; Xu and Small 2002; Leung et al. 2003; Liang et al. 2004a, b, 2012). Most of these studies, however, have treated the CUP as a "black box" without separating the relative contributions of various components that explain the substantial model precipitation errors and the large spread among different schemes.

2) *Precipitation frequency and intensity:* Different combinations of rainfall frequency and intensity can greatly affect surface runoff, evaporation and soil moisture content, and consequently can change the local water recycling and associated hydrological processes (Trenberth et al. 2003; Sun et al. 2005; Dai 2006). Many studies focused on examining the observed changes in extreme rainfall events (e.g., Karl and Knight 1998; Kunkel et al. 1994, 2003; Groisman et al. 2012; Becker et al. 2009) and all showed that the frequency of heavy rainfall has increased during the recent decades over various regions in the U.S. It was found that the contribution from daily precipitation events exceeding 50.8 mm to annual total rainfall amount increased from 9% in 1910s to 11% in 1990s over the U.S., and the largest trends occurred in the eastern and southern U.S. (Karl and Knight 1998). As significant warming occurs in the future, most GCMs predict the total precipitation amount will increase at about 1-2% K^{-1} with warming. However, the changes in rain rates, especially heavy rainfall events, are around 7% K^{-1} according to the Clausius-Clapeyron equation. The implication is that there will be a decrease in light and moderate rains (Hennessey et al. 1997), or fewer but more intense extremely heavy rainfall events (Trenberth et al. 2003). Therefore, accurately predicting the frequency distribution of precipitation especially at the heavy or extreme intensity is as important

as, if not more, than predicting the total rainfall amounts (Trenberth et al. 2003). However, most GCMs generally precipitate too frequently at reduced intensity (drizzling problem), but underestimate the frequency and intensity of heavy precipitation (Dai and Trenberth 2004; Sun et al. 2005). The possible reason is that moist convection in the models is initiated too frequently (Dai 2006) or the model converts the water vapor into precipitation too fast (Sun et al. 2005).

3) *Precipitation diurnal cycle:* The diurnal variations of precipitation (e.g., Janowiak et al. 1994; Dai et al. 1999; Nesbitt and Zipser 2003; Bechtold et al. 2004) and associated convection and cloudiness (e.g., Yang and Slingo 2001; Dai and Trenberth 2004) are of great importance for many aspects of climate studies. Different timing of precipitation during the course of a day affects the partition of surface and atmospheric fluxes of energy and water, leading to changes in the hydrological cycle (Dai and Trenberth 2004). The rainfall diurnal cycle also modulates the surface temperature range via its influence on radiative budgets by convective clouds (Bechtold et al. 2004), and controls the diurnal variation of air quality, such as ozone concentration, by affecting the photochemical production processes, aqueous chemistry, and wet deposition (Lin et al. 2008). However, current models tend to produce early rainfall peaks during summer over both land and oceans, although diurnal phase biases are often model-dependent (Betts and Jakob 2002; Bechtold et al. 2004; Dai and Trenberth 2004; Dai 2006). This common model error is mainly caused by the premature initiation of convection, which prevents the convective available potential energy (CAPE) from accumulating for a sufficient time before the intense convection occurs (Dai and Trenberth 2004). It is also challenging for models to fully capture the regional variations of diurnal features (Liang et al. 2004a; Lee et al. 2007b). In particular, the observed nocturnal rainfall maximum in the vicinity of complex terrain, such as downstream side of the Rocky Mountains, the Sierra Madre Occidental, the Tibetan Plateau, and the Amazon basin, is

generally missed in most GCMs and RCMs (Dai et al. 1999; Lee et al. 2007a). Previous studies have ascribed this failure to three reasons: the improper representation of surface boundary forcing in the GCMs, the unresolved mesoscale convective systems that propagate eastward, and the moist convection problems that are too strongly coupled to surface but insensitive to the large-scale dynamic forcing such as the low level jet over the Central U.S. (e.g., Lee et al. 2007a, b).

Therefore, the ultimate goal is to improve summer precipitation prediction over both land and oceans that distinguishes three key characteristics: geographic variation of total/mean amount, precipitation frequency and intensity, and rainfall diurnal cycle. Limited by the computation domain of the CWRF, this research specifically examines the summer rainfall over the continental U.S. and adjacent coastal oceans along the Atlantic Coast and the Gulf of Mexico, focusing on the effects of CUP. Note that the core problem of CUP is the closure assumption that links the existence and overall intensity of cumulus activity to large-scale processes (Arakawa 2004). Therefore, this study focuses on identifying the effects of the widely used cumulus closures on summer rainfall prediction with respect to the aforementioned three key characteristics. The challenges and major uncertainties in parameterizing the effects of cumulus convection are discussed in more detail in the following section.

1.2. Cumulus parameterization problems

Cumulus convection plays an essential role in the atmospheric general circulation (Pan and Randall 1998) by significantly controlling the vertical transport of moisture, energy and momentum (Wager and Graf 2010). The pioneering study of Riehl and Malkus (1958) illustrated that in the convectively unstable regions, vertical transports of mass and energy were primarily accomplished by individual cumulonimbus clouds instead of synoptic-scale circulations. But

these individual convective-scale clouds, with a diameter generally on the order of 1-10 km, cannot be explicitly resolved by most models. Thus, it has been widely recognized that the effects of cumulus convection have to be represented by the model predicted variables through CUP (Arakawa 2004).

Although various CUP schemes have been developed to predict convective precipitation and associated heat and moisture changes of the atmosphere (Emanuel et al. 1999), the CUP problem is far from solved and remains among the challenges to modeling groups. From the modeling point of view, the basic structure of CUP can be divided into three important components: *dynamic control*, *static control*, and *feedback* (Grell et al. 1991). They involve different physical assumptions that are not fully evaluated and tunable parameters whose actual value are unknown, leading to model deficiency and large uncertainty associated with CUPs.

First, the *dynamic control* of CUP is concerned with how the environment modulates the convection (Grell et al. 1991). Different principal closure assumptions are proposed to link the existence and overall intensity of cumulus activities to large-scale processes (Arakawa 2004), but there is no consensus yet on their application in large-scale or mesoscale models.

For instance, the moisture convective adjustment scheme (Manabe et al. 1965) simply related moist convection to available buoyant energy. The moist convection occurs when and where the air is conditionally unstable and supersaturated, and the air follows the instantaneous adjustment of environmental profiles to an equilibrium status that is neutral and saturated. But this assumption has drawbacks including the requirement of grid-scale saturation for subgrid moist convection to occur and the confinement of convection within the unstable layer (Arakawa 2004). The Quasi-Equilibrium (QE) assumption, proposed by Arakawa and Schubert (1974), followed.

It has been widely used in most mass-flux CUP schemes in which the cloud base mass flux is assumed to adjust rapidly to maintain an instantaneous equilibrium between the destabilization of large-scale processes and the stabilization due to convection. However, Frank and Cohen (1987) suggested that the QE assumption is probably not suitable for RCMs with finer resolutions, although it works well for dynamically large systems. They argued that convection does not respond instantly to externally imposed changes of the large-scale envelope within which mesoscale convective systems develop, and for mesoscale models with 20-50 km resolution only convective drafts need to be parameterized by using low-level wind convergence and grid-scale mass fluxes. The other closure assumptions relate convection to column-integrated quantities, including moist convergence (e.g., Kuo 1974; Kuo and Anthes 1984) and vertical advection of moisture (e.g., Krishnamurti et al. 1983). Under these closures, convection develops to balance the enhanced moisture abundance. Fletch and Bretherton (2010) pointed out that the moisture convergence closure is derived from observations over tropical oceans during long time scales, but may not be applicable for short time predictions because convection is fundamentally a buoyance-driven process. Given that most of closure assumptions are originally developed for large-scale models, their performance is questionable in higher resolution mesoscale models (Molinari and Dudek 1992). Examining their effects on precipitation prediction in CWRF, therefore, will help gain more insights into their applicability in the mesoscale models.

Second, the *static control* of CUP determines the cloud thermodynamic properties in convective updrafts or downdrafts by using simplified cloud models, and includes mechanisms of entrainment, detrainment, and microphysics (Grell 1993). Great uncertainties exist in representing these complicated processes in clouds and their interactions with environment.

For instance, it is not adequately understood what determines the rate of entrainment of environmental air into the cumulus updrafts or how entrainment affects the evolution of cumulus convective system (Randall et al. 2003). There are still controversies about the relative importance of two entrainment processes in previous observations, including the turbulent mixing of dry environment air near the top of clouds (e.g., Raymond 1979; Paluch 1979) and the lateral entrainment around the cloud edges (e.g., Taylor and Baker 1991). The effects of entrainment are incorporated into most CUPs by using simple assumptions that are even more difficult to validate against observations at present (Lin and Arakawa 1997). For instance, Arakawa and Schubert (1974) introduced the idea of explicit cloud spectrum parameterization which assumes that different cloud types are represented by updrafts of varying radii. The entrainment rate is crudely prescribed to be inversely proportional to the cloud radii (Simpson 1971) and assumed to be constant with height. However, most current CUPs are bulk cloud ensemble models in which only one single cloud model is used to represent the average over all the cloud types within a convective ensemble for simplicity. In these schemes, the entrainment and detrainment rates are often set to estimate the maximum cloud-top height (Xie et al. 2002).

It is known that stratiform clouds are formed by the detrainment of condensed water from cumulus clouds, and thus the microphysics properties of detrained air can critically impact the prediction of stratiform cloudiness. However, the representation of the microphysical process in cumulus clouds is usually crude because of the highly simplified cloud dynamics resulting in one of the important sources of uncertainty in the CUP problem (Randall et al. 2003).

The convective downdrafts driven by the evaporation of precipitation usually remove the convective instability by cooling and moistening the environment, which constitutes an important means by which convection stabilizes the atmosphere (Molinari and Dudek 1992).

However, current CUPs assume the convective downdraft mass flux is dependent upon the updraft mass flux with great sensitivity to the precipitation efficiency (Grell and Dévényi 2002). The latter is usually a function of wind shear and subcloud humidity. Randall et al. (2003) argued that the injection of downdraft air into the Planetary Boundary Layer (PBL) can enhance the turbulence and surface flux by further cooling and drying effects, which are generally missed in most downdraft parameterization. Thus, the inadequate representation of the static control processes in the cumulus clouds further complicates the CUP problem.

Third, the *feedback* component primarily specifies the modification of environment by convection. Disparate approaches have been utilized in CUPs to redistribute the total integrated convective heating and drying, but few systematic tests have been made to examine their validity and limitations (Grell et al. 1991). For instance, the Kuo (1974) scheme assumed that convection tends to adjust the atmosphere toward a moist neutral state, and thus the feedback is simply dependent upon the differences between clouds and environment in thermodynamic properties. Arakawa and Schubert (1974) assumed a purely steady-state character for convective clouds and the latent heat released within clouds, and consequently, convection modulates the environment primarily through environment subsidence and convective detrainment. Moreover, the feedback mechanisms also strongly depend on the static control including the entrainment, detrainment, downdrafts, and cloud microphysics. Thus, the uncertainties in the above processes also increase the difficulty in accurately describing the vertical heating and drying distributions in the environment modulated by convection.

In addition, trigger functions are specifically required in mesoscale models to determine when and where deep convection occurs (Kain and Fritsch 1993). They are a set of additional criteria that are often imposed to evaluate the possibility of convection initiation when closure

conditions in the large-scale models are not sufficient for predicting the occurrence of convection. Most triggers in CUP schemes are related to the accessibility of CAPE, or the probability to overcome the negative buoyancy below the level of free convection. However, these trigger functions are highly variable and strongly case-dependent (Kain and Fristch 1993).

Among all of these components, closure assumptions used for *dynamical control* fundamentally determine the location and intensity of convection (Grell and Dévényi 2002). In this regard, they are the primarily causes for the strong sensitivity and regional dependences of CUPs in predicting the summer rainfall mean pattern and amount. Several studies have demonstrated that the closure assumptions have strong impacts on the model rainfall frequency distribution in the Tropics (e.g., Zhang and Mu 2005) and diurnal cycle of convection in North America (e.g., Zhang 2003; Xie et al. 2004). However, these studies mostly focused on improving the closure assumptions in large-scale climate models. Their relative performances in mesoscale models are not yet clear.

Given that the Ensemble Cumulus Parameterization (ECP) scheme in CWRF includes multiple widely used cumulus closure assumptions with relative weights and dependences upon land and oceans (Liang et al. 2012), it provides an unprecedented opportunity to evaluate the isolated effects of each individual closure on summer precipitation prediction over both the U.S. land and coastal oceans. The reason to separately consider the land and oceans is because they generally differ in the environments for the convective system development including the underlying surface characteristics, the atmospheric moisture content, the vertical shear of horizontal wind, the depth of subcloud layer, and the strength of horizontal advective tendencies of temperature or moisture (Xu and Randall 2000).

Several questions can be raised in order to better understand the interactions between cumulus convection and large-scale environments over both land and oceans: 1) What are the relative performance of each closure in predicting the summer precipitation key characteristics? 2) Can they explain the model deficiencies or sensitivities identified among major CUP schemes? 3) Are there any closures that most realistically reproduce all the precipitation variations or complementarily capture certain precipitation features over a given region for further optimization? 4) What assumptions and underlying physical mechanisms are crucial in determining the precipitation spatiotemporal variations over the U.S. land and coastal oceans?

Motivated by answering these questions, five specific objectives are elaborated along with brief background information and original contributions.

1.3. Research objectives

1.3.1. Cumulus closure effects on geographic variation of summer mean precipitation

The first objective is to evaluate CWRF performance using different cumulus closure in the ECP scheme in predicting the geographic variations of summer mean rainfall over the continental U.S. and coastal oceans, with a focus on their regime dependences. Results will form a basis to explain the predictive skill differences of certain CUPs and enhance the understanding of physical mechanisms that control the summer mean pattern over distinct regions.

Over the U.S. coastal oceans, especially along the Atlantic Coast, previous GCMs generally underestimate the summer rainfall amount (e.g., Minobe et al. 2008; Kuwano-Yoshida et al. 2010). Several RCM experiments (e.g., Liang et al. 2004b) showed that the U.S. coastal ocean summer rainfall is sensitive to the CUPs. For instance, the Grell (1993) scheme produces dry biases, but the Kain-Fritsch (1993) scheme yields excessive amounts. Motivated by Zhang and Mu's (2005) finding that the spurious southern ITCZ precipitation band can be significantly

reduced by modifying the Zhang and McFarlane (1995) closure assumption, this study examines the effects of closures in order to identify if any closure can most realistically predict the summer rainfall patterns and amounts over the U.S. coastal oceans.

Over the continental U.S., this thesis focuses on three critical regions where summer rainfall prediction remains challenging to most RCMs and GCMs, including the Central U.S., the North American Monsoon (NAM) region, and the Southeast U.S. (Liang et al. 2012). The summer rainfall over the Central U.S. is controlled by large-scale circulations involving extratropical cyclones and accompanying upper-level westerly jet, and the mesoscale convective complexes and the nocturnal low-level southerly jet (Liang et al. 2012). The difficulty in predicting the NAM rainfall is mainly due to the moist convection and its maintenance mechanisms in the presence of complex terrain and land-sea contrasts (Higgins et al. 1998). The Southeast U.S. summer rainfall is controlled by local convection and affected by the Atlantic subtropical high (Henderson and Vega 1996). Numerous studies have shown that the summer rainfall over the continental U.S. is significantly sensitive to CUPs and has strong regional dependence. Sensitivity experiments by using different cumulus closures in the ECP scheme will be conducted to explain the regime dependence of various assumptions over the U.S. land.

1.3.2. Cumulus closure effects on precipitation frequency and intensity

The second objective is to examine the effects of closure assumptions on frequency distribution of daily precipitation over the continental U.S. and coastal oceans, with a focus on heavy rainfall events. Results will help to identify which closure(s) are able to reproduce observed daily rainfall statistics and have important implications for forecasting extreme events.

Most modeling studies have shown that GCMs tend to precipitate too frequently at light intensity over the land and oceans (Sun et al. 2005; Dai 2006). For instance, Dai (2006)

compared 18 Couple GCMs for precipitation simulations between 50º S-50º N and found that most of them underestimate the contribution from heavy precipitation events (>20 mm day^{-1}) and overestimate the occurrence of light rainfall events (<10 mm day^{-1}). Several RCM studies (e.g., Liang et al. 2006) demonstrate that a full solution to the drizzling problem is difficult and the prediction of daily rainfall frequency distribution is sensitive to CUPs and, varies by region. For example, the daily rainfall frequency simulated by CMM5 (Liang et al. 2001, 2004b) with the Grell (1993) and Kain-Fritsch (1993) schemes are both in agreement with observations for the Central U.S., while the Kain-Fritsch scheme produces more frequent intermediate rainfall in the NAM and Southeast U.S. However, they both overpredict the dry events and generate too few heavy rainfall events in the Gulf States. It is not clear what exact mechanisms in CUPs cause the regional differences.

Efforts have been made to improve the simulations in probability distribution of precipitation intensity, especially for the extreme events through refined cumulus closure assumption. For instance, the revised closure of Zhang and McFarlane (1995) scheme that couples convection with large-scale tropospheric forcing improved the frequency distribution of precipitation intensity over the tropical regions in both summer and winter (Zhang and Mu 2005). Wilcox and Donner (2007) found that the closure that also assumes the convection balances the large-scale instability increase above the boundary layer in the Donner (1993) scheme contributed most to the better prediction of heavy rainfall frequency. However, these studies all focused on the general predictive skills of GCMs using the modified closure to the Zhang-McFarlane scheme, the relative performance of other cumulus closures in simulating daily rainfall statistics at regional scales remains unknown.

1.3.3. Cumulus closure effects on rainfall diurnal cycle

The third objective is to examine the effects of cumulus closure assumptions on regional variations of precipitation diurnal cycle over the U.S. land and coastal oceans. Although increased resolution, refined trigger functions, and improved entrainment process are possible approaches to improve the simulation of diurnal cycle over certain regions, it is imperative to investigate the extent to which the fundamental closure assumption can regulate the diurnal variations.

Previous studies have widely recognized that most GCMs and RCMs have difficulty in faithfully predicting the diurnal cycle of precipitation over land and oceans (e.g., Dai et al. 1999; Liang et al. 2004a; Lee et al. 2007b). Several approaches have been proposed to improve the simulation of the diurnal cycle in GCMs regarding the resolution, trigger functions and entrainment process, but there is still no satisfactory solution yet. First, large errors in phase and amplitude of the precipitation diurnal cycle over the continental U.S. remain when resolution of GCMs is increased to 0.5º (Lee et al. 2007a). Mesoscale circulation associated with coastal convection is difficult to capture even in super-high-resolution GCMs (Sato et al. 2009). Second, the improvement from the trigger function is limited. Bechtold et al. (2004) showed that the trigger function that adds a temperature perturbation to the parcel based on the large-scale vertical velocity at the cloud base in the Kain-Fritsch cumulus scheme can shift the rainfall maximum from 9.5 AM to 12 AM at local solar time (LST) over the Tropical South America and Africa. Further improvements are still required to match the observed peak at 15 PM LST. Third, increasing the entrainment rate can enhance updraft plume dilution, thereby affecting convective precipitation occurrence and intensity (Bechtold et al. 2004). But doubled entrainment rate for penetrative deep convection in the Tiedtke (1989) scheme only slightly delays the time of rainfall peak during the day over the Maritime continent (Wang et al. 2007).

However, the summer rainfall diurnal pattern, especially over the U.S. southern Great Plains can be greatly improved when the cumulus closure is based on large-scale tropospheric forcing, instead of boundary layer forcing in the Zhang-McFarlane scheme (Zhang 2003). Liang et al. (2004a) also demonstrated that the Grell scheme realistically simulates the nocturnal rainfall over the Great Plains because its closure is based on and thus directly responds to the large-scale tropospheric forcing, whereas the Kain-Fritsch scheme shows superiority in the late-afternoon peaks in the Southeast U.S. because its closure is defined and thus controlled by the near-surface forcing that is more favorable there. This indicates that the rainfall diurnal cycle is very sensitive to the interaction between convection and environment that may depends on weather or climate regime. The role of cumulus closure assumptions in determining the rainfall diurnal cycle over different regions is explored here for a better understanding of the coupling processes between convection and large-scale forcing.

1.3.4. Possibility for optimization of the ECP cumulus closure assumptions

The fourth objective is to establish the basis for future optimization of the ECP scheme by examining regime-dependence of various closure assumptions over the continental U.S. and adjacent coastal oceans in predicting the summer precipitation characteristics at different time scales.

Previous studies suggested that various convection schemes work better under different climate regimes (Giorgi and Schields 1999; Xu and Small 2002; Liang et al. 2004a, b, 2007). For instance, the Kain-Fritsch scheme performs well in the NAM and Southeast U.S., but the Grell scheme has its own compelling advantages in realistically reproducing the Midwest summer mean precipitation as well as the nocturnal rainfall peak over the Great Plains. An ensemble

based on these two schemes with equal weights has shown significant improvements in reproducing the U.S. interannual anomalies and climate mean distributions (Liang et al. 2007).

The ECP scheme utilizes a suite of alternative cumulus closure assumptions with tunable relative weights depending upon locations. It facilitates comprehensive evaluation of the relative performance of these closures on the summer rainfall prediction. By identifying whether certain closures can have better performance than others or have complementary effects in predicting different precipitation characteristics, we can gain more insights about the regime-dependences of closure assumptions, and thus shed the light for future optimization of the ECP scheme. The actual optimization of the ECP scheme to improve the overall rainfall prediction is beyond the scope of this thesis, but can be achieved if localized relative weights are well understood for the selected closures.

1.3.5. Sensitivity of Central U.S. summer floods prediction to cumulus parameterization

The fifth objective is to comprehensively evaluate the performance of 12 CUP schemes incorporated in CWRF in predicting the summer precipitation key features over the Central U.S. The emphasis is placed on investigating why the Grell scheme is superior to other schemes in reproducing the nocturnal rainfall peaks by considering its closure and critical trigger.

It has been widely recognized as a common difficulty for most RCMs to accurately predict the Central U.S. summer precipitation (e.g., Takle et al. 1999; Liang et al. 2012). Many studies have documented that model deficiencies over the Central U.S. are strongly sensitive to CUPs with respect to the rainfall amount (Liang et al. 2004b, 2006, 2007); daily rainfall frequency (Liang et al. 2006), and diurnal cycle (Dai et al. 1999; Davis et al. 2003; Liang et al. 2004a; Lee

et al. 2007b, 2008). This study will more comprehensively evaluate the performance of 12 CUPs in order to identify the strength and weakness of each CUP scheme to fuel further improvements.

Liang et al. (2004a) showed that the Grell scheme is superior in reproducing the nocturnal rainfall maximum over the Central U.S. This thesis examines whether the advantage of the Grell scheme exists in CWRF and whether it will be affected when different microphysical schemes are adopted. Sensitivity experiments will be conducted to explore the possible contributions from its closure assumption and the lifting depth trigger that has been found to play a key role in a global model for realistically reproducing the Central U.S. nocturnal rainfall signals (Lee et al. 2008).

The above objectives are accomplished in this thesis by conducting sensitivity experiments and performing diagnostic analyses and critical evaluation of model results. Five major original contributions are summarized as follows:

(1) We develop the ECP scheme on the basis of the G3 scheme with numerous improvements. It not only includes multiple cumulus closures with relative weights, but also allows selecting different closure options over the land and oceans. This revised structure facilitates the optimization of the ECP scheme by determining specific weights for different closures dependent upon the location, time, and climate regimes.

(2) Cumulus closures significantly affect U.S. precipitation patterns, heavy rainfall occurrence, and diurnal cycle, with strong regional dependence differing between land and oceans. None of closure assumptions can fully represent all the observed precipitation spatiotemporal variations. The complementary advantages of closures are

identified in this thesis, forming the basis for further optimization of the ECP scheme if relative weights can be derived for those closures at various time scales.

(3) Cumulus closure effects alone could largely explain the model sensitivity to certain CUPs in summer rainfall predictions. For instance, the total instability adjustment closure consistently produces large wet biases over the NAM and Southeast U.S. and strong deficits over the Central U.S., explaining the systematic errors related to the Kain-Fritsch scheme using the same closure. On the other hand, the instability tendency closure has large deficits over the Southeast U.S. but small biases over the Central and NAM, which is also consistent with the identified biases in the Grell scheme that is based on a similar closure.

(4) The ECP scheme with the moisture convergence and average vertical velocity at the cloud base closures separately over the land and oceans show advantages over the other 11 CUP schemes in simulating the Central U.S. flood amount and, daily rainfall frequency and intensity.

(5) The Grell scheme shows superiority in reproducing the Central U.S. nocturnal rainfall maxima, but other CUP schemes generally fail. This advantage of the Grell scheme is primarily due to the instability tendency closure assumption, indicating that this assumption can be incorporated in the ECP scheme as a trigger function to improve its diurnal cycle simulation over the Central U.S.

CHAPTER 2: MODEL DESCRIPTION AND OBSERVATIONAL DATA

This chapter gives a brief description of the CWRF model used in this thesis, including its basic physical configurations, computation domain, lateral and surface boundary conditions. More details about the Ensemble Cumulus Parameterization scheme that is specifically developed to address the research questions are illustrated, with a focus on its cumulus closure assumptions. This chapter also documents important physical assumptions for fourteen CUP schemes that have been incorporated in the CWRF model, and provides the observational precipitation data for model verification.

2.1. Model descriptions

2.1.1. Basic physics configuration

The CWRF is developed on the basis of the Weather Research and Forecasting model v3.1.1 (WRF, Skamarock et al. 2008) with numerous improvements of physical processes that are essential to climate scales, including the interactions between land-atmosphere-ocean, convection-microphysics, and cloud-aerosol-radiation (Liang et al. 2012). A unique feature of the CWRF is the inclusion of a grand ensemble of alternative parameterization schemes for key physical processes including cloud, aerosol, radiation, surface, PBL, cumulus and microphysics. The current CWRF control physics configuration (Table 2.1) consists of XRL cloud, MISR aerosol, GSFC radiation, CSSP + UOM surface, CAM + ORO PBL, ECP + UW cumulus, and Tao microphysics schemes.

A basic skill evaluation has shown that the CWRF with these control physics configurations has greater application capability and overall better performance than the original WRF in the

contiguous U.S. climate simulations (Liang et al. 2012). By comparing to other alternative options in each physical driver, the GSFC radiation, CSSP surface, and the ECP cumulus schemes have relatively better performances than their counterparts in the U.S. climate simulation, indicating that their consistent integration is the key reason for the substantial improvement in the predictive skills of the CWRF over the original WRF model configuration (Liang et al. 2012).

The GSFC radiation package includes the parameterizations developed by Chou and Suarez (1999) for shortwave and by Chou et al. (2001) for longwave radiation. The solar radiation scheme includes absorption due to water vapor, CO_2, O_3, O_2 and CO_2, and interactions among the gaseous absorption and scattering by cloud condensation, aerosols (sulfate and precursors, dust, black carbon, organic carbon, sea salt), molecules (Rayleigh scattering), and the surface. The spectrum is divided into seven bands in the ultraviolet (UV) region (0.175-0.4 μm), one band in the photosynthetically active radiation region (0.4-0.7 μm), and three bands in the solar near infrared region (0.7-10.0 μm). The infrared parameterization also includes the adsorption due to major gases (H_2O, O_3, CO_2) and minor trace gases (N_2O, CH_4, CFC's), as well as clouds and aerosols in terms of a spectrum with nine bands. The k-distribution method with temperature and/or pressure scaling is used to compute the transmission function in the weak absorption bands of water vapor and trace gases, while a look-up table method is applied to account for the strong absorption bands including the 15-μm CO_2 and the 9.6-μm O_3 bands. These radiative transfer processes allow explicit cloud-radiation interactions and aerosol direct effects, and thus have important applications for high-resolution model simulations.

The CSSP is the core land surface model to predict soil temperature/moisture distributions, terrestrial hydrology variations, and land-atmosphere flux exchanges. It has significant

improvements in representing surface energy and hydrology processes, including an improved dynamic-statistical parameterization of land surface albedo (Liang et al. 2005), a 3-D subsurface hydrologic model with a scalable representation of subgrid topographic control on soil moisture (Choi et al. 2007) and an explicit treatment of surface-subsurface flow interaction (e.g., Choi and Liang 2010).

The ECP scheme is developed from the G3 scheme (Grell and Dévényi 2002) but with numerous improvements on the closure choices and relative weights, depending on land and ocean. The five major groups of closure assumptions in the ECP scheme include the quasi-equilibrium based (AS), the vertical velocity (W), the moisture convergence (MC), the total instability adjustment (KF) and the instability tendency (TD) closure. 16 subensemble algorithms are formulated under these five major assumptions, providing a good opportunity for further optimization by selecting optimal closure(s) for different regions. More details about the differences between the ECP and G3 scheme are given in the Section 2.2.

2.1.2. Computation domain and boundary conditions

The CWRF computation domain is centered at (37.5˚N, 95.5˚W) using the Lambert conformal map projection. It covers the whole continental U.S. and adjacent ocean with 30-km horizontal grid spacing, including total grid points of 197(west-east) × 139 (south-north). The buffer zones are located across 14 grids along 4 domain edges, where varying lateral boundary conditions are specified throughout the entire integration period using a dynamic relaxation technique (Liang et al. 2012). There are 36 vertical levels with refined resolutions near the surface to improve PBL and convection representation, and around the melting altitude (~800-650 hPa) to better simulate the cloud microphysics processes.

A consistent set of surface boundary conditions has been constructed at 30-km grid spacing over North America (Liang et al. 2012). This includes geographic distributions of the characteristics for surface topography (mean elevation, slope, curvature, orientation, shadowing; and their subgrid variability), stream/river and baseflow (direction, channel width, length), soil (bedrock depth, sand, clay and organic matter fraction profiles, bottom temperature), vegetation (land cover category, fractional vegetation cover, leaf and stem area index), ocean (surface temperature, salinity, and current; temperature and salinity profiles; seafloor depth), and crop cultural or management practices (planting type and density, growing area and period, fertilizer rate).

Over oceans, CWRF incorporates observed daily sea surface temperature (SST) distributions using conservative spline fit from the weekly analysis data (Reynolds et al. 2002) available on a 1º × 1º grid mesh from 1981 November to present. A 2-D multi-level upper ocean model is included in CWRF to resolve transient air-sea interactions that essentially determine SST diurnal cycle and daily variation (Ling et al. 2010). The CWRF also updates daily vegetation variations by linear temporal interpolation of the monthly mean climatology derived from the National Oceanic and Atmospheric Administration/Advanced Very High Resolution Radiometer data (Liang et al. 2012).

The initial atmosphere and lateral boundary conditions are constructed from the European Centre for Medium-Range Weather Forecast Interim Reanalysis (ERI, Uppala et al. 2008). The ERI data are available at 6 hourly intervals with 1.5º horizontal grid spacing and 60 vertical levels.

2.2. Cumulus parameterization schemes

The CWRF incorporates 7 new cumulus parameterizations (ZML, CSU, GFDL, MIT, GR, ECP, UW), in addition to the 7 original WRF schemes (BMJ, NKF, SAS, NSAS, TDK, GD, G3). All the cumulus parameterization schemes represented by above abbreviations or acronyms with respective references are defined in Table 2.2. They represent the effects of sub-grid convective updrafts and downdrafts and compensating ambient motions. All schemes are made to predict surface total precipitation rates, cloud base and top levels, and vertical atmospheric heating and moistening profiles, but have some differences in producing the wind tendencies or convective in-cloud liquid or ice water profiles. To consistently evaluate the effects of moist convection parameterization, shallow convection parameterization in 8 CUPs (BMJ, NKF, SAS, NSAS, TDK, ZML, G3, ECP) are switched off internally, and the UW shallow scheme works as an only option with other deep CUPs in all the experiments. According to the cumulus closure assumptions, these fourteen schemes can be generally divided into three major types: 1) Multiple closures (ECP, G3, and GD); 2) Total instability adjustment closure (ZML, NKF, and TDK); 3) Quasi-equilibrium closure-based (BMJ, GR, MIT, GFDL, SAS, NSAS, CSU, UW). The major assumptions and several specific features for each category are illustrated as follows.

2.2.1. Multiple closure schemes

The GD, G3, and ECP schemes are all ensemble mass-flux type schemes with multiple closure assumptions and variants of parameters in the static control including updraft and downdraft entrainment and detrainment and precipitation efficiency. The GD scheme was first introduced by Grell and Devenyi (2002) in which the dynamic control closures are based on convective available potential energy (CAPE or cloud work function), low-level vertical velocity, or integrated vertical advection of moisture. The CAPE-based closures either balance the rate of increase of CAPE or relax the CAPE to a climatological value (QE assumption), or remove the

CAPE in a specific time scale. The G3 scheme is developed from the GD scheme, but excludes the QE assumption from ensemble members, and spreads environmental compensate subsidence to neighboring grid columns.

The ECP scheme is built upon the same parameterization framework of the G3 scheme including the convective trigger functions, cloud models and different dynamic closure control. It differs from the G3 scheme in two main aspects. First, it incorporates major closure assumptions with 16 different algorithms considering the large-scale forcing perturbations from the surrounding nine grid points, while the current version of G3 scheme contains four types of closures by removing the QE assumption. The inclusion of this popular assumption allows sensitivity analyses to better understand systematic precipitation errors in many models that uses CUPs based on it. Second, the ECP scheme adds relative weights for those closures and considers regional dependence between land and oceans, but the G3 scheme uses equal weights for all closures without distinguishing regime contrasts. All the closure assumptions are used to determine the cloud base mass flux by linking the existence and intensity of convection to large-scale processes as shown in Table 2.3.

The AS closure assumes an instantaneous equilibrium between large-scale forcing and subgrid convection by relaxing the cloud work function toward a climatological value (Arakawa and Schubert 1974). Four algorithms differ in the referenced climatology value by implementing the observed average CAPE value table from Lord et al. (1982) and the Global Data Assimilation System above/below cumulus cloud top level, respectively.

The W closure (Brown 1979; Frank and Cohen 1987) assumes that net cloud base mass flux is determined by environmental mass flux averaged from the surrounding nine points at lower tropospheric levels. Specifically, it includes four different algorithms based on the level of free

convection, the updraft originating level, or the level with the maximum or minimum upward vertical velocity below the level of free convection.

The MC closure (Krishnamurti et al. 1983) assumes that convection develops to balance the column integrated moisture convergence. This convergence can be redefined with four different algorithms by selecting maximum, minimum, averaged, or local randomly chosen values from the surrounding nine points.

The KF closure (Kain and Fritsch 1993) assumes that convection acts to reduce the CAPE towards zero over a specific time scale. The TD closure is similar to the assumption in the Grell (1993) scheme, in which convection is determined by the increase of large-scale instability. Both the KF and TD closures contain two different subensembles by defining the large-scale instability locally or averaged over the surrounding nine points.

2.2.2. Total instability adjustment schemes

Three CUPs (ZML, NKF, TDK) are based on the total instability adjustment closure assumption in which the convection acts to reduce the CAPE towards zero over a specific time scale. The ZML is the parameterization of Zhang and McFarlane (1995) with modifications to facilitate its application in high resolution models for deep convection (Liang et al. 2012). The moist convection occurs only when the atmosphere is locally conditionally unstable in the lower troposphere. The updraft ensemble is only comprised of those plumes which can penetrate through this convective layer and these updrafts are assumed to have same initial upward mass flux from the sub-cloud layer to simplify the formulations.

The NKF scheme is a modified version of the Kain-Fritsch scheme (Kain, 2004) which is originally based on Kain and Fritsch (1993). It utilizes a one-dimensional cloud model with explicitly representation of effects of moist updrafts and downdrafts, the entrainment,

detrainment and simple microphysics involved. This scheme triggers the convection when net column convective instability is present and the parcel temperature is higher than the environmental value. To induce stronger convection in the presence of the large-scale upward motion, a perturbation to the parcel temperature which is proportional to the grid-scale vertical motion at the lifting condensation level is incorporated as an additional trigger function.

The TDK scheme is originally designed by Tiedtke (1989) and revised by Nordeng (1994). It is a bulk mass flux model based on the CAPE removal closure. The convection is activated when the moisture convergence is greater than a limit of boundary layer turbulent moisture flux. This scheme considers three types of convection: 1) deep convection that occurs under disturbed, conditionally unstable conditions in the presence of lower tropospheric large-scale moisture convergence; 2) shallow convection that occurs in a suppressed environment and is mainly driven by the turbulent surface moisture flux; 3) mid-level convection that occurs mainly in conditional unstable condition, but with the cloud base above the PBL.

2.2.3. Quasi-equilibrium closure-based schemes

The remaining eight schemes (BMJ, GR, MIT, GFDL, SAS, NSAS, CSU, UW) are all established on the QE closure assumption but with alterations. The BMJ scheme is a moist adjustment parameterization developed by Betts (1986) and Betts and Miller (1986), and modified by Janjic (1994) for both deep and shallow convection. It assumes that the profiles of temperature and moisture in a column with sufficient resolved-scale vertical motion and instability are instantaneously relaxed toward observed neutral structures.

The GR scheme is proposed by Grell (1993) as a simplified mass flux scheme that only consists of a single pair of updraft and downdraft without direct mixing between them. The entrainment and detrainment only occurs at the top or bottom of cloud. Based on the QE

assumption, convection in this scheme is determined by the rate of destabilization in which the change of instability due to convection balances the changes due to nonconvective effects. The convection is not activated until a lifting depth criterion is met.

The MIT scheme is the parameterization of Emanuel (1991) and Emanuel and Živković-Rothman (1999). The closure employs a subcloud-layer quasi-equilibrium hypothesis (Raymond, 1995) which states that convective mass fluxes will adjust so that air within the subcloud layer remains neutrally buoyant with respect to upward displacements to just above the top of the subcloud layer. It utilizes the buoyance-sorting assumption of Raymond and Blyth (1986) which assumes that mixing in clouds is highly episodic, rather than continuous as in the entraining plume model. In its mixing formulations, the entrainment and detrainment rates are functions of the vertical gradients of buoyancy in clouds. Convection occurs whenever the environment is unstable to a parcel in reversible adiabatic ascent from the surface.

The GFDL scheme is the parameterization of Donner (1993) with model implementation of Donner et al. (2001). It determines the cloud base mass flux by requiring that consumption of CAPE by convective systems (subgrid deep convection and associated mesoscale circulations) balances CAPE generation by the large-scale forcing (radiation and surface fluxes). The convection is triggered when the large-scale CAPE generation rate is positive and the maximum convective inhibition cannot exceed 10 J Kg^{-1}. The uniqueness of this scheme is that it augments cloud base mass flux with convective-scale vertical velocities to include the microphysics of mesoscale anvils, leading to a consistent interaction between convection, microphysics and radiation.

The SAS scheme is a simplified version of Arakawa and Schubert (1974) scheme developed by Pan and Wu (1995). The deep CUP determines the cloud base mass flux by relaxing the cloud

work function to a critical value over a fixed timescale. To trigger the convection, this critical cloud work function value must be exceeded and is assumed to be the function of cloud base vertical motion. This scheme also defines the upper limit of convective inhibition using the lifting depth trigger which assumes the depth between the parcel originating level and the level of free convection is less than 150 hPa.

The NSAS scheme is based on the SAS scheme but with several modifications to trigger functions. For instance, the fixed value of lifting depth trigger (150 hPa) is changed to vary within the range of 120-180 hPa, in proportional to the cloud base grid-scale vertical velocity. This intends to produce more convection in large-scale convergence regions but less convection in subsidence areas (Han and Pan 2011).

The CSU scheme is the parameterization of Arakawa and Schubert (1974) but with a prognostic cumulus kinetic energy (CKE) closure (Pan and Randall 1998) and interactive liquid and ice cloud microphysics (Fowler and Randall 2002). This prognostic closure relaxes the QE assumption by explicitly predicting the CKE for each cumulus subensemble. The cloud-base mass flux is determined by the CKE and a dimensional parameter (α) which is related to the adjustment time defined by original QE assumption. In current version of CSU scheme, a constant value of α ($1.0e^{8}$) is given for all cloud types.

The UW scheme is a bulk mass-flux based shallow cumulus parameterization of Bretherton and Park (2009) in which entrainment and detrainment is derived using a buoyancy-sorting algorithm. This scheme has a combined closure and trigger based on convective inhibition. It assumes that shallow convection can only form if the source air has sufficient vertical velocity to penetrate the weak inversion at the top of sub-cloud layer and reach its level of free convection.

The cloud base mass flux is determined as to maintain dynamical equilibrium between the sub-cloud turbulent boundary layer and the base of cumulus cloud layer.

2.3. Observational Data

Over the U.S. coastal oceans, the Tropical Rainfall Measuring Mission (TRMM) 3-hourly and daily product (3B42 version 7, 50º S-50º N, 0.25º grids, 1998-2009) is mapped onto the CWRF 30km-grids using bilinear spatial interpolation to increase the comparability with model simulation. In addition, the TRMM 3A25 product is adopted to provide the monthly mean convective and stratiform precipitation. It is based on the precipitation radar observation and covers 37ºS to 37ºN with a 0.5º grid resolution (Iguchi et al. 2000).

Several major daily precipitation datasets are utilized for model verification over the continental U.S. and Northern Mexico. The primary one is constructed from rain gauge measurements at 7235 stations over the continental U.S. and adjusted by monthly mean of PRISM (Parameter-elevation Regression on Independent Slopes Model, Daly et al. 2008) for the orographic effects particularly important over the western U.S. mountain regions (Liang et al. 2004b). Another one is derived from the National Oceanic and Atmospheric Administration Climate Prediction Center (CPC) global 0.5º analysis of daily gauge measurements (Chen et al. 2008) to supplement data over Canada and Mexico. To examine the diurnal cycle of precipitation, the merged 3-hourly precipitation data from the Tropical Rainfall Measuring Mission (TRMM) product (3B42, 50ºS-50ºN, 0.25º × 0.25º grid, 1998-present) is mapped onto the CWRF 30km grid using bilinear spatial interpolation. In addition, the 3-hourly North American Regional Reanalysis (NARR; Mesinger et al. 2006) and hourly CPC precipitation data over the United States (Higgins et al. 1996) are both used as a supplement to TRMM before 1998.

2.4. Figures and Tables

Table 2.1 The CWRF model control configurations of physics components.

Domain		United States & Adjacent, centered at (37.5˚N, 95.5˚W) Horizontal resolution: 30km (196x139) Vertical resolution: 36 levels, top at 50hPa Buffer zone width: 14-grids (420km)
Physics Configuration	Cloud	XRL (Xu-Randall-Liang cloud cover parameterization, Xu and Randall 1996, Liang et al. 2004b)
	Aerosol	MISR (Multi-angle Imaging SpectroRadiometer, Kahn et al. 2007)
	Radiation	GSFC (NASA Goddard Space Flight Center, Chou and Suarez 1999; Chou et al. 2001)
	Surface	CSSP (Conjunctive Surface-Subsurface Process Model, Choi and Liang 2010)
	PBL	CAM (NCAR Community Atmosphere Model) + ORO (Module for orographic turbulence stress and gravity-wave drag, Rontu 2006)
	Deep Cumulus	ECP (Ensemble Cumulus Parameterization modified from G3, Grell and Dvénéyi 2002)
	Shallow Cumulus	UW (University of Washington, Park and Bretherton 2009)
	Microphysics	GSFCGCE (Goddard Cumulus Ensemble Model, Tao et al. 2003)
	Ocean	UOM (upper ocean model) (Ling et al. 2010; Liang et al. 2012)

Table 2.2 The summary of CWRF cumulus parameterization schemes with the related references [Qc, Qi, Qr, Qs: mixing ratio of cloud water, ice, rain, and snow].

CUP	References	Closure	Trigger	Momentum Tendencies	Moisture Tendencies	Shallow
ECP	modified from G3	Multiple	Maximum cap strength	no	Qc, Qi	yes
G3	Grell and Dvénéyi (2002)	Multiple without QE	Maximum cap strength	no	Qc, Qi	yes
GD	Grell and Dvénéyi (2002)	Multiple	Maximum cap strength	no	Qc, Qi	no
ZML	Zhang and McFarlane (1995)	Total instability adjustment	CAPE > 0	yes	Qc, Qi	no
NKF	Kain and Fritsch (1993); Kain (2004)	Total instability adjustment	CAPE > 0; Parcel temperature perturbation	no	Qc, Qi, Qr, Qs	yes
TDK	Tiedtke (1989); Nordeng (1995)	Total instability adjustment	Moisture convergence	yes	Qc, Qi	yes
BMJ	Betts and Miller (1986); Janic (1994)	QE assumption	Positive CWF threshold	no	-	yes
GR	Grell (1993)	QE assumption (instability tendency)	Lifting depth trigger	no	-	no
MIT	Emanuel and Živković-Rothman (1999)	subcloud layer-based QE assumption	Environment is unstable to a parcel	yes	-	no
GFDL	Donner (1993); Donner et al. (2001)	QE assumption	CAPE > 0; ΔCAPE > 0	no	Qc, Qi	no
SAS	Pan and Wu (1995)	QE assumption	Critical CWF; Lifting depth trigger	yes	Qc, Qi	yes
NSAS	Han and Pan (2011)	QE assumption	Lifting depth trigger	yes	Qc, Qi	yes
CSU	Fowler and Randall (2002)	QE assumption (prognostic CKE)	CKE dissipation rate	no	Qc, Qi, Qr, Qs	no
UW	Bretherton and Park (2009)	subcloud layer-based QE	Turbulent kinetic energy	yes	Qc, Qi, Qr, Qs	yes

Table 2.3 Cumulus closure assumptions in the ECP scheme (five major groups with variants).

Closures	Variants in closure	Calculation Methods
AS (Arakawa and Schubert 1974)	Climatological cloud work function	AS_1: use table 1 in Lord et al. (1982) above the cumulus cloud top AS_2: use table 1 in Lord et al. (1982) below the cumulus cloud top AS_3: calculated from GDAS above the cumulus cloud top AS_4: from GDAS below the cumulus cloud top
W (Brown 1979; Frank and Cohen1987)	Upward vertical velocity	W_1: minimum value below the cloud base (LFC) W_2: average value at the cloud base (LFC) W_3: maximum value below the cloud base (LFC) W_4: average value at the updraft originating level;
MC (Krishnamurti et al. 1983)	Integrated vertical advection of moisture	MC_1: maximum value MC_2: minimum value MC_3: average value MC_4: local value
KF (Kain and Fritsch 1993)	CAPE or cloud work function	KF_1: average value among the spread of forcing perturbations KF_2: local value
TD (Grell 1993)	Large scale instability forcing tendency	TD_1: averaged over the spread of forcing perturbations TD_2: local value

CHAPTER 3: CUMULUS CLOSURE EFFECTS ON SUMMER PRECIPITATION PREDICTION OVER THE U.S. COASTAL OCEANS

This chapter evaluates CWRF's ability to simulate the summer precipitation characteristics over the U.S. Atlantic Coasts and Gulf of Mexico, focusing on the effects of cumulus closure assumptions in an Ensemble Cumulus Parameterization (ECP) scheme. It is compiled from an article submitted to *Journal of Climate* titled "CWRF summer precipitation prediction over the United States coastal oceans: Effects of ensemble cumulus parameterization closures". The model physics configuration and evaluation data are described in Chapter 2. This Chapter presents the model experiments and results with respect to precipitation spatial pattern, frequency and intensity, and diurnal cycle. Additional discussions explore possible causes for model discrepancies among the cumulus closures in terms of cloud base mass flux, convective-to-total precipitation ratio, and associated thermodynamic and large-scale circulation characteristics.

3.1. Introduction

Many efforts have been made on reducing the modeling precipitation biases over oceans by improving cumulus closure assumptions that is the fundamental component of CUPs (Arakawa 2004). For instance, Zhang and Mu (2005) revised the cumulus closure of Zhang and McFarlane (1995) to base it on the large-scale forcing in the free troposphere rather than CAPE in the whole atmosphere. This modification greatly reduced the dry bias in the western Pacific monsoon region and also significantly mitigates the double ITCZ problem (Zhang and Wang 2006). Wilcox and Donner (2007) also found that the closure which assumes convection balances the

increase in large-scale instability above the boundary layer in the Donner (1993) scheme contributed most to a realistic prediction of heavy rainfall frequency. In addition, previous studies mainly focused on investigating the effects of refined cumulus closures on the diurnal cycle of continental convection (Zhang 2003). Given that convective systems over oceans generally have different structures and life cycles from those over land (Sato et al. 2009), the question about how cumulus closure assumption affects the diurnal cycle of convection and precipitation over the oceans remains open.

We will focus on the U.S. Atlantic Coast and the Gulf of Mexico (hereafter, U.S. coastal oceans) because they are significantly affected by hurricanes or tropical storms and their associated storm-surge floods and waves could pose severe threat to the people along the shorelines (Maloney and Hartmann 2000). Current GCMs with coarse resolutions mostly focused on predicting the seasonal and annual means of precipitation over the U.S. coastal oceans and they generally predict insufficient amounts (Kuwano-Yoshida et al. 2010), whereas the RCM simulations of summer coastal ocean rainfall are sensitive to CUP (Liang et al. 2004b; 2012).

On the other hand, current CUP schemes are generally based on several principle cumulus closure assumptions including integrated moisture convergence (Kuo 1974), or the vertical moisture assumption (e.g., Krishnamurti et al. 1983), the widely used QE assumption proposed by Arakawa and Schubert (1974), and the environmental low-level wind convergence closure (Frank and Cohen 1987). Previous studies have recognized that large controversies exist about the applicability and performance of these cumulus closures for weather forecasts or climate prediction (Frank and Cohen 1987; Arakawa 2004; Fletch and Bretherton 2010). Therefore, in order to improve the U.S. coastal ocean summer rainfall prediction, this study will investigate the

effects of CUP, focusing on the predictive skills of different cumulus closures by adopting the ECP scheme.

3.2. Model Experiments

Figure 3.1 (a-d) shows the observed seasonal mean precipitation distributions over the CWRF computation domain during 1998-2009. There is a clear precipitation band along the U.S. Atlantic Ocean in all four seasons. The rainband is widest in winter (DJF) and narrowest in summer (JJA), but slightly discontinued in autumn (SON) along the U.S. East coastlines and more widespread to further east. The rainfall intensity is weakest in spring (MAM) and strongest in summer. Figure 3.1 (e-h) present the interannual standard deviations of the four seasonal mean precipitation from the climatology mean of 1998-2009. Large variances are exhibited over three key coastal ocean regions located at the north and south portion of the U.S. Atlantic Coast and Gulf of Mexico (hereafter, U.S. North Atlantic, U.S. South Atlantic and Gulf of Mexico shown in the boxes). This study will focus on the summer because it has the largest amount of precipitation accompanied with most intense convection along the U.S. coast oceans (Kuwano-Yoshida et al. 2010). The outcome will allow us to gain insights into the cumulus convection effects.

Figure 3.2 specifically shows precipitation anomalies averaged over the above three key regions in summer and autumn relative to the 1998-2009 climatology. We will focus on three heavy summer precipitation anomalies including 2008 (U.S. South Atlantic), 2003 (Gulf of Mexico) and 1999 (U.S. North Atlantic), and also compare the 2008 autumn with largest precipitation anomaly along the U.S. North Atlantic to further examine whether the cumulus closure effects have seasonal dependence. This study will conduct integrations for all these cases with one month model spin-up, utilizing ECP five ensemble closures (AS, W, MC, KF, and TD)

and 16 individual subensemble algorithms respectively over oceans. The land closure uses the MC assumption as in the CWRF control configuration (Liang et al. 2012).

3.3. Results

3.3.1. Effects of ensemble cumulus closures

a. Geographic distribution of summer mean precipitation

Figure 3.3 shows summer (2008, 2003, 1999) mean precipitation biases of the CWRF simulations using the ECP scheme with the five cumulus ensemble closures (AS, W, MC, KF, TD) averaged over the three key regions and the entire U.S. East plus South coastal oceans. For all three cases, the AS, MC and KF closures largely overestimate rainfall amounts, while the TD closure systematically produces deficits. Nevertheless, the W closure generates the smallest summer mean biases over these ocean regions.

Figure 3.4 presents the geographic distributions of 2008 summer mean precipitation, the number of rainy days (daily rainfall >1 mm day^{-1}), and the averaged rain intensity (daily rainfall > 1 mm day^{-1}) over the U.S. coastal oceans as observed and simulated by CWRF using the ECP scheme with five different ensemble closures. Results show that the AS, MC and KF closures all produce widespread excessive precipitation bands over the coastal oceans. The wet biases are caused by too many rainy days and unrealistically strong rain intensities. In contrast, the TD closure underestimates the rainfall amount and produces reduced number of rainy days compared to other closures, but still more than observations. The W closure better captures the heavy rain band observed along the Gulf Stream, but yields excessive amounts further east mainly due to the frequent rainy days.

b. Precipitation frequency and intensity

Figure 3.5 shows the frequency distribution of 2008 summer point-wise daily precipitation and relative contribution from each daily precipitation rate to the summer total precipitation over the entire U.S. coastal oceans simulated by CWRF using the ECP scheme with five different ensemble cumulus closures as compared to the ERI reanalysis and the TRMM observations. The range of precipitation rates is divided into 1 mm/day bin from 0 to 55 mm day^{-1}, with daily rainfall higher than 55 mm day^{-1} accumulated into the last bin. The frequency calculation is based on daily rainfall of all CWRF grids within the U.S. coastal oceans without any spatial or temporal average. The relative contribution to the total precipitation from each bin is the product of the frequency of rainfall occurrence and the precipitation rate within the bin divided by the summer total amount.

The ERI largely overestimates the frequency of light rain events with daily intensity less than 15 mm day^{-1}, but hardly produces heavy rain events exceeding 25 mm day^{-1}. The ECP scheme with five ensemble cumulus closures all produce much wider spectra than the ERI, though they still have deficiencies from the reality. In particular, the AS, MC, and KF closures generally predict more frequent rainy events than the TRMM for daily rate greater than 5 mm day^{-1}, leading to the large wet biases. In contrast, the W and TD closures both underestimate the occurrence of heavy rain events with different frequency distribution. For instance, the W closure underpredicts the occurrence of daily rainfall greater than 20 mm day^{-1}, while the TD closure largely underestimates the contribution of daily rate greater than 5 mm day^{-1}. Therefore, the precipitation frequency distribution substantially varies with the choice of cumulus closures.

c. Precipitation diurnal cycle

The observed ocean rainfall diurnal cycle is characterized by an early morning maximum (Janowiak et al. 1994) over the open areas but with distinguished regional differences, such as

the near-continental variations caused by the coastline effects and gravity wave forcing from the adjacent land (e.g., Yang and Slingo 2001). Despite the regional variations, the true physical mechanisms responsible for this early morning rainfall peak are still not well known. Nesbitt and Zipser (2003) briefly summarized the possible causes into four general categories: 1) the differential radiative heating between convective and surrounding cloud-free regions; 2) the increased instability produced by nighttime radiative cooling near the cloud top; 3) the reduced cloud entrainment effects due to increased relative humidity at night; 4) the daily SST variations. These mechanisms suggested that the ocean rainfall diurnal cycle is modulated by the interaction between moist convection, cloud formation, radiation and surface processes (Yang and Slingo 2001). Thus, precipitation diurnal simulation provides an excellent test bed for evaluating these interactive physics processes (Dai 2006).

Figure 3.6 compares the 2008 summer mean diurnal cycles of rainfall averaged over the three selected U.S. coastal ocean regions as observed by the TRMM and simulated by CWRF using the ECP scheme with five ensemble closures. The observed diurnal cycles varied in their phases and amplitudes along the U.S. coastal oceans. There exhibits a clear phase transition from the early morning around 3AM in the U.S. North Atlantic to 8AM in the U.S. South Atlantic, and then around 9AM-11AM in the Gulf of Mexico. This phase behavior is different from previous findings in the tropic oceans where the mean rainfall peaks tend to appear around 6-7AM (Nesbitt and Zipser 2003), indicating that distinct physical mechanisms are responsible for the regional variation of rainfall diurnal cycle over the coast oceans. For instance, the delayed rainfall peaks over the latter two regions might be due to the effects of land convection migrated to the offshore areas that has been suggested by earlier studies (Zhou and Wang 2006).

The model results show that the TD closure is most capable of capturing the diurnal phase over these three ocean regions with the highest correlations (0.97, 0.84 and 0.97), but largely underestimates rainfall peak amounts. For the U.S. North Atlantic Coast, all the five closures tend to well capture the timing of diurnal cycle, but with much weaker amplitudes than observations. For the U.S. South Atlantic Coast, the W closure captures the observed diurnal magnitudes but yields somewhat earlier peaks than TRMM, while the AS, MC, and KF closures significantly overpredict the rainfall magnitude with 3-hour earlier peaks. Over the Gulf of Mexico, the W and TD closures tend to produce a precipitation maximum around 9AM close to TRMM, but the other closures (AS, MC, and KF) predict much earlier rainfall peaks. These sensitivity studies suggest that the cumulus closure assumptions affect the regional variations of the U.S. coastal ocean rainfall diurnal cycle. The systematic underestimated amplitudes of diurnal cycle in all simulations over the U.S. North Atlantic and the Gulf of Mexico is consistent with the previous modeling studies, which suggested a lack of appreciable SST diurnal forcing as one of primary causes (Dai et al. 1999). This model error also indicates that future studies are required to examine how precipitation diurnal cycles are actually related to the SST variations by conducting sensitivity experiments with UOM.

d. Overall performance of the ECP five ensemble closures

Several typical characteristics of these five ensemble cumulus closure assumptions are identified as follows. First, the AS, KF, and MC closures tend to overestimate the number of rainy days and the mean rain intensity, resulting in widespread large wet biases along the U.S. coastal oceans. Second, the W and TD closures reduce such biases, but still contain important deficiencies. For instance, the TD closure substantially overestimates the frequency of light rain less than 5 mm day^{-1}, leading to weaker rain intensities and total amount deficits, while the W

closure unfaithfully predicts wet biases further east and overestimates the number of rainy days, mostly attributed to the daily precipitation less than 20 mm day^{-1}. Third, the AS, MC, and KF closures overestimate diurnal magnitudes and generate earlier rainfall peaks than the observations, while the TD closure better captures the diurnal phase, but underestimates the amplitude. Although the W closure produces a more realistic magnitude, falling between the above two groups, it still has nontrivial phase errors. Therefore, none of these ensemble closure assumptions can fully represent all the observed precipitation characteristics. The inherent biases and distinct sensitivities among these ensemble cumulus closures suggest that improvements for the prediction of U.S. coastal ocean precipitation are possible by refining the ECP ensemble closures.

3.3.2. Effects of subensemble closure algorithms

Each ensemble cumulus closure includes multiple algorithms in the ECP scheme. It is unknown how these algorithms under the same conceptual assumption contribute to the typical behavior of the ensemble. By investigating the effects of individual closure algorithms, we attempt to explain whether different algorithms in each ensemble tend to produce systematic errors or they complement each other to generate smaller biases. The results here can also provide guidance for future optimization of the ECP scheme by deriving appropriate weights for certain cumulus closure algorithms that can complementarily capture the observed signals (Liang et al. 2007).

a. Geographic distribution of summer mean precipitation

Figure 3.7 compares CWRF biases using the ECP scheme with 16 subensemble closure algorithms for precipitation in three summer cases averaged over the three key regions and the entire U.S. East plus South coastal oceans. Biases are widely spread and some are systematic in

certain ensemble closures. For instance, the AS and KF subensemble algorithms all overpredict the rainfall amounts, resulting in large wet biases in their ensembles, while all the TD algorithms systematically produce dry biases. The W and MC closure algorithms exhibit a wide distribution of biases, where the use of maximum vertical velocity at sub-cloud layer (W_3) and moisture convergence (MC_1) yield large wet biases, while that of the minimum vertical velocity at cloud base (W_1) and moisture convergence (MC_2) produce significant deficits. Thus, the AS, KF and TD ensemble closures generate errors that are systematic across all their subensemble algorithms, while the W and MC ensemble closures simulate reduced biases by cancellation of compensatory errors among their member algorithms. An important finding is that algorithms based on the average vertical velocity at the cloud base or updraft originating level (W_2 or W_4), and moisture convergence (MC_3) consistently have smaller biases than other members.

The study below evaluates the relative performance of three algorithms all based on the averaged large-scale forcings: the W_2, MC_3, and TD_1 that computes the CAPE increase rate from average instability. Figure 3.8 shows precipitation geographic distributions of three summer cases simulated by CWRF using the ECP scheme with the above three subensemble algorithms (W_2, MC_3, TD_1) compared to the ERI reanalysis, and TRMM observations. The ERI generally underestimates the summer rainfall along the U.S. coastal oceans, consistent with the prediction of most GCMs (Kuwano-Yoshida et al. 2010). Among the three subensemble algorithms, the TD_1 produces significant deficits over coastal oceans, but the W_2 and MC_3 complementarily reproduces the observed precipitation pattern and amount. Compared to TRMM, the W_2 better captures the location of major rainband along the Gulf Stream but with insufficient amounts, while the MC_3 improves the prediction of rainfall amounts but with a much wider coverage.

Table 3.1 lists the pattern correlation coefficients and root mean square (rms) errors of summer (2008, 2003, 1999) mean precipitation, rainy days and intensity between CWRF simulations using the ECP scheme with W_2, MC_3 and TD_1 and their corresponding ensemble (W, MC, TD) closures and TRMM observations. The W_2 and MC_3 better capture the geographic distribution of summer mean amounts with comparable higher pattern correlations and smaller rms errors than the TD_1. Particularly, the W_2 greatly reduces the overestimation of rainy days in the W ensemble, while the MC_3 improves rain intensity over the MC ensemble. Thus, the other algorithms of these two ensemble closures produce relatively poor skills and are better eliminated.

b. Precipitation frequency and intensity

Figure 3.9 shows the frequency distribution of 2008 summer pointwise daily rainfall and relative contribution to the total amount over the U.S. coastal oceans simulated by CWRF using the ECP scheme with three subensemble algorithms (W_2, MC_3, TD_1) as compared to the driving ERI reanalysis and TRMM observations. All three CWRF simulations significantly improve the frequency distribution in the ERI, especially for heavy rain events greater than 25 mm day^{-1}. The TD_1 produces a similar distribution as its TD ensemble, both generating too many events of light rain (< 5 mm day^{-1}), but insufficient occurrences of higher intensities. The W_2 and MC_3 both overpredict the events of rainfall weaker than 25 mm day^{-1}, but slightly underestimate heavier rainfall events. Compared to the corresponding ensembles, the W_2 improves the contribution of daily rainfall greater than 40 mm day^{-1} that are totally missed in the W ensemble, while the MC_3 inhibits the higher frequency of daily rainfall greater than 5 mm day^{-1} in the MC ensemble.

Figure 3.10 shows spatial frequency distributions of pointwise correlation coefficients and rms errors of daily rainfall variations for three summer cases (2008, 2003, 1999) over the U.S. coastal oceans between TRMM observations and CWRF simulations using the ECP scheme with three subensemble closures (W_2, MC_3, TD_1). Following Liang et al. (2012), the statistics are based on daily precipitation for all the grids over the U.S. coastal oceans in the CWRF domain. If the frequencies curve of correlation coefficient (rms errors) shifts more toward the right (left), model ability in capturing the daily precipitation variation of temporal correspondence and magnitude is higher. Clearly, the TD_1 is worst overall, producing lowest correlation and largest rms errors for all three cases. In contrast, the MC_3 is superior in reproducing the observed temporal structure, with the correlation frequency shifting more to the right.

c. Precipitation diurnal cycle

Figure 3.11 compares the 2008 summer precipitation diurnal cycles simulated by CWRF using the ECP scheme with three subensembles (W_2, MC_3, TD_1), and from the ERI reanalysis and TRMM observations over the three coastal ocean regions. The TD_1 has the typical characteristics of TD ensemble, better capturing the diurnal cycle phase than other closures but largely underestimating the magnitude. The MC_3 greatly reduces the overestimated magnitudes in the MC ensemble, and produces the diurnal amplitude comparable with the W_2. Both W_2 and MC_3 produce weaker and earlier rainfall peaks than observations, suggesting that deep convection starts prematurely due to the lack of effective convective inhibition mechanisms involved (Dai and Trenberth 2004). In the ECP scheme, the convection trigger function is basically determined by maximum cap inversion which is 50 hPa over oceans. The success of TD_1 or TD ensemble in reproducing the diurnal phase may result from the inclusion

of increased CAPE as an additional constraint for convection initiation. This can be more generally implemented as a convective inhibiting trigger function (Xie et al. 2004).

3.3.3. Effects of cumulus closures on autumn precipitation

Above has shown that major rainbands in autumn have seasonal mean distribution similar to summer, but much stronger interannual variances over three distinct coastal regions. This section investigates the effects of cumulus closures on autumn precipitation, focusing on the seasonal contrast to summer.

Figure 3.12 compares the 2008 autumn mean precipitation biases of simulations with subensemble algorithms using average assumptions (W_2, TD_1, MC_3) and their corresponding ensemble closures (W, TD, MC) compared to the TRMM observations averaged over three key coastal regions and the entire U.S. coastal oceans. Consistent with the summer cases, all the AS and KF algorithms systematically overestimate the autumn precipitation, but the TD algorithms tend to produce large deficits especially over the U.S. North Atlantic Coast. The W and MC closures produce a wide range of autumn mean biases, where the subensemble algorithms using the average vertical velocity at cloud base (W_2) or moisture convergence (MC_3) have the smallest biases. Note that the W_2 produces relatively larger deficit over the U.S. North Atlantic Coast but the smallest biases over the other two regions. In contrast, the MC_3 has smallest dry bias over the U.S. North Atlantic Coast but larger wet biases over the others. As such, the W_2 and MC_3 show their complementary advantages in capturing the autumn mean pattern and intensity.

Figure 3.13 compares the frequency distribution of 2008 autumn pointwise daily precipitation and relative contribution to total rainfall over the U.S. coastal oceans simulated by CWRF using the ECP scheme with the three subensemble algorithms (W_2, MC_3, TD_1), and

from the driving ERI reanalysis and TRMM observations. Impacts of different cumulus closures on the precipitation frequency and intensity have weak seasonal dependence, where major features in autumn are very similar to summer. In particular, the TD_1 tends to overpredict the frequency of light rainfall less than 5 mm day^{-1}, but substantially underestimate the occurrence of events of heavier intensities. The W_2 and MC_3 overpredict the frequency and contribution of daily rainfall less than 25 mm day^{-1}, but capture the distribution of extreme tails better than the ERI and TD_1.

Figure 3.14 compares 2008 autumn and summer mean diurnal cycles of precipitation averaged over the U.S. coastal oceans simulated by CWRF using the ECP scheme with three subensemble algorithms (W_2, MC_3, TD_1), and from the ERI reanalysis and TRMM observation. Observations reveal a morning rainfall peak around 09AM in both seasons. A secondary maximum occurs in autumn around 15PM, as shown in Dai and Trenberth (2004). The ERI reanalysis systematically produces earlier rainfall peaks with weaker amplitudes in both summer and autumn. The CWRF simulations with three closure algorithms exhibit coherent behaviors in both seasons. The W_2 shows better performance in capturing the diurnal cycle amplitude, while the TD_1 substantially underestimates the total rainfall amount. Nevertheless, the TD_1 is superior over others in capturing the diurnal phase with higher temporal correlation for summer (0.94) and autumn (0.75), compared to the W_2 closure (0.75, 0.51). On the other hand, the MC_3 significantly overestimates the total rainfall amount and produces somewhat earlier peaks than observations.

Thus, cumulus closures have systematic effects on the U.S. coastal ocean precipitation with weak seasonal dependence. The W_2 and MC_3 show complementary advantages in capturing the seasonal mean pattern and intensity and more realistically predict extreme event occurrence,

whereas the TD_1 better represents the rainfall diurnal phase. These findings are supported by previous studies that have suggested the large-scale ascent as an important dynamical control of precipitation occurrence in the Tropics (Barlow et al. 1998) and the moisture flux convergence as a significant contributor to U.S. daily precipitation variations (Becker et al. 2009).

3.4. Possible causes for different cumulus closure effects

The following first explores the spectra across the cumulus closures in simulating cloud base mass flux and convective-to-total precipitation ratio, and then explains possible causes for complementary advantages of the W_2 and MC_3 in predicting summer mean precipitation pattern and intensity. The specific focus is on their differences in simulating the convective precipitation and associated atmospheric instability, upward motion, and wind convergence.

3.4.1. Cloud base mass flux

The convective precipitation in CUP is parameterized by the precipitation efficiency with total condensate and cloud base mass flux, which determined by different cumulus closure assumptions (Arakawa 2004). Thus, the cloud base mass flux directly affects the convective rainfall amount, and results in different predictive skills among various closure assumptions. Figure 3.15 compares the frequency distributions of cloud base mass flux among 16 algorithms in 2008 June over the three key coastal ocean regions. There exist two distinct groups of cloud base mass flux distribution that differ in magnitude over one order. The group with systematically greater magnitudes contains all the AS and KF closures, and algorithms of maximum vertical velocity (W_3), maximum, average, and local random moisture convergence (MC_1, MC_3, MC_4). Accordingly, all these closures tend to overestimate mean precipitation in both summer and autumn experiments.

The other group with one order smaller magnitudes includes algorithms of minimum vertical velocity (W_1) and moisture convergence (MC_2), and average vertical velocity at cloud base (W_2) and at updraft originating level (W_4), as well as two instability tendency assumptions (TD_1, TD_2). These closures, however, differ in their frequency distributions of cloud base mass flux. For instance, the W_2 and W_4 both have much broader spectrum, but the others have a narrow band toward the lower end that may explain their larger rainfall deficits.

3.4.2. Convective-to-total precipitation ratio

Most GCMs produce incorrect combination of precipitation types, with largely excessive convective but much insufficient stratiform precipitation (Dai and Trenberth 2004; Dai 2006). In particular, Dai (2006) showed that most couple GCMs generally produce higher convective-to-total ratios (>90%) over the tropical oceans, compared to the 45-65% in the TRMM. In these GCMs, most CUPs adopt the CAPE-based closure assumptions such as the Zhang and McFarlane (1995) scheme in which convection simply removes the CAPE over a given time scale (Dai 2006). As CAPE mainly depends on SST conditions over the tropical marine atmosphere (Fu et al. 1994), the overestimation of the convective-to-total precipitation ratio suggests the tropical oceanic convection in these models couples too strongly to the local SST (Dai 2006). It is thus understood that the analysis of this ratio can help reveal model deficiencies in CUPs.

Table 3.2 compares the 2008 summer convective-to-total precipitation ratio from the TRMM3A25 observations and the simulations of 16 subensemble closures over the three key and entire coastal ocean regions. The TRMM 3A25 data gives an average ratio of 64% over the U.S. entire coastal oceans. The group of the closures with a large magnitude of cloud base mass flux attribute total rainfall amount predominantly by convection, with the ratio generally greater

than 85%. In contrast, the closures with much smaller cloud base mass flux, such as W_1 and MC_2, produce inadequate convective contribution, 18% or less of the total. In this regard, it is encouraging that the W_2 (or W_4) closure well reproduces the observed ratio, albeit with slight underestimation of total precipitation over the U.S. coastal oceans. As compared with TRMM, the MC_3, on the other hand, produces a much higher ratio (88%), but better captures the total precipitation amount as previously described.

3.4.3. Atmospheric instability and wind vertical structure

Previous studies suggested that the intensity of convective rainband over the U.S. Atlantic Coast are largely determined by the vertical structure of wind convergence, and the horizontal structure of upward motions associated with the convection displays similar seasonal variations with the precipitation distribution (Minobe et al. 2008; Kuwano-Yoshida et al. 2010). Below examined are the effects of cumulus closures on the distribution of atmospheric instability (CAPE) and upward motions along with vertical structure of wind convergence. This attempts to explain why the W_2 most realistically locates the major rainband along the Gulf Stream but with insufficient amount, and the MC_3 has enhanced precipitation but overestimated rainband coverage.

Figure 3.16 presents geographic distributions of 2008 summer mean observed SST, CWRF simulated CAPE and convective precipitation, as well as upward motions at 500 hPa by using the ECP scheme with three subensemble closures (W_2, MC_3, TD_1). In all cases, the maximum convective rainbands are associated with high CAPE tongue that slants from the southwest to northeast, nearly parallel with the observed SST front. But substantial differences exist in convective rainfall amounts and CAPE distribution. Specifically, the TD_1 produces less frequent convection and thus too little rainfall accompanied with relatively small CAPE near the

U.S. South Atlantic. The MC_3 produces a spreading band of strong convective precipitation associated with the widest CAPE tongue over the U.S. Atlantic Coast, but the W_2 generates a narrow distribution of convective precipitation and CAPE tongue with weaker intensities than the MC_3.

Following Kuwano-Yoshida et al. (2010), we analyze the geographic distribution of model simulated vertical velocities at different altitudes (here, only show the 500 hPa) to display the relation between the convective rainfall and upward motions. The W_2 produces a narrow band of upward motion extending throughout the whole troposphere, closely following the rain band along the U.S. Atlantic Coast. However, the TD_1 simulates much weaker and scattered upward motions, leading to insufficient convective precipitation, whereas the MC_3 produces a much wider band of stronger updrafts, explaining its relative poor performance in precipitation pattern.

Figure 3.17 shows the 2008 summer mean vertical structures of wind convergence averaged over the three coastal ocean regions simulated by CWRF using the three subensemble closures (W_2, MC_3, TD_1). Over the U.S. Atlantic Coast, the MC_3 generates the strongest wind convergence near the surface and also the largest divergence in the upper troposphere, resulting in the strongest upward motions and convective rainfall. In contrast, the TD_1 produces the weakest surface convergence and upper-level divergence, and thus has much smaller upward motions and convective precipitation. The analyses suggest that cumulus closures significantly affect the distribution of atmospheric instability (CAPE), and upward motions associated with wind convergence, and thereby produce large differences in convective rainfall patterns and amounts.

3.5. Summary and Concluding remarks

TRMM observations show that large interannual precipitation variability exists over the U.S. coastal oceans, especially, north and south portions of the U.S. Atlantic and the Gulf of Mexico. A series of CWRF integrations utilizing the ECP scheme with five ensemble closures (AS, W, MC, KF, and TD) are performed for three summers (2008, 2003, 1999) when abnormally heavy rainfall occurred over the above key areas. The results show that closure assumptions largely affect the CWRF predictions of the U.S. coastal ocean summer precipitation. The AS, KF, and MC closures produce widespread wet biases along the entire U.S. coastal oceans due to overestimated rainy days and stronger rain intensity. The TD closure better captures the occurrence of rainy days than other closures, but it overestimates the frequency of light rain events and thus yields large amount deficits. The W closure better captures the rainband along the U.S. Atlantic Coast, but overestimates the rainy days and total amounts further east. Although showing superiority in predicting the diurnal phase, the TD closure systematically underestimates rainfall amounts. Thus, none of these ensemble closure assumptions can fully represent all the observed precipitation characteristics.

Further experiments using the ECP scheme with 16 subensemble closure algorithms show that different algorithms under the same physical concept can have pronounced impacts on ocean precipitation simulation. The algorithms based on the average vertical velocity at cloud base (W_2) and moisture convergence (MC_3) complementarily reproduce the observed precipitation pattern and amount, and perform better than other closures in capturing the frequency of heavy rainfall events. For the diurnal cycle, the instability tendency closures (TD_1 or TD) are superior in capturing the rainfall diurnal phase but with larger deficits. These results suggest that cloud base vertical velocity and moisture convergence are the primary factors controlling precipitation seasonal mean and daily variation, while the instability tendency plays a more critical role in

regulating the diurnal phase. Our findings are supported by previous studies that have suggested the large-scale ascent as an important dynamical control of precipitation occurrence in the Tropics (Barlow et al. 1998) and the moisture flux convergence as a significant contributor to U.S. daily precipitation variations (Becker et al. 2009). The complementary effects of these three closures in precipitation variations provide an opportunity for further optimization of the ECP scheme if specific weights can be derived for each closure at various time scales.

The large disparities of model biases among these cumulus closures directly arise from their formulation differences in computing the cloud base mass flux. The ECP closures can be categorized as two major groups that differ in cloud base mass flux magnitude. One group with one order larger magnitude encompasses all the closure algorithms that produce excessive precipitation, while the other group that has smaller cloud base mass flux systematically generates precipitation deficits. Note that several critical variants in closure algorithms are highly empirical with strong scale dependence. For example, the AS closure assumes a specific time interval (1200 seconds) to consume the CAPE departure from a prescribed climatological value; the KF closure assume a relaxation time scale (2400 seconds) to remove the total CAPE; the TD closure employs a shorter time scale (240 seconds) to deplete the increase of CAPE. Although precipitation biases may be reduced to a certain extent through reasonable adjustment of the time scale, yet our sensitivity experiments showed that their effects are relatively small as compared to the contrasts between the closures discussed above.

Cumulus closures affect the coastal ocean precipitation simulation mainly through their impacts on the atmospheric instability and wind structures. In particular, the W_2 generates, as observed, a narrow band of upward motion, CAPE tongue and convective precipitation, but the MC_3 produces a widespread distribution of stronger upward motion and convective

precipitation associated with a wide CAPE tongue. It explains why the W_2 most realistically captures the spatial distribution of a major rainband but with an insufficient amount, while the MC_3 improves the precipitation amount but with an unrealistically widespread pattern.

Nevertheless, the W_2 and MC_3 still overpredict the rainy days, despite the fairly realistic pattern of summer mean rainfall amounts. This indicates that the moist convection in the ECP scheme is triggered prematurely and occurs too often. This deficiency is also evident in the diurnal cycle prediction as the W_2 and MC_3 tend to produce earlier rainfall peaks than observations. On the other hand, the TD_1 generates reduced rainy days and better reproduces the diurnal phase. Thus, it is likely to inhibit the convection by adding the instability tendency as an additional trigger function in the ECP scheme to improve the frequency distribution and diurnal cycle.

However, the difficulties in accurately predicting the ocean precipitation diurnal cycle could also be caused by the deficiencies in other related physical processes, such as SST, the planetary boundary layer, and cloud microphysics (Dai and Trenberth 2004). Thus, the improvement of ocean rainfall diurnal simulation requires a better understanding and representation of these processes. Additionally, the model verification is influenced by the observational data uncertainty. This work was originally evaluated against TRMM 3B42 version 6 data. Yet the latest version 7 has improved rainfall intensity estimates with substantial differences from the previous release. Hence, our evaluation has been revisited against the new TRMM data, leading to some nontrivial modifications of the result interpretation. Further deviations are expected as the TRMM data accuracy is still uncertain. Nevertheless, the ECP scheme provides an unprecedented opportunity to identify the typical behaviors of these cumulus closures, and the objective diagnostic procedure established in this study can effectively guide future refinements

of the ECP scheme through ensemble closure optimization to enhance precipitation predictive skills against more accurate observations as emerged.

3.6. Figures and Tables

Table 3.1 Spatial pattern correlation coefficient and rms error between simulated by the ECP scheme with subensembles (W_2, TD_1, MC_3) and ensemble (W, TD, MC) closures and observed precipitation (summer mean, number of rainy days, and rain intensity) over the U.S. Atlantic Coasts and Gulf of Mexico for three summer experiments (2008, 2003, 1999).

Summer Cases	**ECP closures**	**Summer Mean**		**Number of Rainy Days**		**Intensity**	
		Correlation	RMSE	Correlation	RMSE	Correlation	RMSE
2008	W_2	**0.69**	**1.79**	0.57	16	0.41	5.68
	W	**0.63**	**2.15**	0.47	23	0.40	5.26
	TD_1	0.62	2.34	**0.58**	**12**	0.19	7.02
	TD	0.59	2.19	**0.47**	**12**	0.15	6.52
	MC_3	**0.64**	**1.91**	0.48	22	**0.41**	**5.40**
	MC	**0.53**	**5.51**	0.41	23	**0.40**	**5.50**
2003	W_2	**0.62**	**2.34**	**0.56**	**14**	0.43	5.28
	W	**0.54**	**2.52**	**0.48**	**22**	0.41	4.88
	TD_1	0.55	3.04	0.51	17	0.33	5.65
	TD	0.52	2.93	0.43	19	0.28	5.84
	MC_3	**0.63**	**2.38**	0.51	21	**0.48**	**4.57**
	MC	**0.52**	**4.90**	0.46	22	**0.43**	**5.00**
1999	W_2	**0.53**	**2.86**	**0.51**	**14**	0.37	5.74
	W	**0.49**	**2.61**	**0.51**	**19**	0.41	5.09
	TD_1	0.50	2.61	0.46	13	0.22	6.24
	TD	0.54	2.52	0.43	11	0.33	6.17
	MC_3	**0.54**	**2.35**	0.50	18	**0.41**	**5.19**
	MC	**0.38**	**4.82**	0.45	18	**0.32**	**6.72**

Table 3.2 Simulated convective-to-total precipitation ratios (%) averaged over the three key coastal ocean regions for 2008 summer by CWRF using the ECP scheme with 16 subensemble closures.

Regions	**TRMM**	**AS**				**W**				**MC**				**KF**		**TD**	
		1	2	3	4	1	2	3	4	1	2	3	4	1	2	1	2
U.S. North Atlantic	**65**	86	92	72	77	5	**61**	86	46	88	8	89	91	88	93	25	44
U.S. South Atlantic	**57**	89	93	81	81	11	**72**	95	64	97	15	91	95	88	98	29	50
Gulf of Mexico	**62**	98	95	94	94	10	**75**	98	63	98	16	92	99	95	99	30	56
Total	**64**	87	89	81	82	13	**69**	91	60	91	18	88	92	88	91	32	53

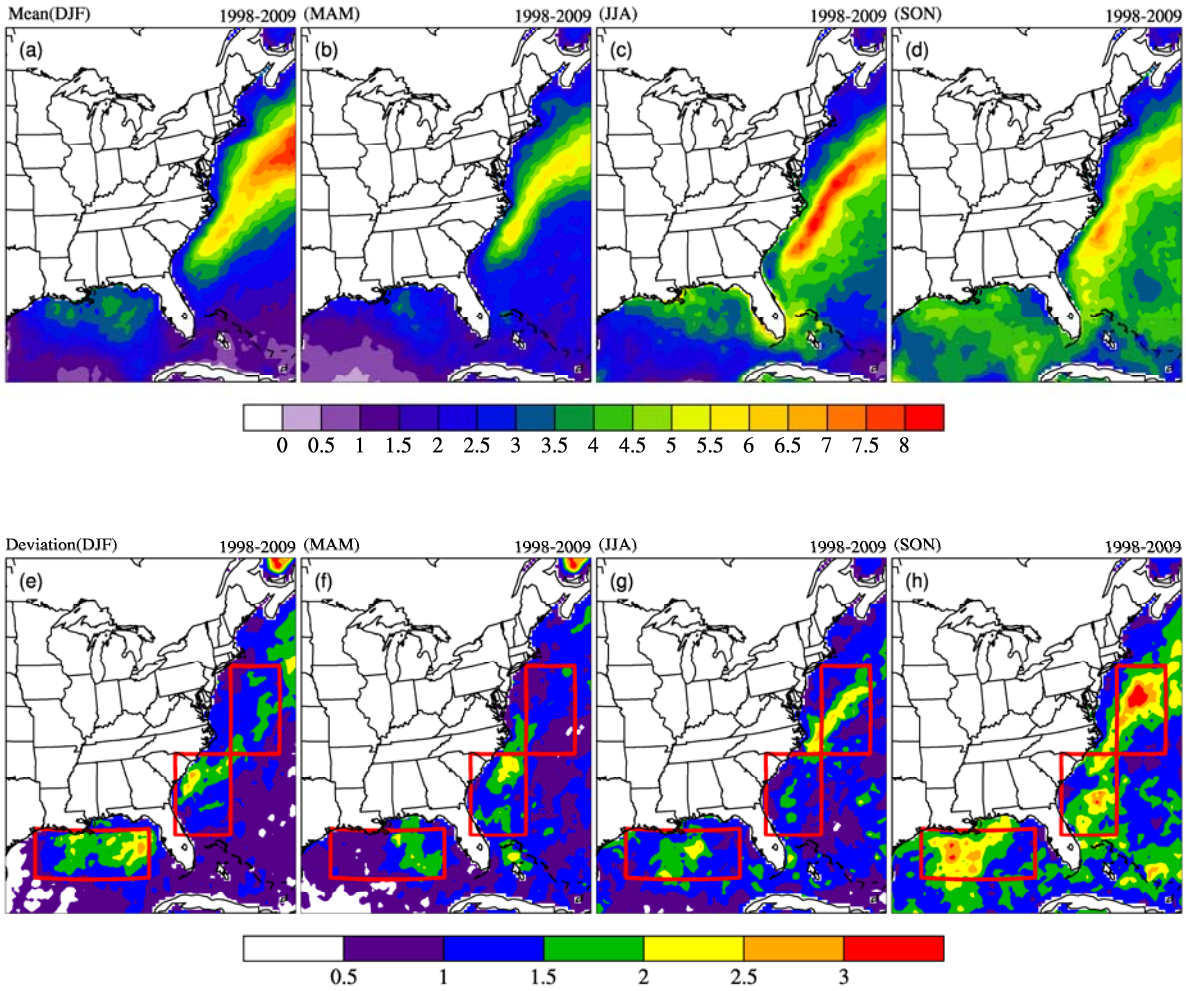

Figure 3.1 Geographic distribution of TRMM precipitation (mm day^{-1}) seasonal climatology (*upper panels*) and interannual standard deviation (*bottom panels*) for winter (DJF), spring (MAM), summer (JJA), and fall (SON) averaged during 1998-2009. Outlined in the bottom figures are three key regions which are U.S. North Atlantic Coast (34°-39°N, 75°-67°W), U.S. South Atlantic Coast (28° -34°N, 82° -75°W), and the Gulf of Mexico (25°-29°N, 95° -84°W).

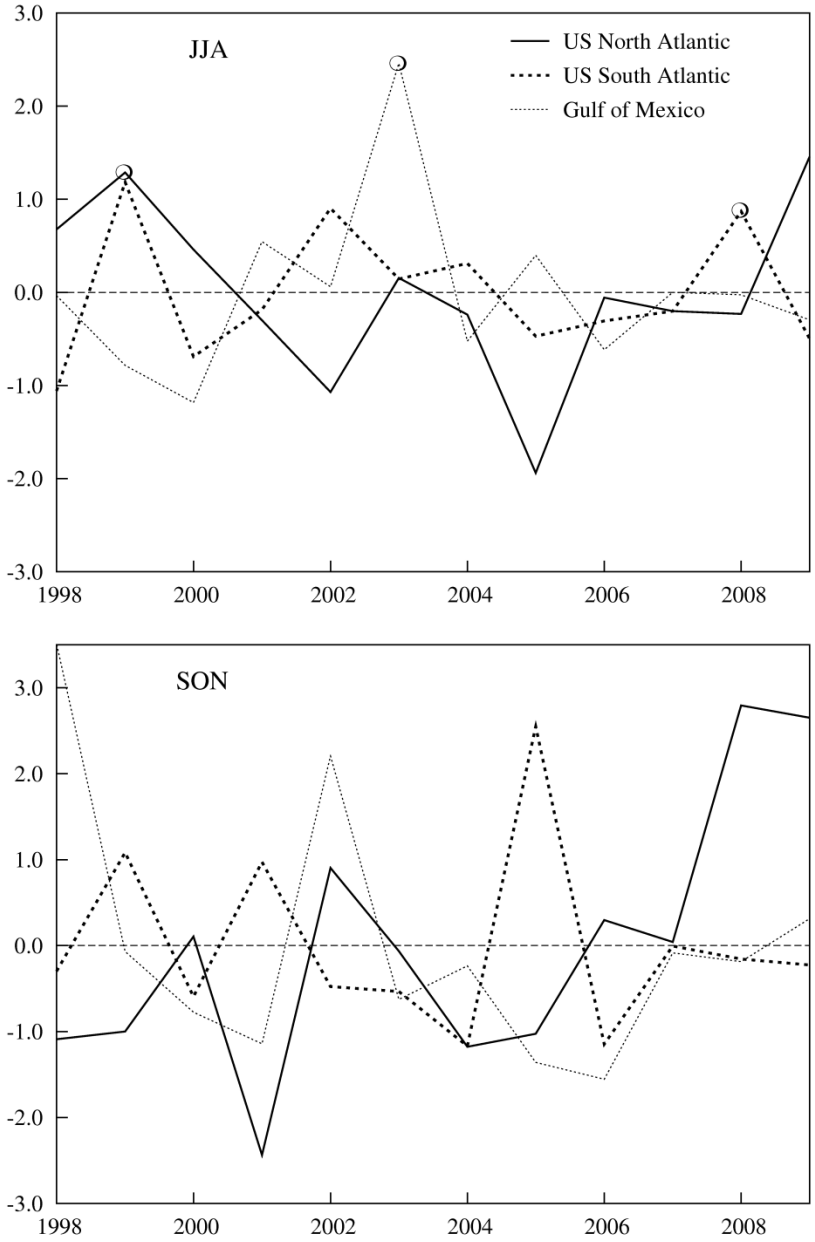

Figure 3.2 Summer (JJA) and Autumn (SON) seasonal mean precipitation (mm day^{-1}) anomalies from the 1998-2009 climatology from the TRMM observations averaged over the three key coastal ocean regions outlined in Figure 3.1. Three summer cases are marked by circles.

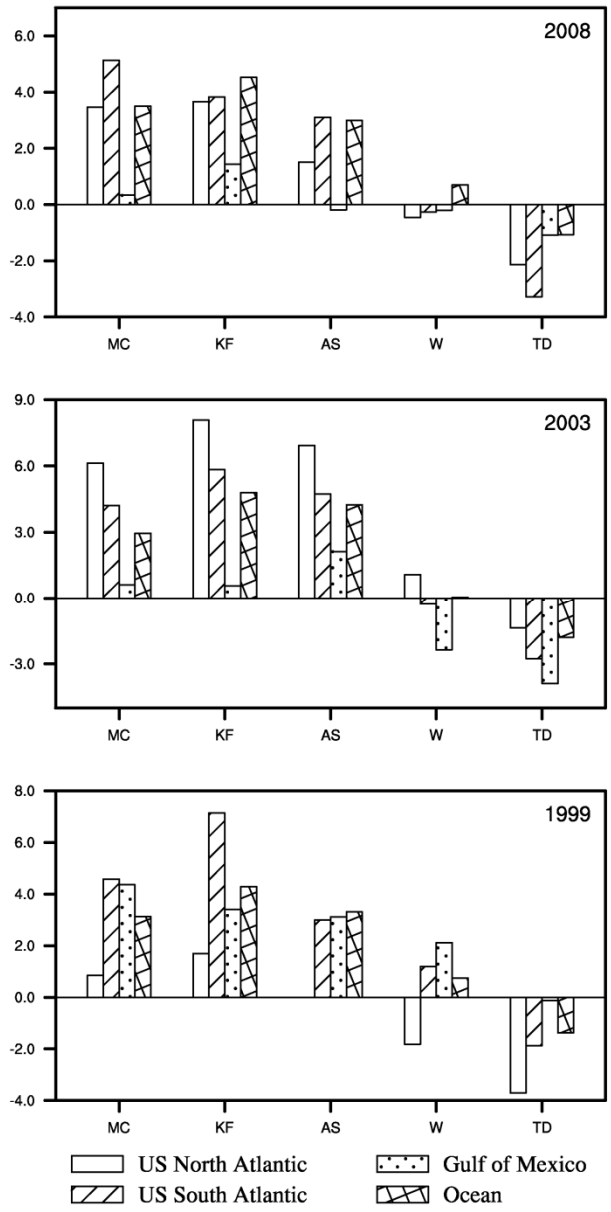

Figure 3.3 Three summer (2008, 2003, 1999) mean precipitation biases averaged over the three coastal regions (U.S. North Atlantic Coast, U.S. South Atlantic Coast, Gulf of Mexico) and the entire U.S. East and South coastal ocean simulated by CWRF using the ECP scheme with five ensemble closures (AS, W, MC, KF, TD) as compared to the TRMM observations.

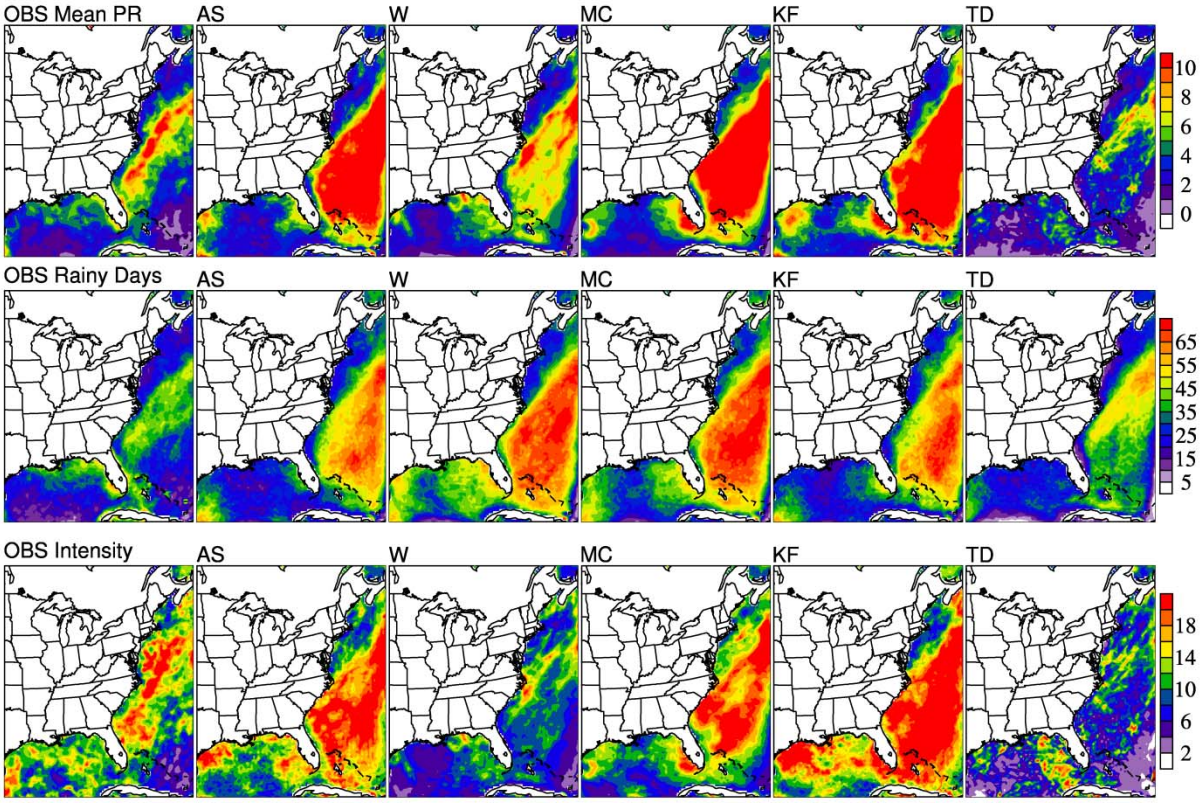

Figure 3.4 Geographic distributions of 2008 summer mean precipitation (*upper panels*, unit: mm day^{-1}), the number of rainy days (for daily precipitation > 1mm day^{-1}, *middle panels*), and the mean rain intensity (*bottom panels*, unit: mm day^{-1}) simulated by CWRF using the ECP scheme with five ensemble closures (AS, W, MC, KF, TD) and the TRMM observations (OBS).

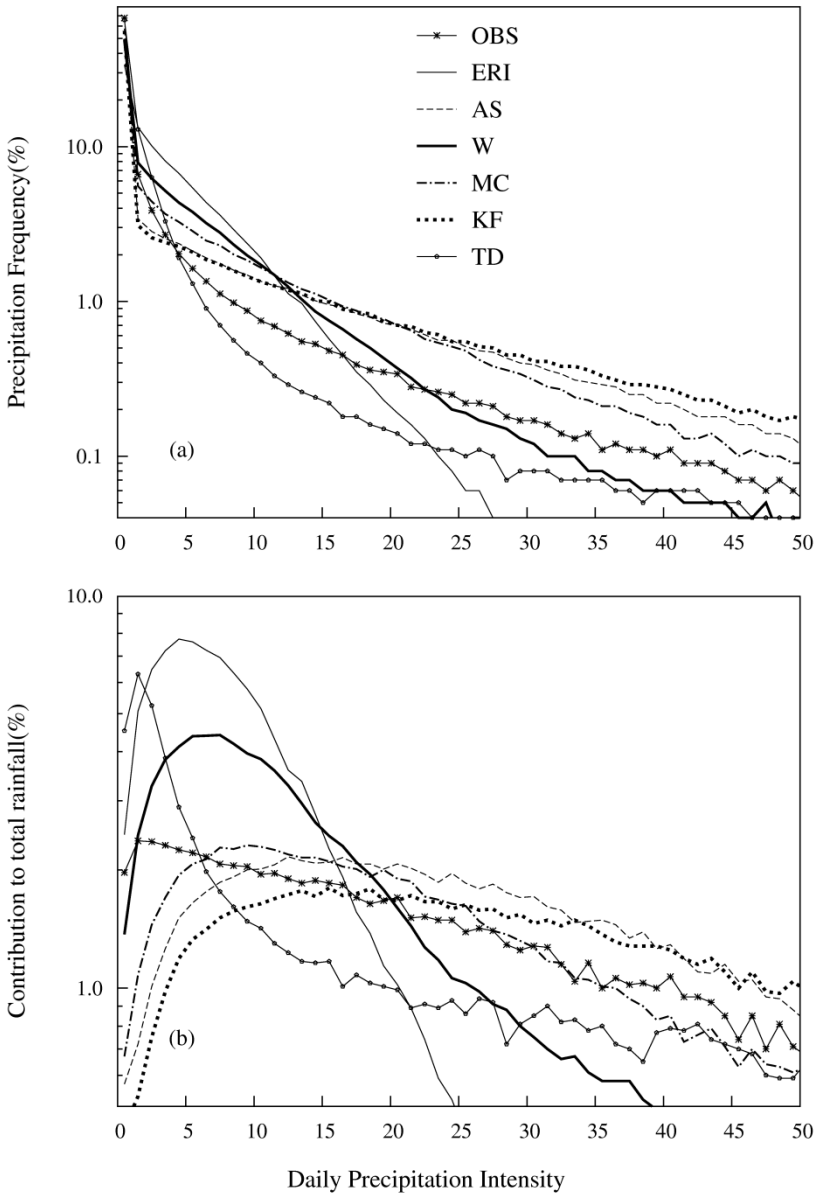

Figure 3.5 Frequency distributions (in logarithm scales) of 2008 summer pointwise daily precipitation (a) and the relative contribution to total precipitation (b) from each binned precipitation (1 mm day^{-1}) over the entire U.S. coastal oceans simulated by CWRF using the ECP scheme with five ensemble closures (AS, W, MC, KF, TD) and the ERI reanalysis as compared to the TRMM observation.

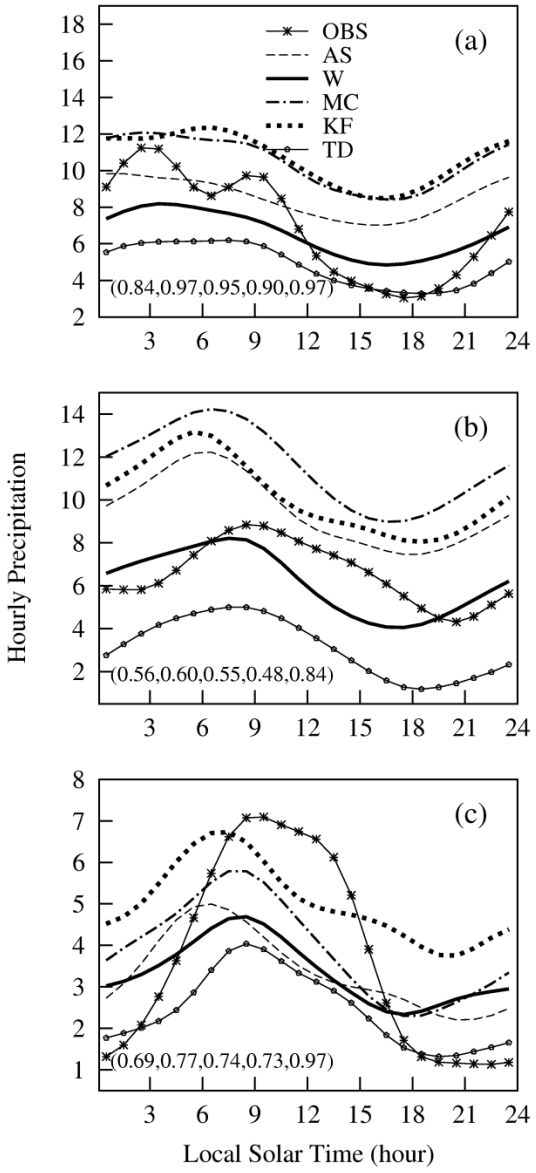

Figure 3.6 Mean diurnal variation (relative to local solar time) of the precipitation (correlation coefficients in the boxes) simulated by CWRF using the ECP scheme with five ensemble closures (AS, W, MC, KF, TD) as observed by TRMM averaged over the three key regions: (a) U.S. North Atlantic Coast, (b) U.S. South Atlantic Coast, and (c) Gulf of Mexico, corresponding to the boxes in Figure 3.1.

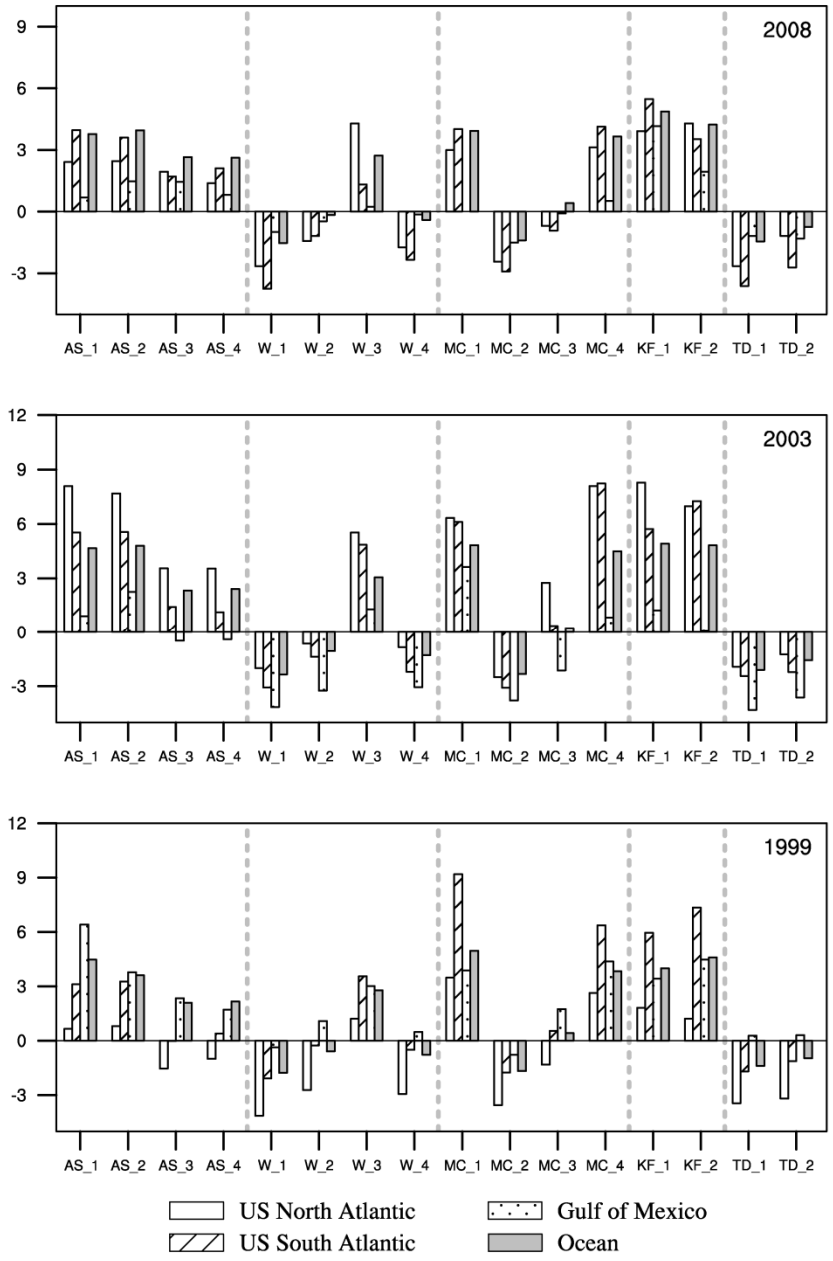

Figure 3.7 Mean precipitation biases in three summer cases (2008, 2003, and 1999) averaged over the key coastal regions (U.S. North Atlantic Coast, U.S. South Atlantic Coast, and Gulf of Mexico) and the whole U.S. East and South coastal oceans simulated by CWRF using the ECP scheme with 16 subensemble closures as compared to the TRMM observations.

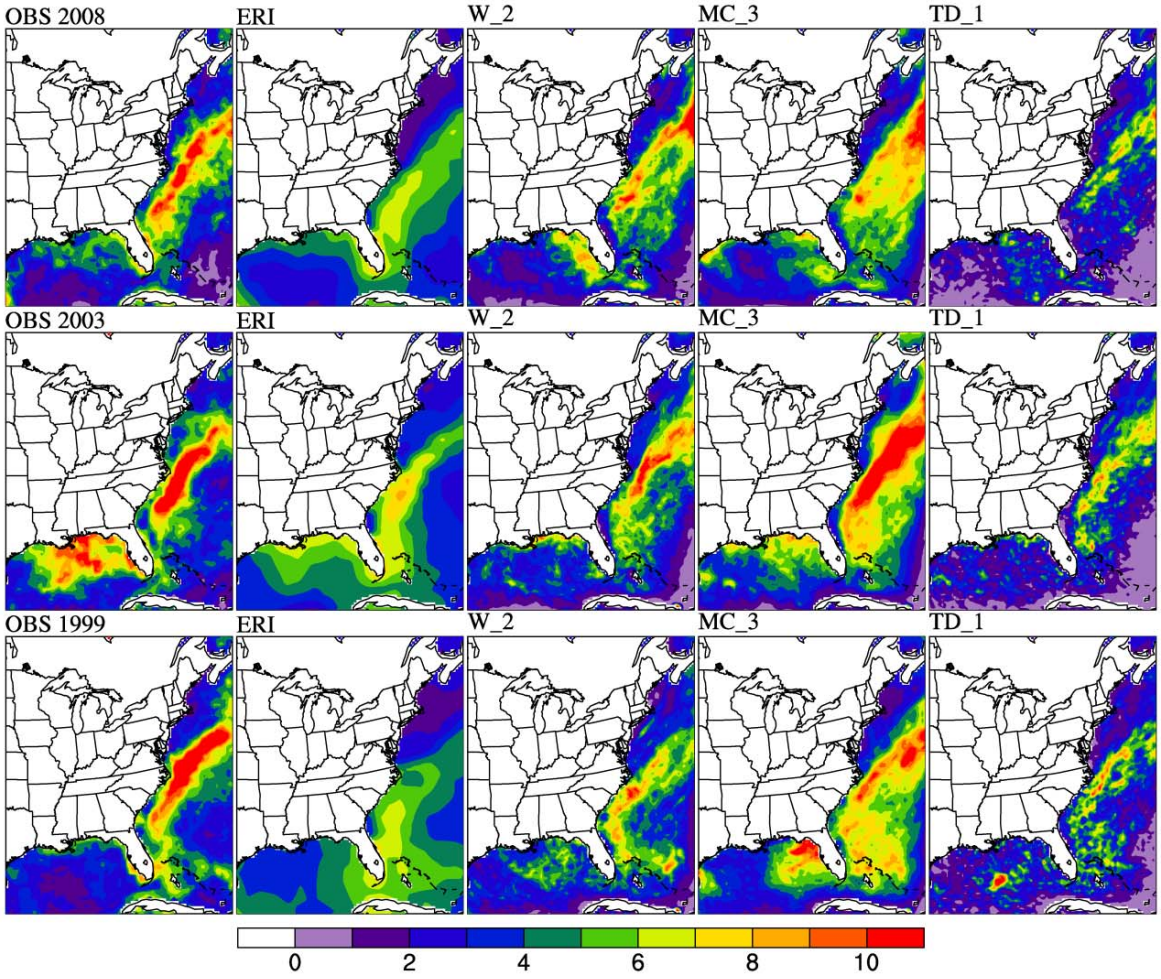

Figure 3.8 Geographic distributions of 2008, 2003, 1999 summer mean precipitation (upper panels, unit: mm day^{-1}) simulated by CWRF using the ECP scheme with three subsensemble closures (W_2, MC_3, TD_1), from the ERI reanalysis and TRMM observations (OBS).

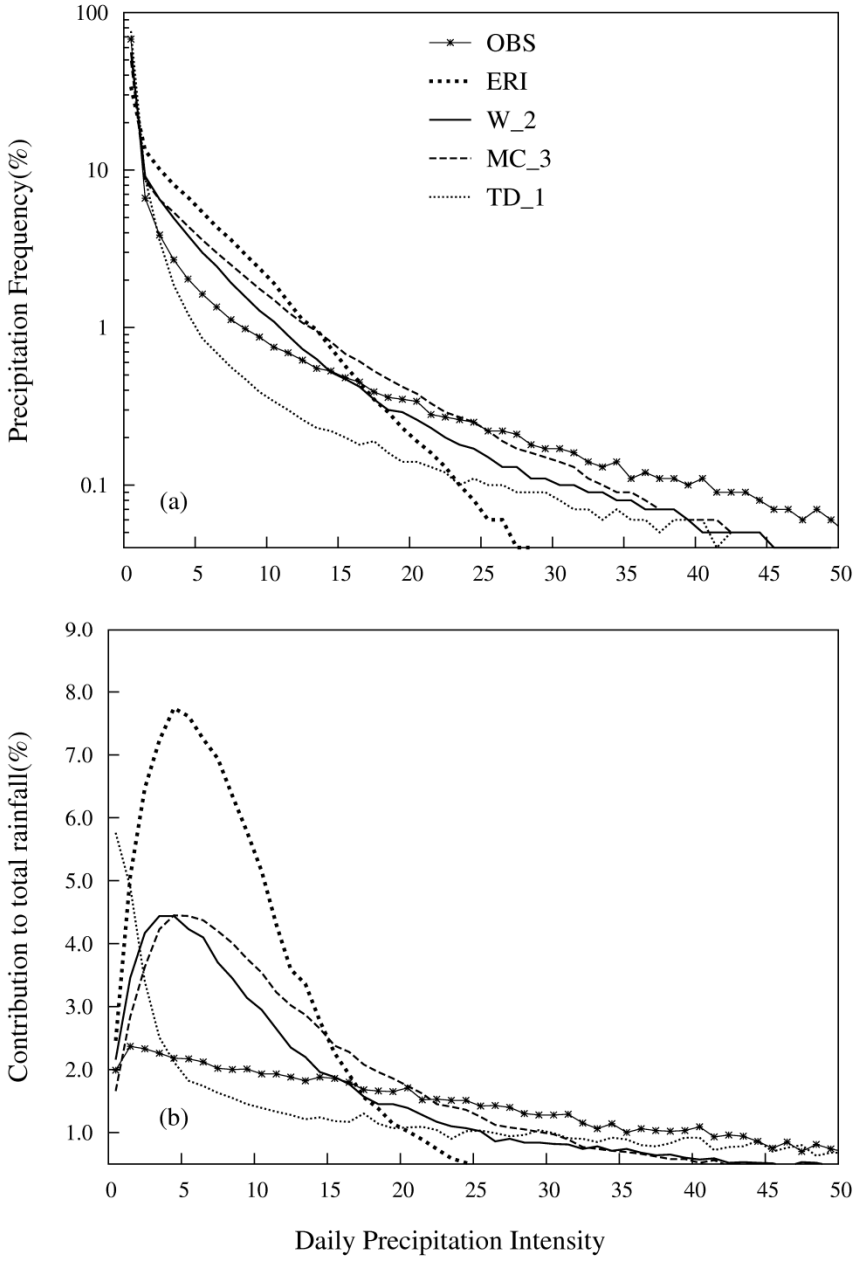

Figure 3.9 Frequency distributions (in logarithm scales) of 2008 summer daily precipitation (a) and the relative contribution to total precipitation (b) from each binned precipitation (1 mm day^{-1}) over the entire U.S. coastal oceans simulated by CWRF using the ECP scheme with the three subsensemble closures (W_2, TD_1, MC_3), and from the ERI, compared to the TRMM observations (TRMM).

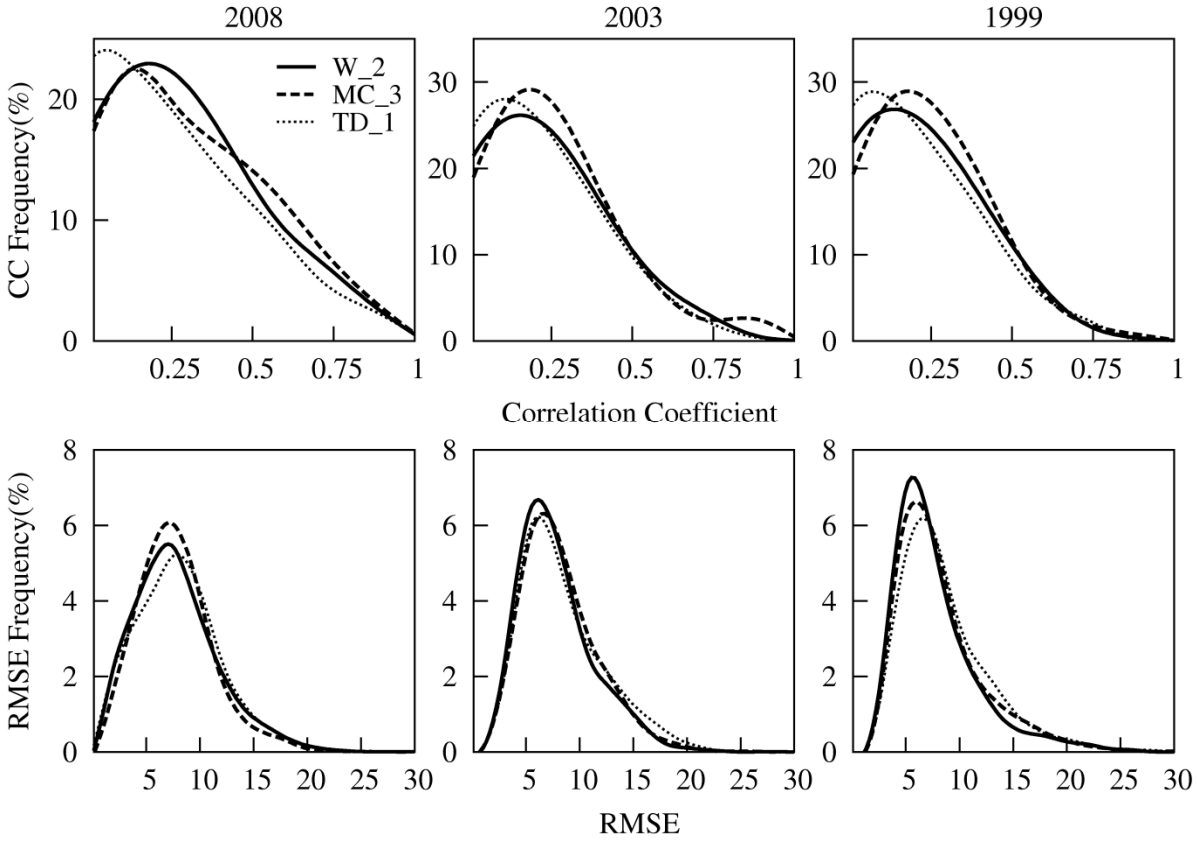

Figure 3.10 Spatial frequency distributions of pointwise correlation coefficients and rms errors of daily rainfall variations for three summer cases (2008, 2003, 1999) over the U.S. coastal oceans grids between the TRMM observations and simulations by CWRF with the ECP scheme using three subensembles (W_2, MC_3, TD_1).

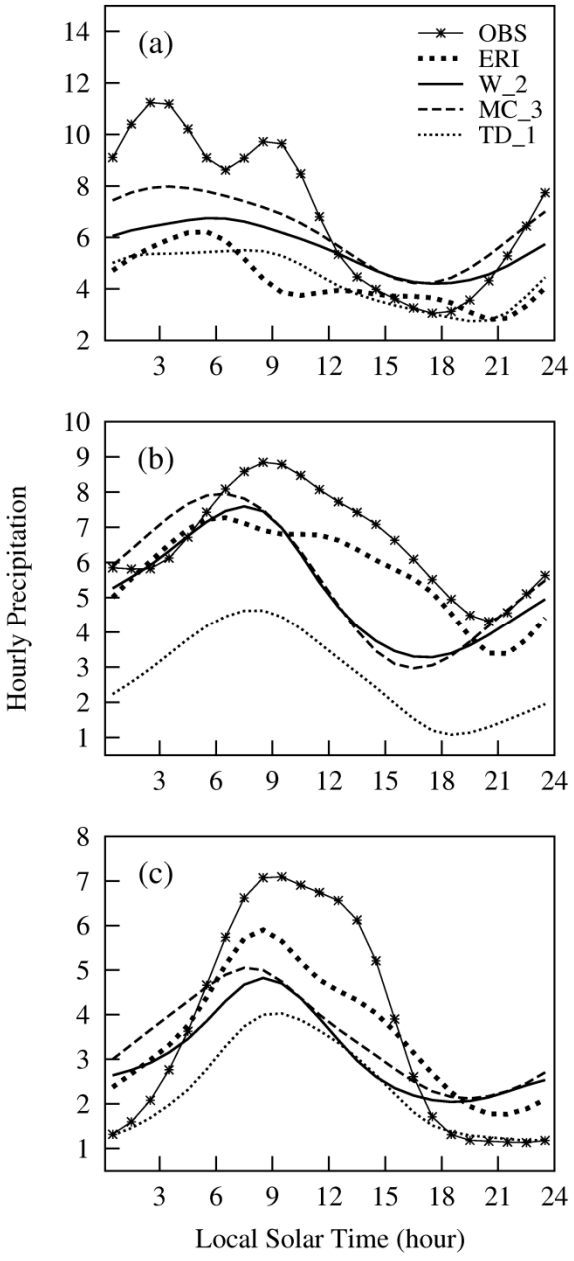

Figure 3.11 2008 summer precipitation diurnal cycle (mm day^{-1}, relative to local solar time) simulated by the CWRF/ECP with three subensemble closures (W_2, MC_3, TD_1) compared to the ERI and TRMM observations, all averaged over (a) U.S. North Atlantic Coast, (b) U.S. South Atlantic Coast, and (c) Gulf of Mexico.

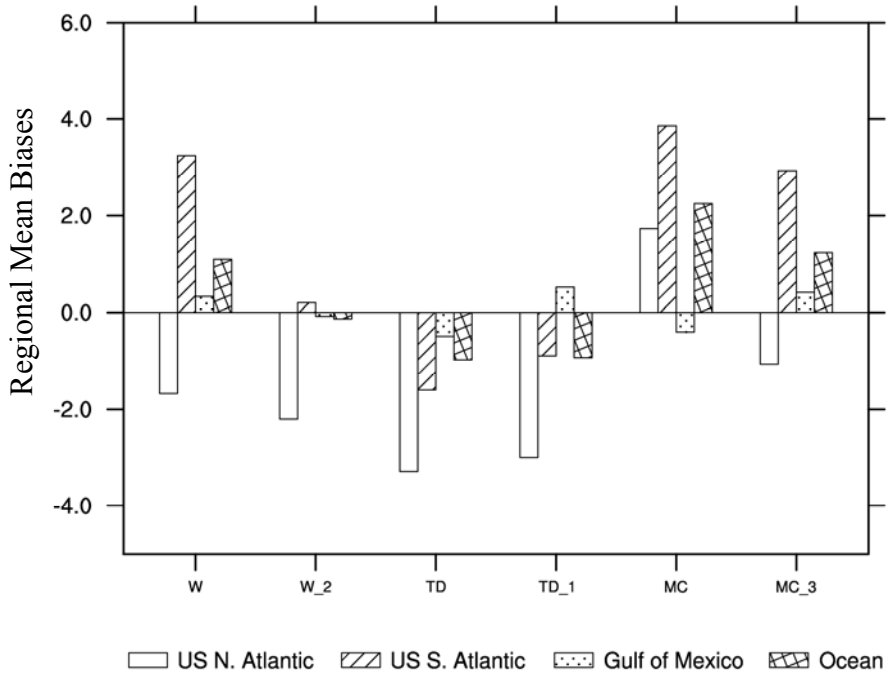

Figure 3.12 2008 autumn mean precipitation biases (mm day^{-1}) of simulations with subensemble algorithms using averaged assumptions (W_2, TD_1, MC_3) and their corresponding ensemble closures (W, TD, MC) compared to the TRMM observations averaged over three key coastal regions and the entire U.S. coastal oceans.

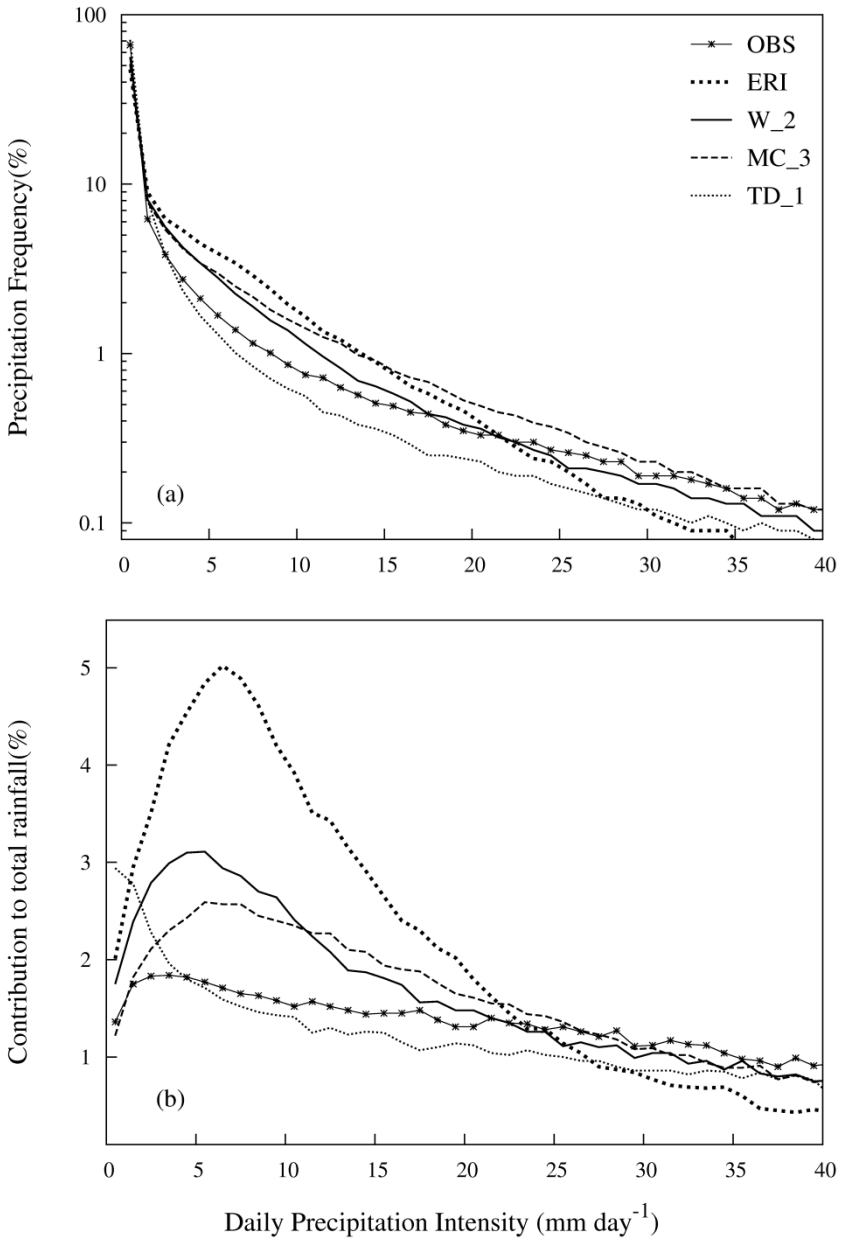

Figure 3.13 Frequency distribution (in logarithm scales) of 2008 autumn pointwise daily precipitation (a) and relative contributions from each daily precipitation rate bin to the total amount (b) over the U.S. coastal oceans simulated by CWRF with the ECP scheme using three subensemble algorithms (W_2, MC_3, TD_1) as compared to the driving ERI reanalysis and TRMM observations.

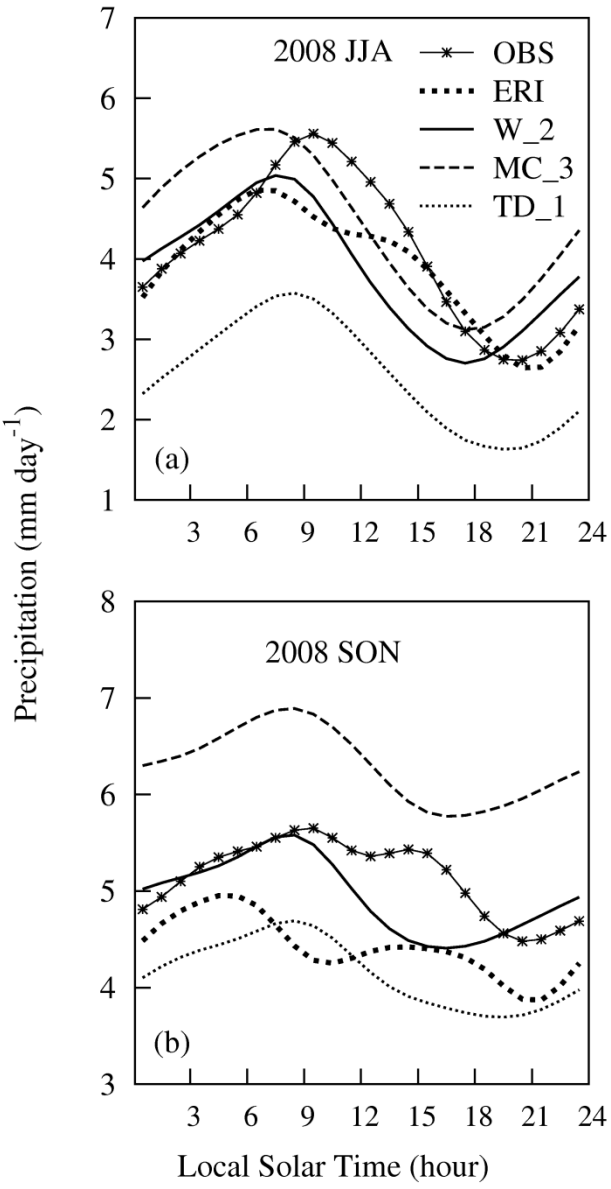

Figure 3.14 2008 summer and autumn mean diurnal cycles of precipitation averaged over the U.S. coastal ocean grids simulated by CWRF with the ECP scheme using three subensemble algorithms (W_2, MC_3, TD_1) and from the ERI reanalysis and the TRMM observation.

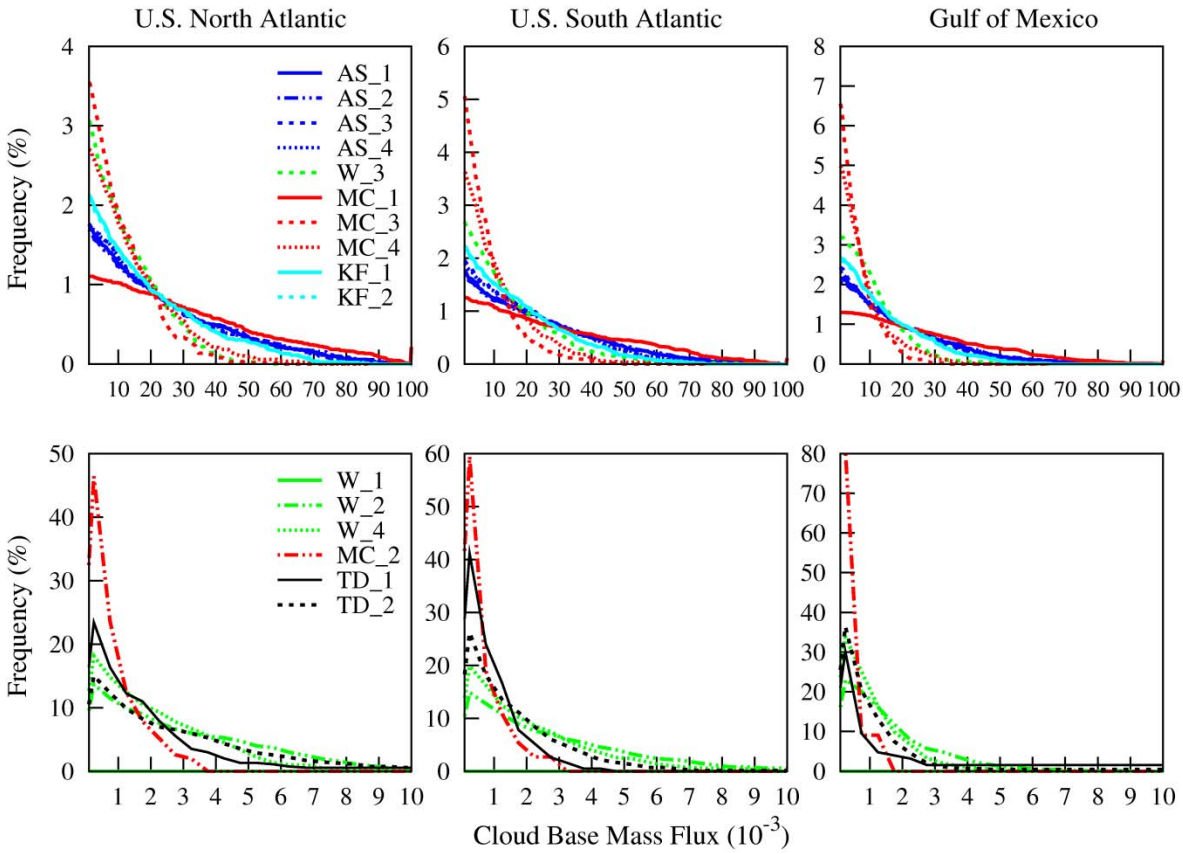

Figure 3.15 Spatial frequency distributions of 3-hourly pointwise cloud base mass flux simulated by CWRF with the ECP scheme using 16 subensemble closures in 2008 June over three U.S. coastal ocean regions.

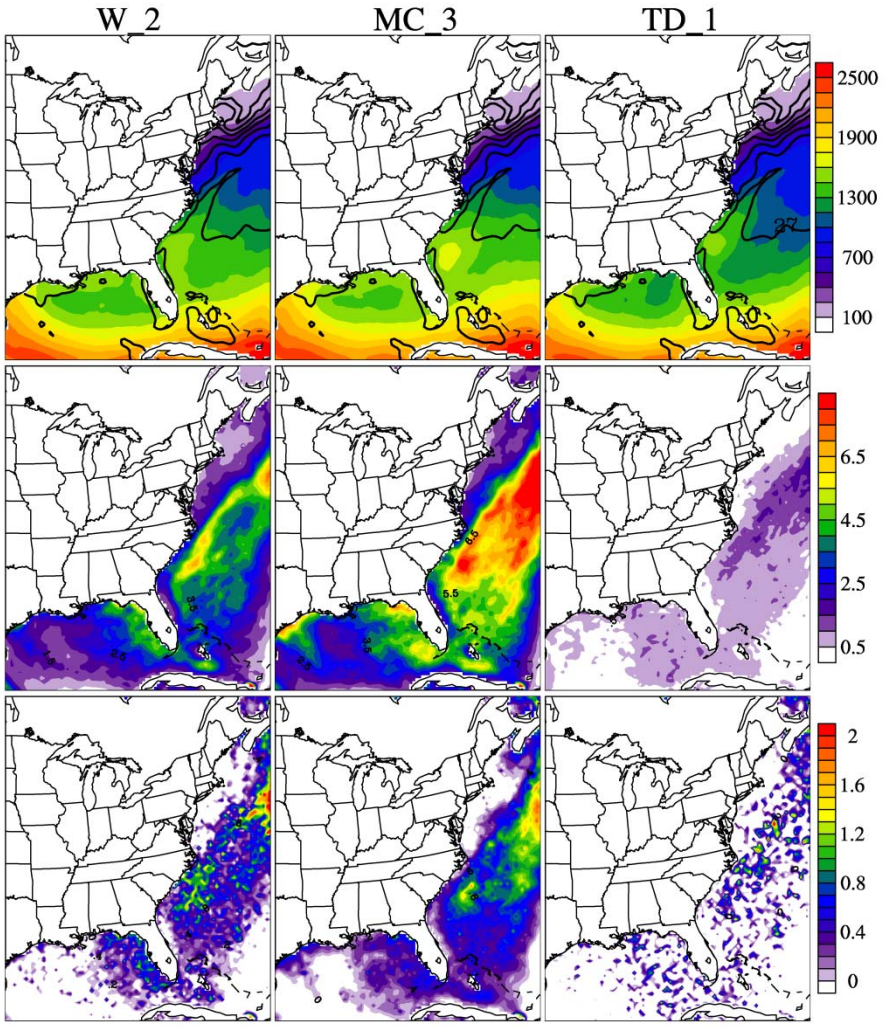

Figure 3.16 Geographic distributions of 2008 summer mean observed SST (solid lines in *upper panels* with interval of 1ºC), simulated CAPE (shaded in *upper panels*, $J \cdot kg^{-1}$), convective precipitation (*middle panels*, mm day^{-1}), and mean vertical velocity (*bottom panels*, 10^{-2} m s^{-1}) at 500 hPa by CWRF using the ECP scheme with three subensemble closures (W_2, MC_3, TD_1).

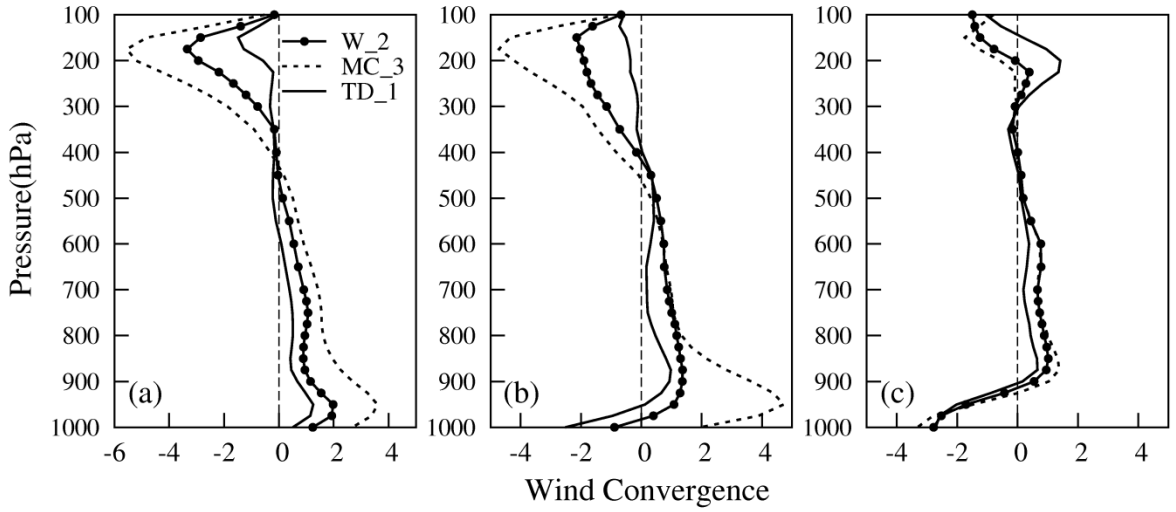

Figure 3.17 Vertical profiles of wind convergence (10^{-6} s^{-1}) in the 2008 summer simulations by the CWRF using the ECP scheme with three subensemble closures (W_2, MC_3, TD_1) respectively, averaged over (a) U.S. North Atlantic Coast, (b) U.S. South Atlantic Coast, and (c) Gulf of Mexico.

CHAPTER 4: CUMULUS CLOSURE EFFECTS ON SUMMER PRECIPITATION PREDICTION OVER THE CONTINENTAL U.S.

This chapter utilizes the ECP scheme incorporated in the CWRF to examine the effects of cumulus closure assumptions on the continental U.S. summer precipitation prediction with respect to the mean pattern and amount, daily rainfall frequency distribution, and regional variations of diurnal cycle. It is compiled from an article in preparation for submission to *Journal of Climate* titled "CWRF summer precipitation prediction over the continental United States: Effects of ensemble cumulus parameterization closures". The detailed model experiments and results along with discussions for further ECP optimization are summarized in this chapter.

4.1. Introduction

Numerous studies have demonstrated the U.S. summer mean precipitation simulation is significantly sensitive to CUPs, with strong regional dependence and large controversies (Giorgi and Shields 1999; Gochis et al. 2002; Xu and Small 2002; Leung et al. 2003; Liang et al. 2004b, 2008). However, these studies only compared the performance of CUP as an integral "black box" without explicitly interpreting which component causes the model differences (Neggers et al. 2004). As the CUPs differ in closure assumption, trigger function and other parameters, it is difficult to fully determine the specific causes for model errors. It is essential to examine cumulus closures, being fundamental to CUP, to explain model deficiencies in precipitation prediction in a systematic manner such that specific assumptions can be identified with distinguished typical behaviors.

It is also important to examine the precipitation frequency and intensity, especially the extreme events, as well as the rainfall diurnal cycle. These precipitation characteristics are more difficult to predict and yet critical for many impacts applications (Liang et al. 2006). Previous studies have suggested that cumulus closure improvements have important influences on the model simulated rainfall frequency distribution and diurnal variation. For instance, Wilcox and Donner (2007) showed that modeled precipitation frequency distribution is shaped by cumulus closures, trigger functions, and cloud spectrum parameters, among which the cumulus closure most likely affects the occurrence of extreme events. Liang et al. (2004a) illustrated that the Grell scheme realistically simulates the nocturnal rainfall over the Great Plains because its closure is based on and thus directly in response to the large-scale tropospheric forcing, whereas the Kain-Fritsch scheme shows superiority in the late-afternoon peaks in the Southeast U.S. because its closure is defined and thus controlled by the near-surface forcing that is more favorable there. This indicates that the rainfall diurnal cycle is strongly sensitive to the interaction between convection and large-scale forcing, which is represented by cumulus closure assumptions in the CUPs.

The present study, therefore, will use the CWRF to more comprehensively examine the cumulus closure effects on the continental U.S. summer precipitation prediction, regarding its mean distribution, frequency and intensity, and diurnal cycle. This is facilitated by the Ensemble Cumulus Parameterization (ECP) scheme incorporated in the CWRF. Implementing different cumulus closures in the ECP scheme where other components (e.g., trigger function and cloud models) are identical provides a unique opportunity to isolate the effects of cumulus closures.

Section 4.2 describes the model experiments of three typical summers (1993, 2003, and 2006) when large rainfall anomalies occur over the Central U.S., NAM region and Southeast U.S. It has

been a longstanding challenge for current RCMs to accurately simulate precipitation variations over these three regions during the summer (Liang et al. 2012). Section 4.3 presents the respective effects of five cumulus closures on CWRF prediction of the continental U.S. summer mean precipitation pattern, and also illustrates the relative contributions of large-scale circulation and regional features to the modeled summer mean biases. Section 4.4 focuses on their effects on rainfall frequency and intensity, while Section 4.5 on the rainfall diurnal cycle. Section 4.6 briefly demonstrates the model sensitivity to 16 subensemble closure algorithms in order to explore possibility for further rigorous optimization of the ECP scheme. Major conclusions are summarized in Section 4.7.

4.2. Model experimental design

Figure 4.1 shows the observed geographic distributions of summer mean precipitation and interannual deviation averaged during 1979-2009 over the continental U.S. and Northern Mexico. Observation exhibits a concentrated precipitation region (around 4 mm day^{-1}) east of 100º W over the Central U.S. and more intense precipitation over 5.5 mm day^{-1} along the U.S. southern coastlines and Florida. Along the downstream slopes of Rockies, there is a dry zone transition due to the precipitation shadowing by mountains (Liang et al. 2012). Rainfall increases over the Southwest U.S. and Northern Mexico mainly contributed by the North American monsoon system. The standard deviation clearly shows that three regions have large summer precipitation anomalies: the Central U.S., NAM, and Southeast U.S. Thus, the following analysis will focus on these critical regions.

Figure 4.2 depicts the interannual variations of summer mean precipitation anomalies relative to the 1979-2009 climatology averaged over above three key regions. There appears an out-of-phase relationship between the NAM and Central U.S. summer precipitation anomalies for which

Higgins et al. (1998) provided several possible mechanisms: 1) Enhanced Great Plains low-level jet increases the Central U.S. precipitation, while consequently suppresses rainfall over the NAM region and the U.S. East Coast; 2) Accompanied with intensified NAM rainfall, the elevated heating over this region forces sinking motions in adjoining regions and thus dynamically inhibits the convection over the South-Central U.S.

We select the summer of 1993 that is characterized by extreme flood over the Central U.S. and drought over the Southeast U.S. The 2003 summer is also chosen because opposite patterns are observed with severe drought over the Central U.S. and the NAM region but strong wet anomaly over the Southeast U.S. The 2006 summer is additionally selected because it represents a wet NAM in order to compare with the dry NAM event in the 2003 case. As such, these three summer cases facilitate the examination of cumulus impacts for contrasting hydrological conditions over different regions.

A series of experiments using the five ensemble closures and their 16 subensembles in the ECP scheme are conducted over the continental U.S. and Northern Mexico for these three summers with one month model spin-up, respectively. Over the coastal oceans, the ECP scheme adopts the average cloud base vertical velocity closure due to its superiority in predicting the summer rainfall distribution in previous chapter.

4.3. Effects on the U.S. summer precipitation mean and daily variation

Figure 4.3 illustrates summer (1993, 2003, and 2006) mean precipitation biases of the CWRF simulations using the ECP scheme with the five ensemble closures (AS, W, MC, KF, TD) averaged over the three key regions. The MC closure systematically overestimates the rainfall amount over the NAM and Southeast U.S., but produces relatively small biases over the Central U.S. Also, the KF closure behaves consistently under various climate regimes by producing even

larger wet biases than the MC closure over the NAM and Southeast U.S., and substantially underestimating the rainfall over the Central U.S. It agrees with Liang et al. (2004b) who found that the cumulus parameterization scheme of Kain and Fritsch (1993) yields excessive rainfall in the NAM and Southeast U.S., but large deficits over the Central U.S. In contrast, the TD closure systematically produces large deficits over the Southeast U.S., but small biases over the Central U.S. and NAM. This may explain the summer dry biases over the Southeast U.S. that has been identified in the Grell scheme (1993) based on the same instability tendency assumption.

Table 4.1 compares the pattern correlation coefficients and rms errors between the CWRF simulations using the ECP scheme separately with five ensemble closures and observations over the continental U.S. and Northern Mexico. The W and MC closures are comparable in predicting the summer rainfall pattern with higher pattern correlation coefficients than others. However, the W closure more realistically reproduces rainfall amounts with smaller rms errors compared to the MC closure.

Figure 4.4 compares spatial frequency distributions of pointwise correlation coefficients and rms errors of daily precipitation over all the grids of the continental U.S. and Northern Mexico for three summer cases between observations and CWRF simulations using the ECP scheme with five different ensemble closures. All the experiments show that the TD closure poorly captures the overall daily precipitation variation because it has the largest rms errors and lowest correlation coefficients. In contrast, the MC closure systematically produces higher correlation coefficients than other closures in three cases, indicating that the MC closure is superior in capturing the temporal variation of daily precipitation over the U.S. land. But compared to the W closure, the MC closure tends to produce larger rms errors due to overestimated rainfall amount over the NAM and Southeast U.S. shown above.

Figure 4.5 compares the performances of W and MC closures over the Central U.S. The MC closure systematically better captures the observed daily rainfall variation than the W closure in both temporal correspondence and magnitude over the Central U.S., although the MC closure does not always show its advantages over the NAM and Southeast U.S. In contrast, the W closure generally better reproduces the observed daily rainfall magnitude by having smaller rms errors than the MC closure over the NAM and Southeast U.S. Thus, among the five closures, the MC closure has clear advantages than others in capturing both summer precipitation mean and daily variability over the Central U.S., but systematically overestimates the rainfall amount over the NAM and Southeast U.S. It is encouraging that the wet biases over these two regions can be significantly reduced by using the W closure.

The largest model discrepancy of regional mean precipitation among the five cumulus closures exist over the Southeast U.S as shown in Figure 4.3. Most closures (AS, KF, and MC) produce significantly wet biases, while the TD closure produces dry biases. However, the W closure systematically produces the smallest precipitation biases over this region. The 1993 summer is taken as an example to examine the relative contributions of the regional circulation features simulated by the CWRF using the ECP scheme with the MC (too wet), TD (too dry), and W (most realistic) closures for precipitation biases over this critical region.

Figure 4.6 shows the 1993 summer mean geographic distributions of the CWRF minus NARR (as a proxy for observations) differences in wind at 850-hPa and 200-hPa and vertically integrated moisture flux comparing the result sensitivity between the MC, W, and TD closures. There are several prominent differences that are consistent with regional precipitation biases, especially over the Southeast U.S. First, the 850 hPa wind anomalies suggest that the TD closure produces a much stronger and farther inland Atlantic subtropical high, causing greater

subsidence that inhibits the precipitation over the Southeast U.S. Conversely, the subtropical high in the MC closure shifts more eastward with stronger southeasterly flows on its south flank, leading to enhanced moisture convergence and consequently increased rainfall over the Southeast U.S. Clearly, the W closure most realistically produces the intensity and location of subtropical high, resulting in the smallest precipitation bias over this region. Second, 200-hPa wind biases in the TD closure exhibits a clear cyclonic flow departure over the eastern U.S., implying stronger upper level convergence which suppresses the upward motion and precipitation. Both the W and MC have relatively small upper level wind biases, but the MC closure produces a cyclonic perturbation of moist transport over the Southeast U.S. greatly contributing to the wet biases. Third, the MC closure has the smallest biases for both upper and lower level wind circulation over the Central U.S., resulting in a more realistic simulation of summer rainfall than other closures. Results demonstrate that cumulus closures substantially influence the interaction of large-scale circulation and convection, and consequently cause regional precipitation differences.

4.4. Effects on the U.S. summer precipitation frequency and intensity

Figure 4.7 compares the 1993 summer frequency distribution of pointwise daily precipitation and relative contribution to the total amount over the continental U.S. and Northern Mexico from the observations, ERI reanalysis, and CWRF simulations with the ECP scheme using five ensemble cumulus closures respectively. We only show 1993 case because three summer cases exhibit similar probability distributions. The precipitation in the ERI reanalysis has a very narrow distribution, with much more frequent daily rainfall occurring less than 15 mm day^{-1}, and almost no occurrence exceeding 30 mm day^{-1}. All the CWRF simulations are more capable of capturing observed frequency distribution of daily precipitation greater than 15 mm day^{-1}. They

even produce more frequent heavy rain events than observations for intensity exceeding 40 mm day^{-1}. The AS and KF closures tend to underestimate the frequency of light precipitation (<15 mm day^{-1}), while yield too many heavy rainfall events than other closures. The TD closure significantly underestimates the frequency of light to medium rainfall (<30 mm day^{-1}), but generates too many heavy rain events (>40 mm day^{-1}).

Among these five closures, the W and MC closures more realistically predict the overall frequency distribution of the U.S. daily precipitation, primarily differing in the light and medium range. But both closures tend to slightly overestimate the frequency of heavy rainfall tail, which has also been shown in Wilcox and Donner (2007). They found that the precipitation frequency spectrum would shift toward more intense rain events if turning off the convective trigger such as the deep convective inhibition threshold (100 J kg^{-1}), or removing the representation of mesoscale anvil stratiform clouds. Therefore, further improving the precipitation frequency distribution, specifically decreasing the occurrence of extreme rainfall events in the W and MC closures, can be made from refinements in the cumulus triggers or cloud parameterizations (Wilcox and Donner 2007).

Figure 4.8 compares the frequency distribution of daily precipitation simulated by CWRF using the ECP scheme with the W and MC closures for all three summer cases over the three key regions. All the experiments consistently show that over the Central U.S., the MC closure better captures the frequency distributions especially for the extreme rainfall tails than the W closure, implying that the MC closure not only has superiority in capturing the summer mean precipitation and daily variability, but also in reproducing the daily rainfall frequency over the Central U.S. But the W and MC closures have mixed effects in predicting the observed heavy rainfall frequency over the other two regions.

Figure 4.9 compares the geographic distributions of seasonal mean precipitation, the number of rainy days, and the averaged rain intensity, as well as the daily rainfall 95th percentile intensity for 1993 summer simulated by the CWRF using the ECP scheme with the W and MC ensemble closures, respectively. Results further depict that the ERI hardly captures the observed heavy rainfall pattern with overall weak intensity over the Central U.S., while the W and MC closures both better reproduce the rainfall amount, the occurrence of rainy days and the averaged rain intensity over this region. But the MC closure generates a more reasonable distribution of the extreme events with more accurate regional details over the Central U.S. than the W closure which overpredicts the intensity of extreme events. On the other hand, the deficiency of MC closure in overestimating the rainy days and intensity over the NAM and Southeast U.S. can be greatly reduced by using the W closure.

4.5. Effects on precipitation diurnal cycle

The observed diurnal cycle of summer precipitation over the U.S. exhibits large regional differences and variations in its phase and magnitudes. It is generally characterized by late afternoon maxima over the western and southeastern U.S., but has a prominent nocturnal rainfall peaks to the east of the Rockies and the adjacent Great Plains (Dai et al. 1999; Liang et al. 2004a, Lee et al. 2007a, b). However, considerable regional deficiencies have been found in numerous modeling studies. These include the common difficulty in adequately capturing the nocturnal rainfall peaks over the Great Plains (Lee et al 2007a, b), a general phase bias, depending on the models, in the diurnal cycle of precipitation with a tendency to rain 2-5 hours earlier than observations over the Southeast U.S. and the NAM region (Lee et al. 2007b), and overactive diurnal cycle of convection manifested by the overestimated frequency and underestimated intensity of rainfall diurnal peaks (Dai et al. 1999).

Figure 4.10 shows the summer mean diurnal cycle of precipitation averaged over the three key regions simulated by CWRF using the ECP scheme with the five ensemble closures, and from the driving ERI, as compared with the NARR as well as the CPC (for 1993 case) and TRMM (for 2006 case). In 1993 summer, the NARR and CPC exhibit similar precipitation diurnal amplitudes and phases over the Central and Southeast U.S., but the CPC has a weaker nocturnal peak over the Central U.S. primarily due to its lower spatial resolution. Note that the CPC value for the NAM region is not given because the CPC analysis data only covers the U.S. without the Northern Mexico. In 2006 summer, the diurnal rainfall peaks occur somewhat earlier in the TRMM than NARR and exhibit larger amplitudes over all three regions. Positive biases of precipitation estimates from the satellite over the land have been suggested by Janowiak et al. (2007). The TRMM diurnal timing over the three regions is coincident with that shown by Liang et al. (2004a) in the National Centers for Environmental Prediction Stage-IV multi-sensor analysis data where the radar detection of evaporating precipitation and changing droplet size during storms causes an earlier peak.

The ERI reanalysis fails in reproducing the phase of diurnal cycle, consistently producing unrealistic noon to early afternoon rainfall peaks over all three regions. This has also been found in previous studies (Yang and Slingo 2001; Trenberth et al. 2003). The CWRF using the ECP scheme with five ensemble closures exhibits different skills in capturing the regional diurnal variations. The AS, MC and KF closures all produce a diurnal cycle with the peak locked at 15 PM over the three regions, and peak amount comparable over the Central U.S. In contrast, the TD closure shows superiority in producing an early morning rainfall peak over the Central U.S., albeit with 3 hours earlier than observations. A similar advantage was identified with the Grell scheme that uses a closure based on the large-scale forcing tendency (Liang et al. 2004a). The W

closure greatly inhibits the afternoon rainfall peaks appeared in AS, MC, and KF closures over the Central U.S., but yields a weaker peak in the late evening to early morning. However, all the closures could not accurately predict the diurnal phase over the Southeast U.S. with peaks about 3-hour earlier than observations. One exception is for the TD closure that predicts a much weaker peak with about 1-3 hours lags the observations.

Thus, the TD closure more likely depicts the primary diurnal signal over the Central U.S., but poorly simulates the diurnal phase over the NAM and strongly underestimates the peak amount over the Southeast U.S., while the KF closure qualitatively captures the diurnal timing with overestimated magnitudes over the NAM. These two features correspond well with the behavior of the Grell and Kain-Fritsch scheme, respectively (Liang et al. 2004a).

Different vertical heating profiles of convective and stratiform precipitation can affect the propagation speed of mesoscale convective systems in the model (Lee et al. 2007a), and thereby influence the diurnal cycle pattern particularly across the Rocky Mountains to the Great Plains. In this regard, it is imperative to examine how CWRF partitions total precipitation into convective and stratiform rainfall using the ECP scheme with different cumulus closures and determine their relative contributions to the simulated diurnal cycle deficiencies in different regions. Figure 4.11 compares the 1993 summer mean diurnal variations of convective and resolved rainfall over three key regions simulated by CWRF using the ECP scheme with five different cumulus ensemble closures and an experiment without any CUP scheme. The TD closure systematically produces smaller convective but greater resolved precipitation over all the three regions, while the other closures generally have the opposite contributions. A similar smaller convective rainfall contribution is also evident in the result of Zhang (2003) in which the nocturnal rainfall peak over the southern Great Plains is well captured when the closure is based

on the tropospheric forcing. Moreover, the Grell scheme with a similar large-scale forcing tendency closure also produces relatively smaller convective precipitation shown in Liang et al. (2004b).

Results suggest that greater resolved precipitation from the explicit microphysics schemes largely contributes to the nocturnal rainfall amount over the Central U.S. In a preliminary CWRF experiment without the CUP, the simulated nighttime rainfall peaks somewhat earlier (around 21 LST) than that in the CWRF simulation with the ECP scheme using the TD closure (around 03-06 LST). This suggests that over the Central U.S. the CUP is important in regulating the occurring time of rain peak, albeit having smaller contribution to the magnitude.

4.6. Further refinement of the closure assumption

Figure 4.12 summaries the summer (1993, 2003, and 2006) mean biases over three key regions for the CWRF sensitivity experiments using 16 subensemble closures, respectively. Several systematic deficiencies are identified to explain the model errors shown in the previous ensemble simulations. First, all AS subensemble closures consistently produce large wet biases over the Southeast U.S. but small biases in other two regions. The KF closure algorithms systematically yield excessive amounts over the NAM and Southeast U.S. but large deficits over the Central U.S. In contrast, the TD closure algorithms consistently underestimate the Southeast U.S. summer rainfall but with small biases over the Central U.S. and NAM. Second, the average closure assumptions, such as the vertical velocity at the cloud base (W_2) or at the updraft originating level (W_4) and the integrated vertical moisture convergence (MC_3), more likely produce smaller biases than other subensemble closures in their groups accordingly.

It is generally agreed that ensembles of multiple models or physical configurations tend to have superior skill over those using a single model or physical configuration (Murphy et al. 2004;

Liang et al. 2007). As such, we specifically compare the three subensemble closures that all use averaged controlling factors including the vertical velocity at the cloud base (W_2), the moisture convergence (MC_3) and the large-scale forcing tendency (TD_1) with their ensembles which are W, MC, and TD closures, respectively. Table 4.1 clearly demonstrates that the W ensemble closure better reproduces the overall precipitation mean pattern and amount over the continental U.S. and Northern Mexico by having larger pattern correlation coefficients and smaller rms errors than the W_2 closure, while the MC_3 closure comparably well captures the summer mean pattern with the MC ensemble but improves rainfall amount simulations by producing smaller rms errors than the MC ensemble. Further comparison of the two optimal closures (W and MC_3) shows that the W ensemble closure more realistically reproduces the rainfall amount by having smaller rms errors than the MC_3 closure. On the other hand, the TD ensemble and its subensemble closures poorly capture the summer mean precipitation pattern and amount. All suggest that the W ensemble still has compelling advantages over others in reproducing the overall summer mean pattern and rainfall amount.

Figure 4.13 compares spatial frequency distributions of pointwise correlation coefficients and rms error of daily precipitation between observations and simulations by CWRF using the ECP scheme with the W ensemble and the MC_3 subensemble closure for the 1993 and 2003 summer. Two closures have comparable predictive skills over the Central and NAM in contrasting climate regimes, but over the Southeast U.S., the W ensemble closure is more capable of capturing the daily variations during the dry events (1993), while the MC_3 closure better simulates the wet condition (2003). This suggests that although the W ensemble is superior in reproducing the overall U.S. summer mean pattern and rainfall amount, a better simulation of regional precipitation characteristics at various time scales by the ECP scheme can be achievable through

further intelligent optimization of its closure assumptions. For example, we can derive appropriate regime-specific weights for W ensemble and MC_3 closure to improve the daily precipitation prediction over the Southeast U.S. due to their complementary advantages for dry and wet climate regimes over this area. This will be the focus of future work.

4.7. Conclusion

This study utilizes the ECP scheme incorporated in the CWRF to examine the effects of cumulus closure assumptions on the continental U.S. summer precipitation prediction, regarding the mean pattern and amount, the daily rainfall frequency and intensity, and the diurnal variation. Three summers (1993, 2003, 2006) are chosen because they represent distinguished climate conditions over three key regions including the Central U.S., NAM and Southeast U.S. By implementing the CWRF using the ECP scheme with five different ensemble closures separately to these summer cases, several important model deficiencies and typical characteristics associated with these cumulus closures are identified.

First, cumulus closure effects alone could largely explain the model sensitivity to certain CUPs in summer mean precipitation simulations over the continental U.S. For instance, the KF closure consistently produces large wet biases over the NAM and Southeast U.S. and strong deficit over the Central U.S., explaining the systematic errors suggested by Liang et al. (2004) related to the Kain-Fritsch scheme using the same closure. Conversely, the TD closure systematically produces large deficits over the Southeast U.S., but small biases over the Central U.S. and NAM region. This is also consistent with the identified biases in the Grell cumulus scheme that is based on a similar closure with large-scale instability tendency assumption.

Second, cumulus closures have different impacts on the summer mean precipitation and daily variation over the continental U.S. with regional dependence. Among the five major closures, the

MC closure most realistically reproduces the summer precipitation mean and daily variability over the Central U.S., but overestimates the rainfall amount over the NAM and Southeast U.S. However, these wet biases over the latter two regions can be significantly reduced by using the W closure. These findings suggest that the moisture convergence plays a dominant role in controlling the summer precipitation pattern and daily variability over the Central U.S., but the low-level wind convergence and associated upward velocity is a good candidate depicting the primary physical process which organizes the mesoscale deep convection and precipitation over the NAM and Southeast U.S.

Third, cumulus closures significantly affect the combination of daily rainfall frequency and intensity, depending upon the region. The AS, KF, and TD closures, buoyance-based assumption, generally exhibit too fewer light rain events and more frequent heavy precipitation than observations. Both the W and MC closures better capture the frequency distribution of heavy rain events over all the grids of the continental U.S. and Northern Mexico than other closure assumptions, but mainly differ in their predictions of light and medium intensity. A robust signal from all experiments is that the MC closure shows clear advantage over the Central U.S. for most realistically reproducing the daily rainfall frequency distribution especially for the extreme tails.

Fourth, cumulus closures fundamentally differ in representing the interactions between the subgrid convection and the large-scale forcing, leading to distinct predictive skills in capturing the key regional diurnal variations. The AS, KF, and MC closures all fail to produce the nocturnal maxima over the Central U.S. and produce locked diurnal precipitation peaks at around 15 PM LST over the three key regions. Because convection in these cumulus closures is assumed to strongly couple with near-surface forcing and thus tends to generate excessive convective precipitation at early afternoon. However, the TD closure more likely depicts the observed

nocturnal rainfall maximum over the Central U.S., but poorly simulates the diurnal phase over the NAM and strongly underestimates the peak amount over the Southeast U.S. On the other hand, the KF closure qualitatively captures the diurnal timing but with overestimated magnitude over the NAM. All the cumulus closures did not accurately predict the diurnal phase over the Southeast. Further improvements in the simulation of diurnal cycle may require refining critical triggers functions such as the convective initiation level and relaxation time scale (Lee et al. 2007a).

Sensitivity experiments using 16 individual closure algorithms demonstrate that cumulus closure algorithms have significant impacts on the continental U.S. summer precipitation simulation, especially over the Southeast U.S. The cumulus closures using the average vertical velocity at the cloud base (W_2) or at the updraft originating level (W_4), and average moisture convergence (MC_3) produce smaller summer mean biases than other subensemble closures in their groups accordingly. Detailed comparison of these subensemble algorithms with their corresponding ensemble closures shows that the W ensemble closure has overall superior in reproducing the U.S. summer mean status, although the MC_3 greatly reduces the biases in the MC ensemble. More importantly, the MC_3 subensemble complements the W ensemble on the daily variation prediction for the dry and wet events over the Southeast U.S. This implies that in future work, enhanced predictive skills for daily variability over different climate regimes can be achieved if specific weights for these closures are derived locally by yielding overall minimum rms errors and/or maximum temporal correlations with observations.

4.8. Figures and Tables

Table 4.1 Spatial pattern correlation coefficient and rms errors between CWRF simulations using the ECP scheme with five ensemble closures (AS, W, MC, KF, TD) compared to three subensemble closures (W_2, MC_3, TD_1) and the observations over the continental U.S. and Northern Mexico for 1993, 2003 and 2006 cases.

ECP	**1993 Summer**		**2003 Summer**		**2006 Summer**	
closures	Correlation	RMSE	Correlation	RMSE	Correlation	RMSE
AS	0.60	2.07	0.72	2.84	0.64	2.62
W	0.74	1.37	0.77	1.45	0.71	1.51
MC	0.70	1.71	0.78	1.99	0.73	1.76
KF	0.53	2.68	0.70	3.42	0.65	3.27
TD	0.66	1.71	0.60	2.04	0.67	1.66
W_2	0.72	1.43	0.69	1.71	0.62	1.70
MC_3	0.73	1.50	0.79	1.56	0.68	1.54
TD_1	0.67	1.69	0.59	2.07	0.63	1.70

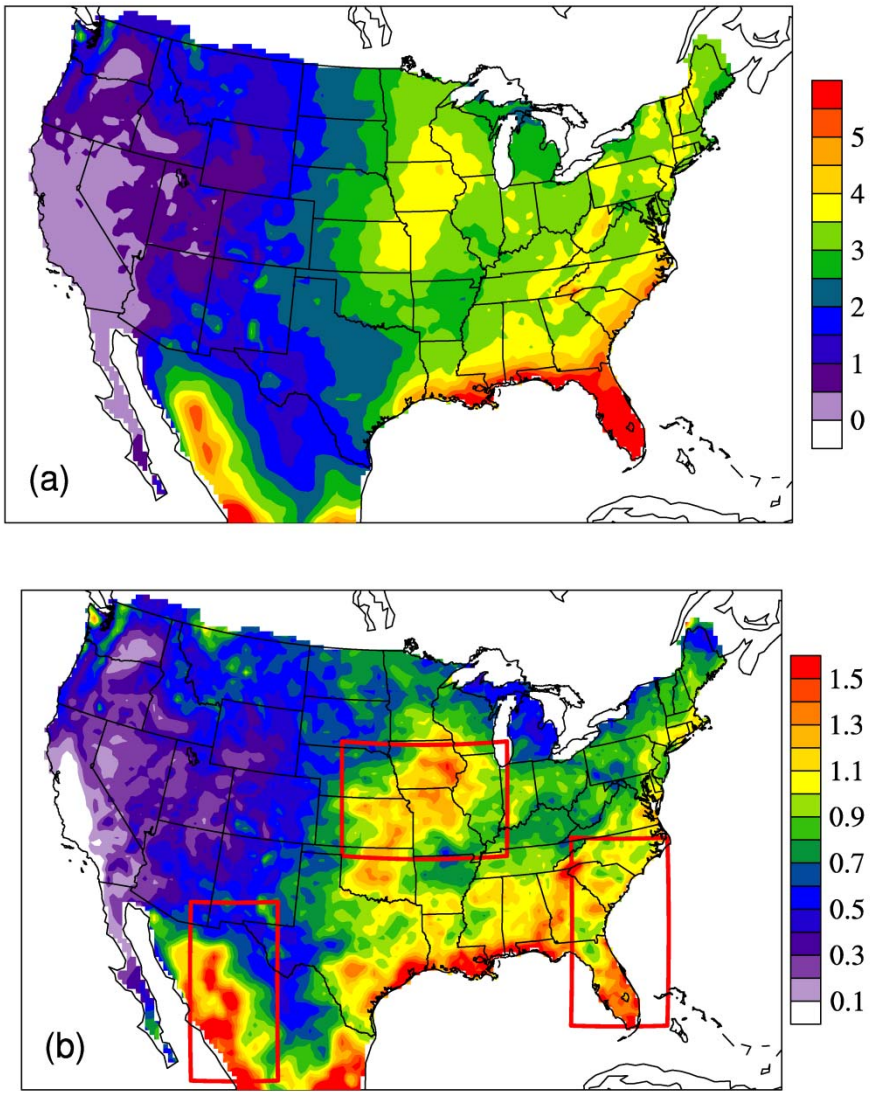

Figure 4.1 The geographic distributions of observed summer mean precipitation (a, mm day^{-1}) and interannual standard deviation (b, mm day^{-1}) averaged during 1979-2009 over the continental U.S. and Northern Mexico. Outlined in the bottom figure are three key regions which are the Central U.S. (36º-43ºN, 100º -87ºW), North American Monsoon region (NAM, 22º -33ºN, 109º -104ºW), and the Southeast U.S. (26º -35ºN, 85º -76º W).

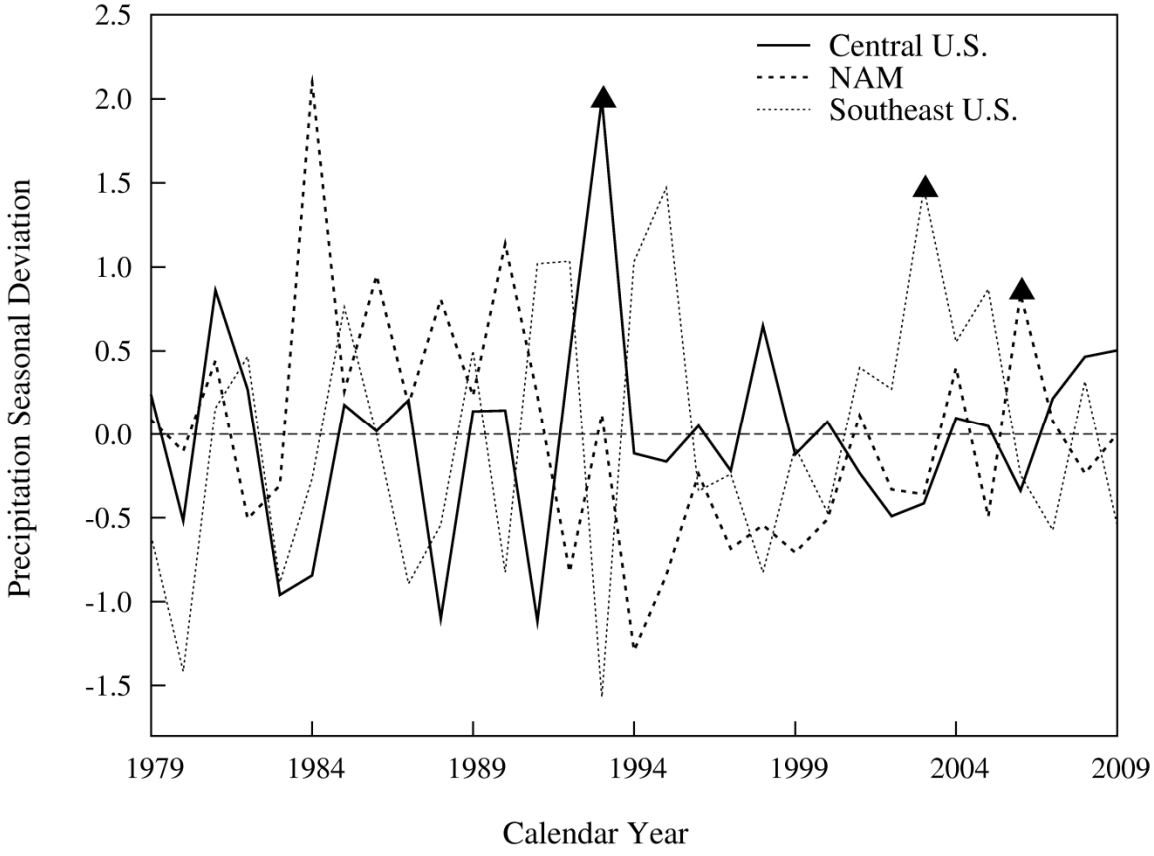

Figure 4.2 Summer mean precipitation anomalies (mm day^{-1}) from the 1979-2009 climatology averaged over the three key regions outlined in Figure 4.1. Three summer cases are marked by triangles.

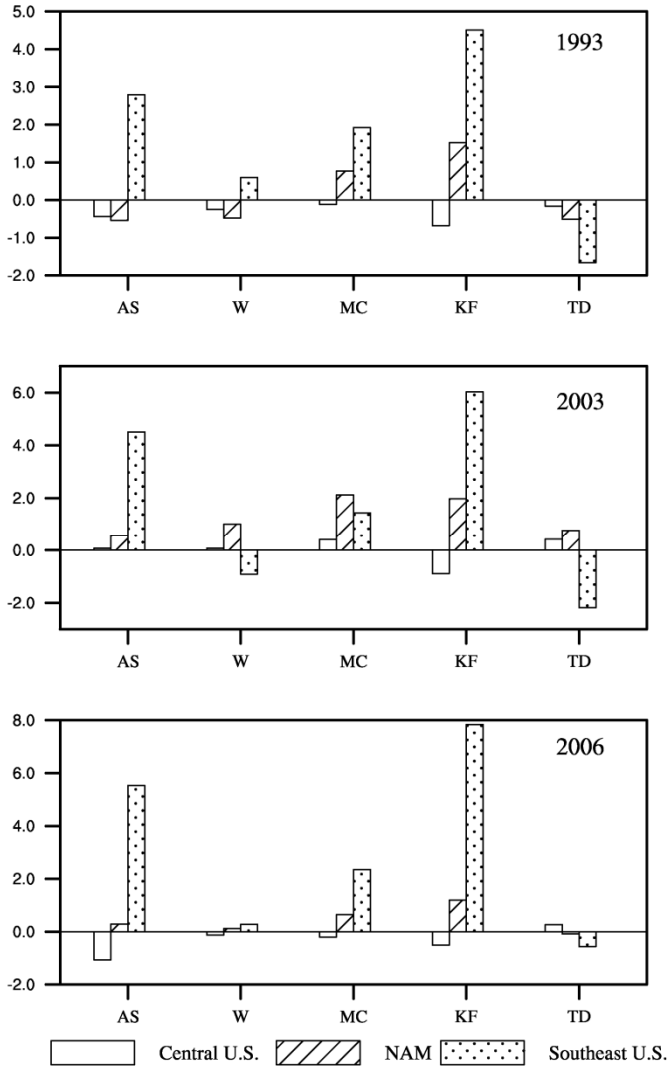

Figure 4.3 Three summer (1993, 2003 and 2006) mean precipitation biases (mm day^{-1}) averaged over the three key regions (Central U.S., NAM, and Southeast U.S.) simulated by the CWRF using the ECP scheme with five ensemble closures (AS, W, MC, KF, TD) as compared to the observations.

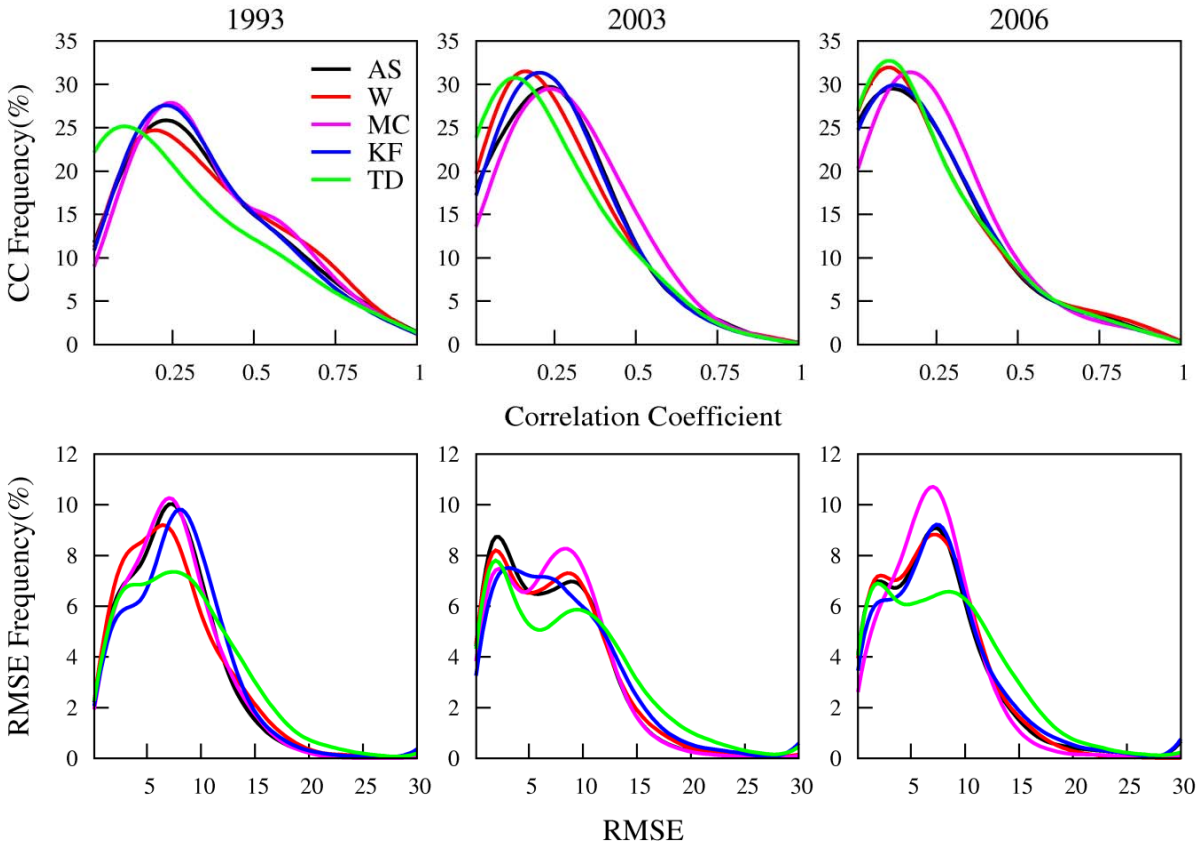

Figure 4.4 Spatial frequency distributions of pointwise correlation coefficients and rms errors of daily rainfall variations over the entire U.S. continental grids between observations and the CWRF simulations using the ECP scheme with five ensemble closures (AS, W, MC, KF, TD) for three summer cases (1993, 2003, 2006).

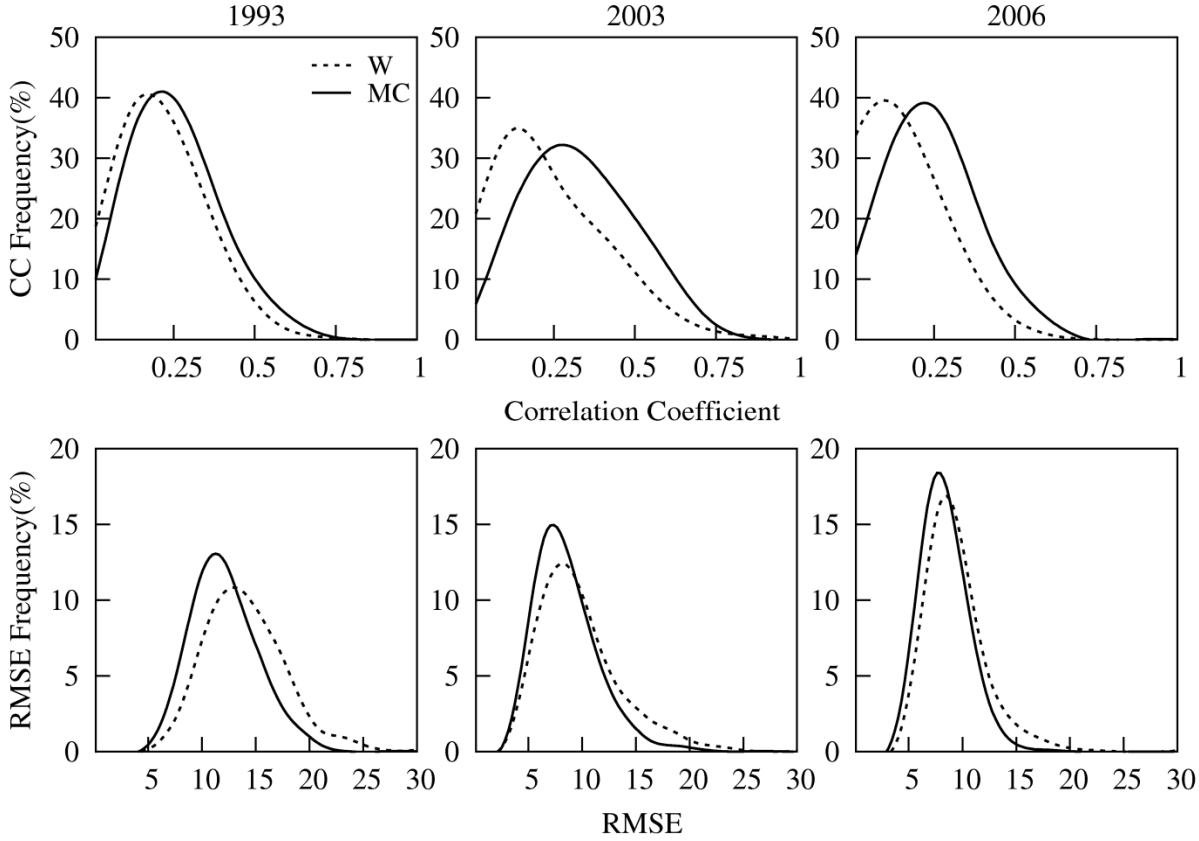

Figure 4.5 Spatial frequency distributions of three summers (1993, 2003, 2006) pointwise correlation coefficients and rms errors of daily rainfall variations over the Central U.S. between observations and the CWRF simulations using the ECP scheme with W and MC closures.

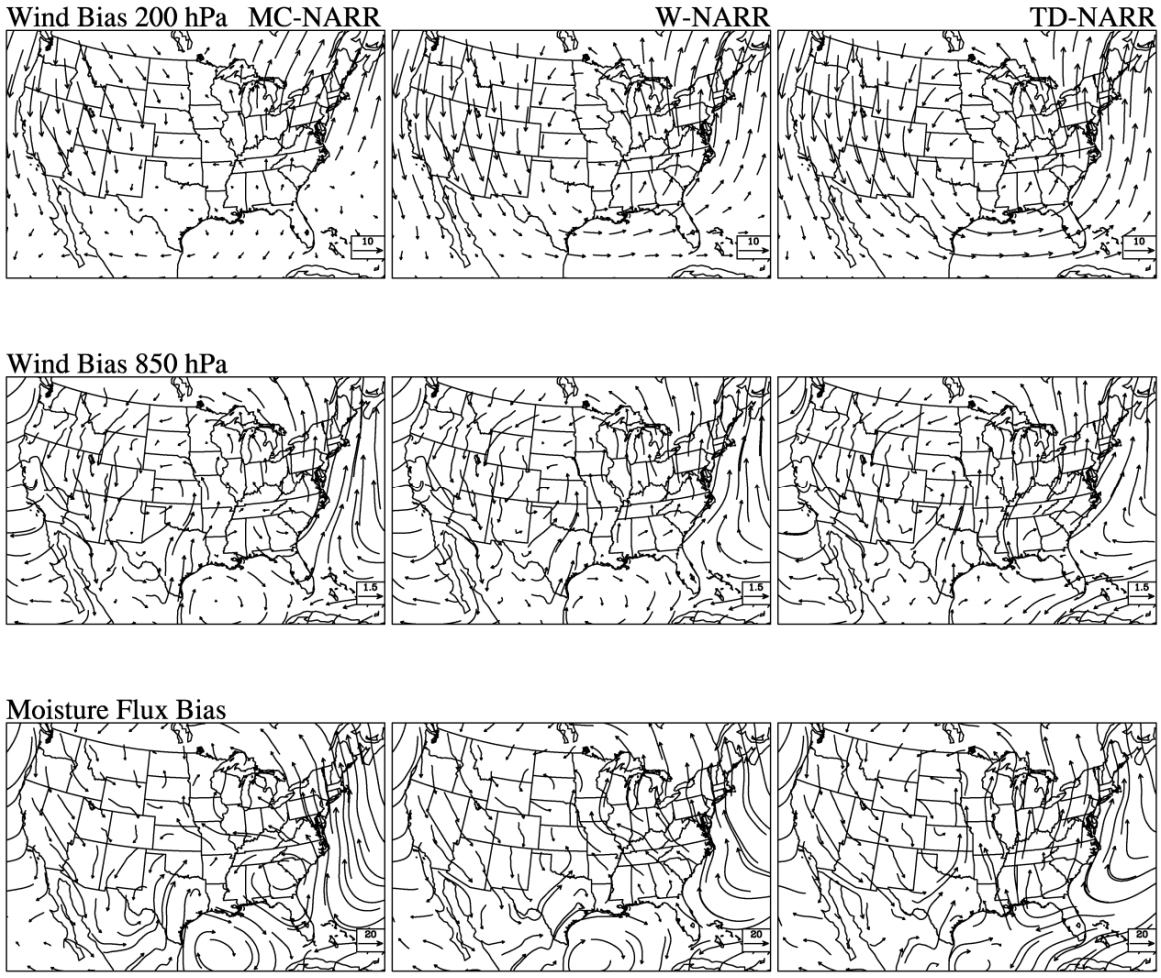

Figure 4.6 1993 summer mean geographic distributions of the CWRF minus NARR (as a proxy for observations) differences in wind (m s^{-1}) at 200 hPa (*upper panels*) and 850 hPa (*middle panels*) and vertically integrated moisture flux (*bottom panels*, kg m^{-1} s^{-1}) comparing between the MC, W, and TD closures.

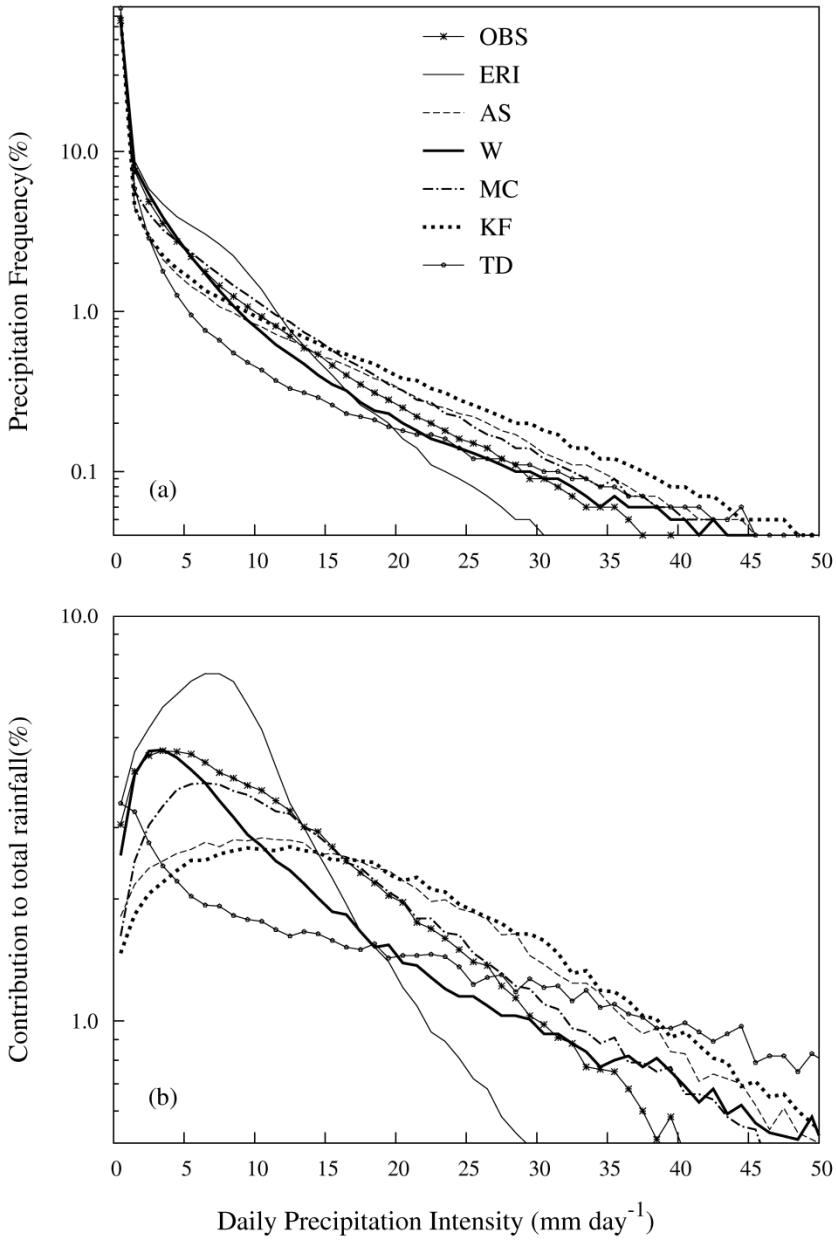

Figure 4.7 Frequency distributions (in logarithm scales) of 1993 summer daily precipitation (a) and the relative contribution to total precipitation (b) from each unit binned precipitation (1mm day^{-1}) for all grids over the continental U.S. and Northern Mexico as observed, and simulated by the CWRF using the ECP scheme with five ensemble closures (AS, W, MC, KF, TD) and the ERI reanalysis.

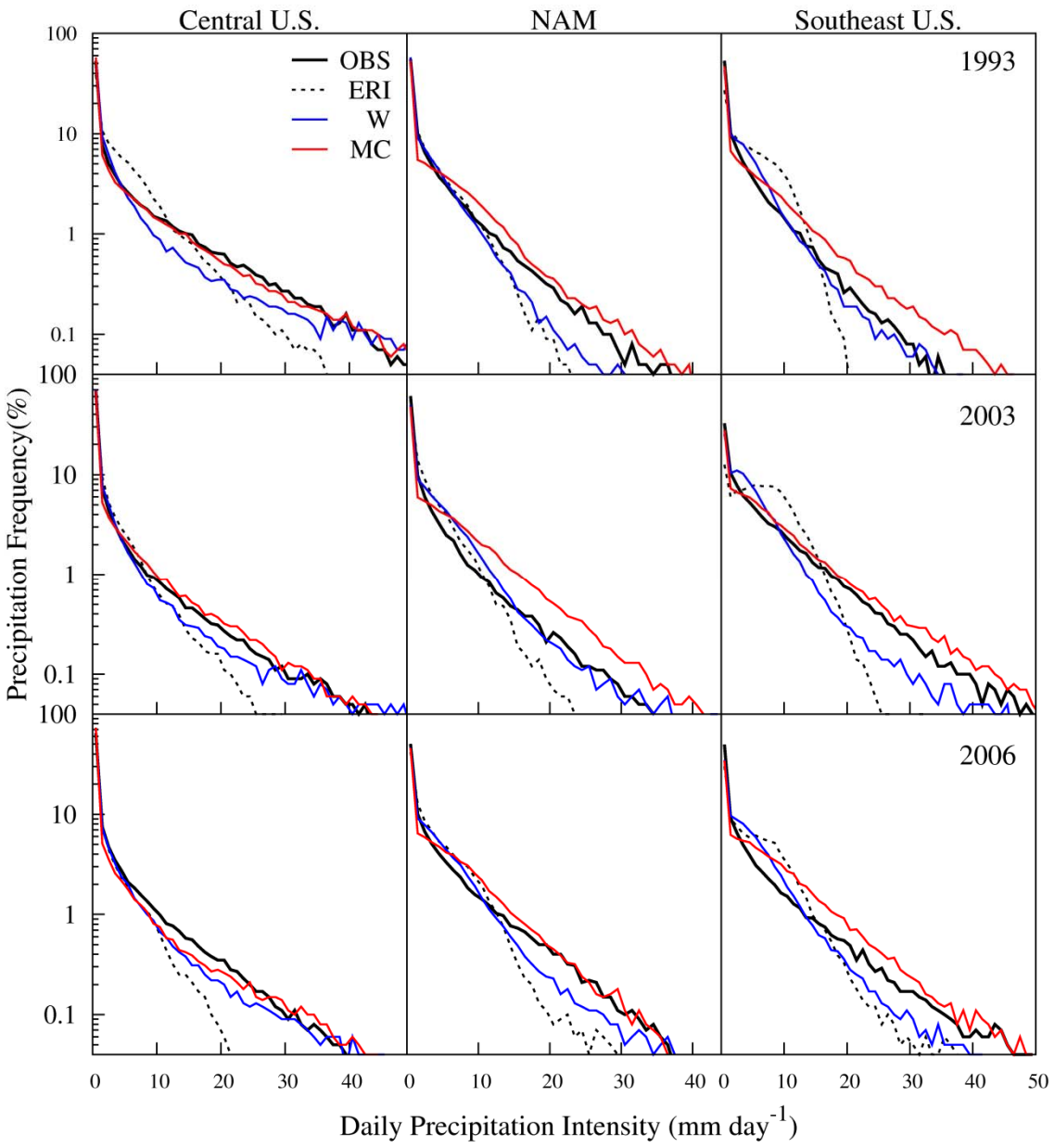

Figure 4.8 Frequency distributions (in logarithm scales) of daily precipitation for three summer cases (1993, 2003, 2006) over three key regions (Central U.S., NAM, Southeast U.S.) simulated by the CWRF using the ECP scheme with W and MC ensemble closures as compared to the observations and the ERI reanalysis.

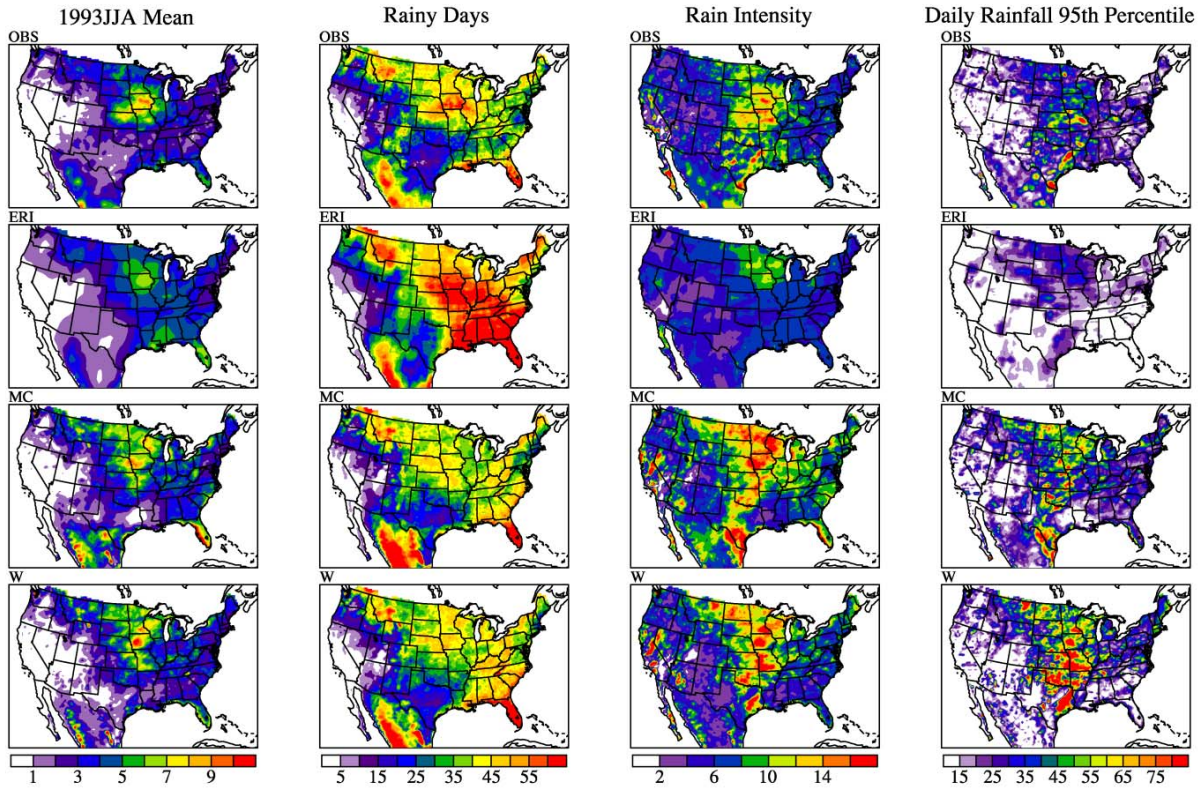

Figure 4.9 The geographic distributions of 1993 summer mean precipitation (mm day^{-1}), the number of rainy days (daily rainfall >1.0 mm day^{-1}), and the averaged rain intensity (mm day^{-1}) as well as the daily rainfall 95th percentile intensity (mm day^{-1}) simulated by the CWRF using the ECP scheme with the W and MC ensemble closures as compared to the observations and ERI reanalysis.

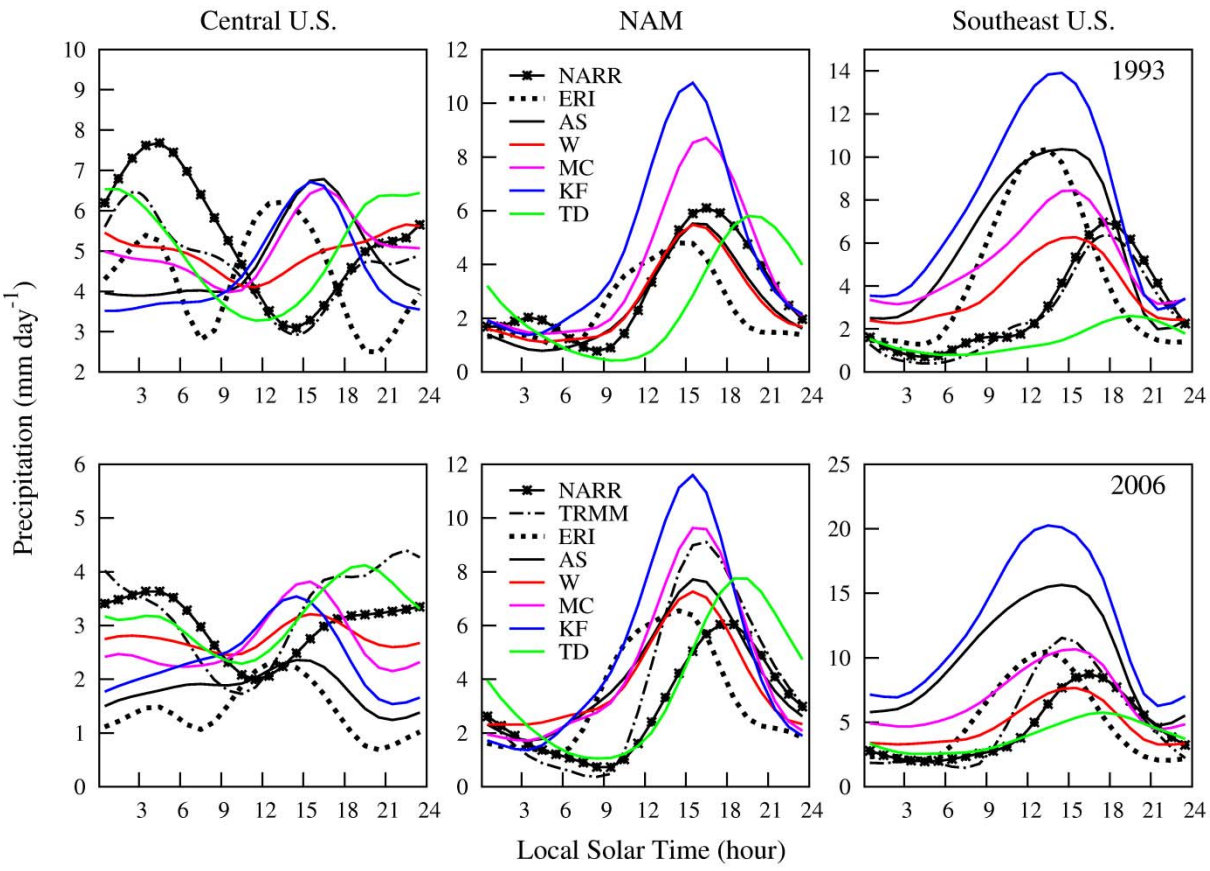

Figure 4.10 Summer mean precipitation diurnal cycle (mm day^{-1}, local solar time) averaged over three key regions (Central U.S., NAM and Southeast U.S.) as observed (NARR and CPC for 1993 case, NARR and TRMM for 2006 case) and simulated by the CWRF using the ECP scheme with five ensemble closures (AS, W, MC, KF, TD) compared to the driving ERI reanalysis.

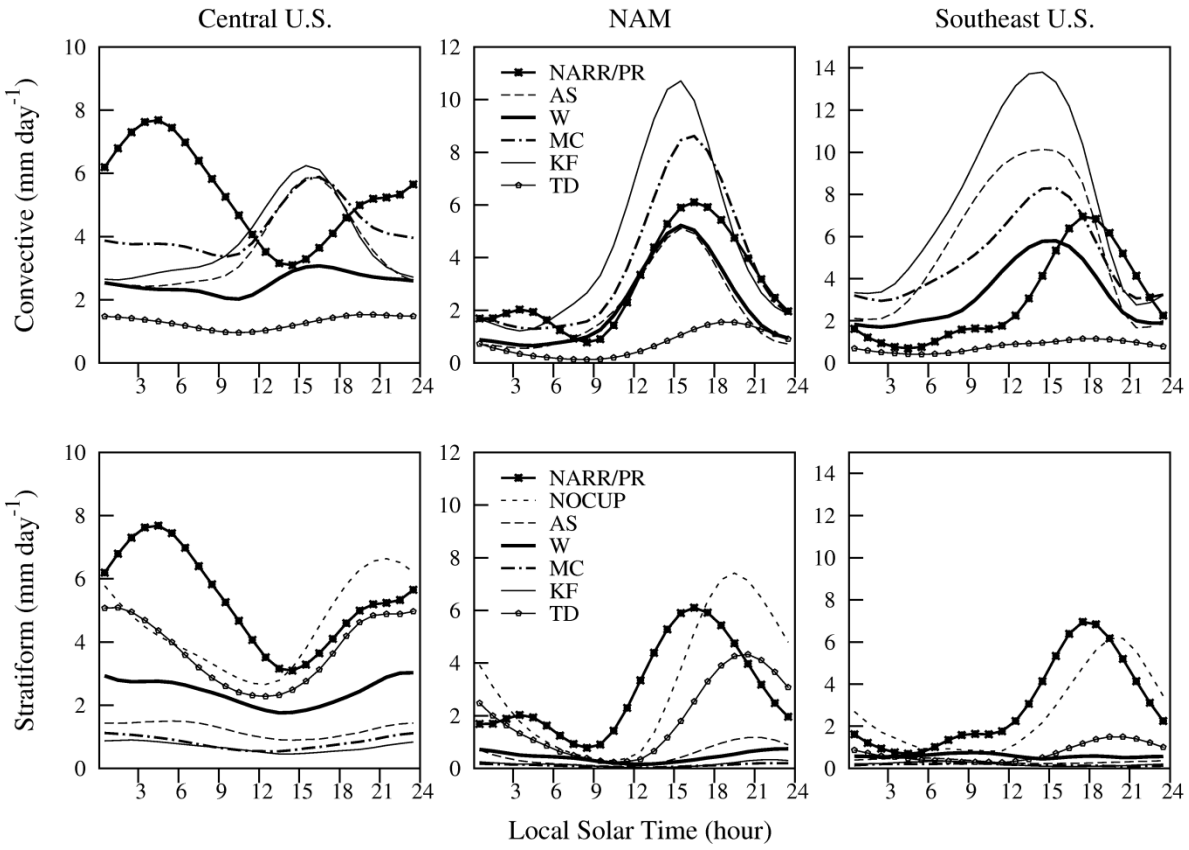

Figure 4.11 1993 summer mean diurnal cycle of convective (*upper panels*, mm day^{-1}) and stratiform precipitation (*bottom panels*, mm day^{-1}) averaged over three key regions (Central U.S., NAM and Southeast U.S.) simulated by CWRF using the ECP scheme with five ensemble closures (AS, W, MC, KF, TD) and a sensitivity experiment without CUP scheme (NOCUP), as compared to total observed precipitation (NARR/PR).

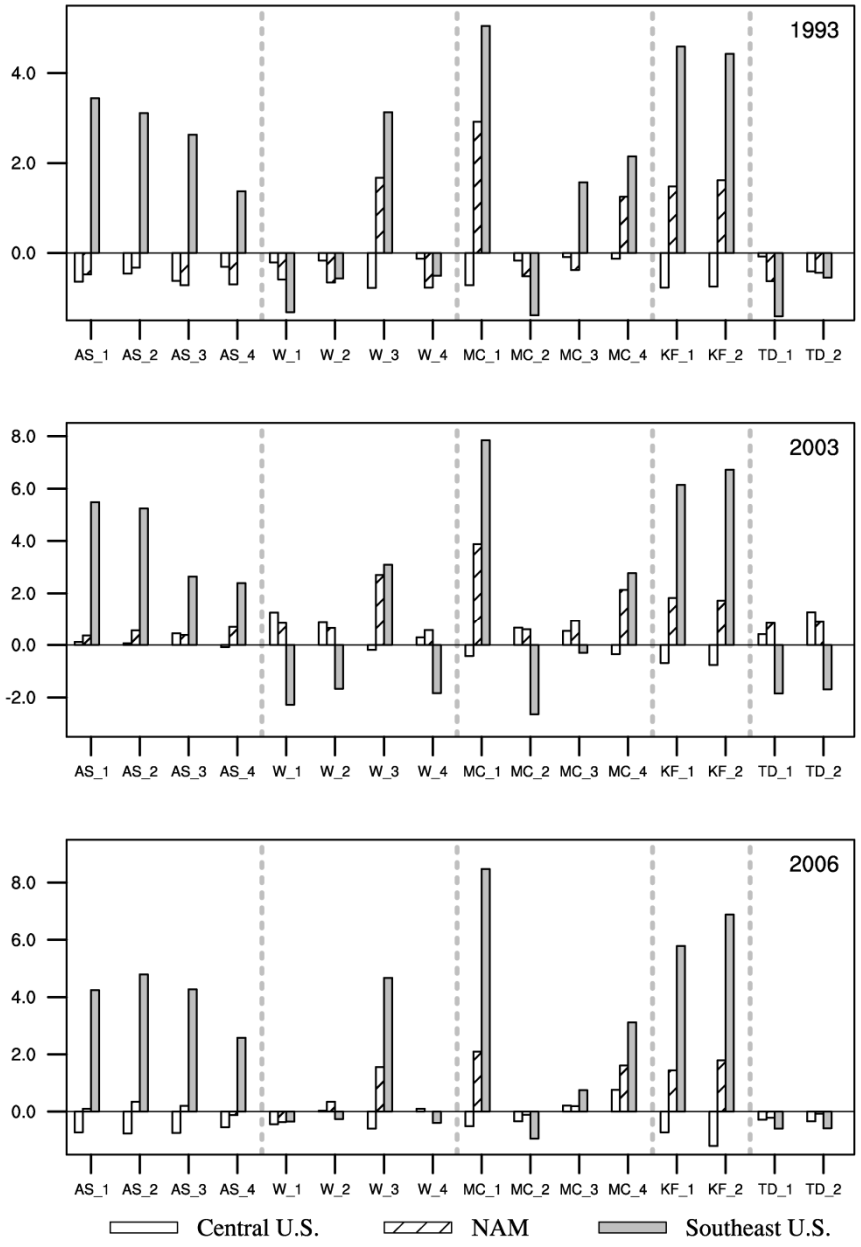

Figure 4.12 Three summer (1993, 2003, and 2006) mean precipitation biases (mm day^{-1}) averaged over the three key regions (Central U.S., NAM, and Southeast U.S.) simulated by CWRF using the ECP scheme with 16 subensemble closures as compared to the observations.

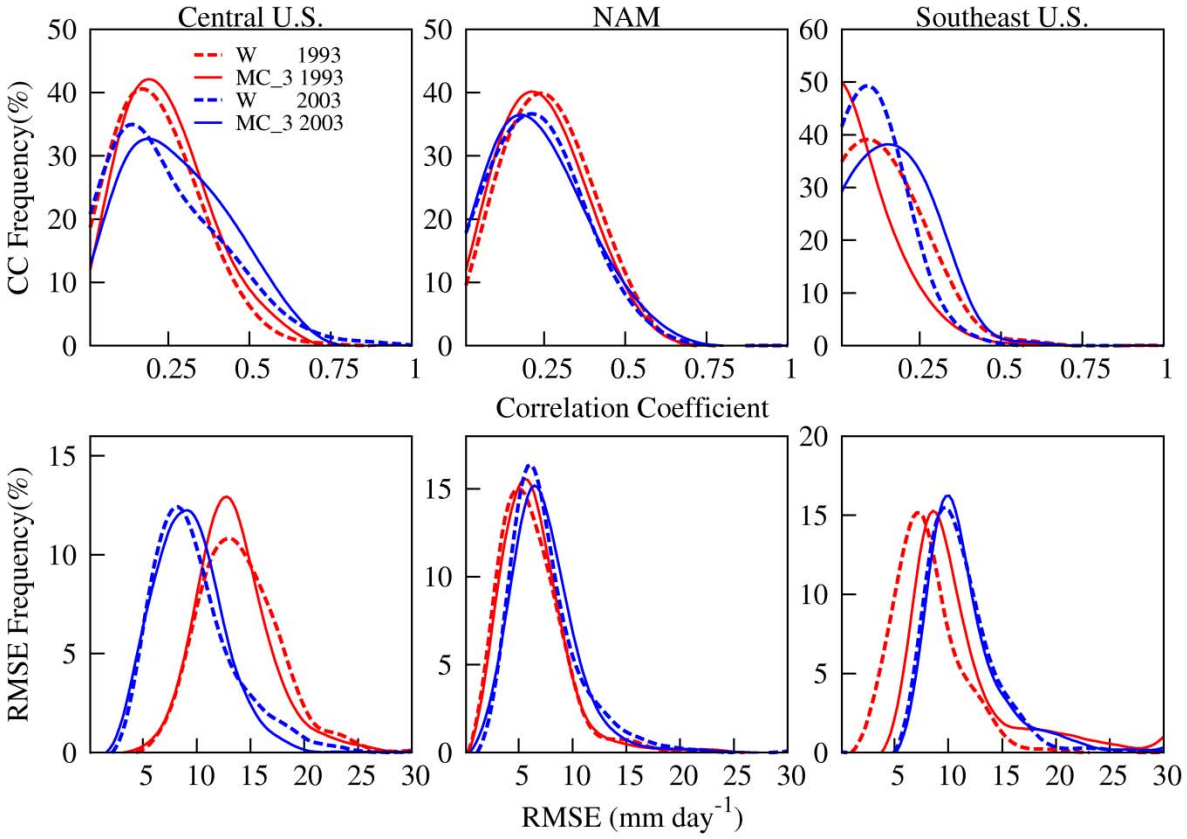

Figure 4.13 Spatial frequency distributions of pointwise correlation coefficients and rms errors of daily rainfall variations over three key regions (Central U.S., NAM, and Southeast U.S.) between observations and the CWRF simulations using the ECP scheme with W ensemble and MC_3 subensemble closures for 1993 and 2003 summer.

CHAPTER 5: SENSITIVITY OF CENTRAL U.S. SUMMER FLOODS PREDICTION TO CUMULUS PARAMETERIZATION

This chapter comprehensively evaluates the relative performance of CWRF using twelve CUP schemes in predicting the Central U.S. summer precipitation pattern, frequency distribution, and diurnal cycle. It is compiled from an article in preparation for submission to *Journal of Climate* titled "Evaluation of cumulus parameterization schemes in the CWRF simulations of summer floods over the Central United States". This chapter presents the strength and weakness of individual CUP schemes, with a focus on examining their capabilities of reproducing the observed nocturnal rainfall peaks over the Central U.S. The description of all these CUP schemes incorporated in the CWRF is given in the Chapter 2. A brief introduction, model experiments and results are shown as follows.

5.1. Introduction

The Central United States is the world's most productive, agriculture region. During the summer, heavy precipitation frequently occurs over this area and cause severe floods with devastating damages and considerable socioeconomic consequences (Kunkel et al. 1994). These extreme rainfall events have been identified with complicated physical mechanisms at different scales. The primarily processes include the large-scale circulation anomalies (Bell and Janowiak 1995; Mo et al. 1997), the sub-continental moisture transport from the Great Plain low-level jet (Mo et al. 1997; Ting and Wang 2006), and the remote supplies from the Caribbean region (Dirmeyer and Kinter 2010), as well as the local effects of land surface processes with debates (Beljaars et al. 1996; Paegle et al. 1996; Bosilovich and Sun 1999). Therefore, summer floods

over the Central U.S. provide an ideal test for the evaluation of the regional climate model (RCM) performance.

However, it is still a great challenge for most RCMs to make accurate predictions of precipitation at relatively flat region such as the Central U.S. (Takle et al. 1999; Liang et al. 2012), especially during the summer when moist convective systems prevail (Liang et al. 2001, 2004b). Previous studies have suggested that systematic errors still exist in the predictions of the Central U.S. summer rainfall and large model uncertainties are associated with the choice of CUP schemes, with respect to three precipitation characteristics: rainfall total amount (e.g., Liang et al. 2004b, 2006, 2012), daily precipitation frequency and intensity (e.g., Liang et al. 2006), and the rainfall diurnal cycle (e.g., Dai et al. 1999; Davis et al. 2003; Liang et al. 2004a; Lee et al. 2007b, 2008).

Given that the CWRF incorporates the most comprehensive list of CUPs that have been widely used in current GCMs and RCMs (Liang et al. 2012), therefore, this study will comprehensively evaluate the CWRF performance using different CUPs in predicting the summer floods over the Central U.S. The main objective is to identify the strength and weakness of individual CUP schemes in predicting the above key precipitation characteristics, with a major focus on their performances in simulating the nocturnal rainfall peaks over the Central U.S.

This study later will demonstrate that the cumulus parameterization of Grell (GR) scheme has clear advantages over cumulus schemes in capturing this nocturnal rainfall signals. As such, a set of sensitivity experiments are designed to address three specific questions: 1) What is the important role of the GR cumulus scheme in regulating the simulated precipitation diurnal cycle over the Central U.S.? 2) Whether its superiority is affected by the representation of large-scale

microphysics? 3) What is the relative contribution of the closure assumption and critical trigger function for this success of the GR scheme?

5.2. Model Experiments

Table 5.1 lists four groups of sensitivity experiments that have been carried out in this research. Their different physical configurations and research objectives are illustrated as follows. First, twelve individual CUP schemes in the CWRF are used to conduct integrations from May 1 to August 31 for 1993 and 2008 when both record floods occurred over the Central U.S. (Dirmeyer and Kinter 2010). Among the 14 CUP schemes incorporated in CWRF, only 12 schemes are specifically evaluated in this study without including the UW and GD schemes because the UW scheme is utilized as a common shallow convection option and the GD scheme has been further modified by the G3 scheme.

The second group compares the CWRF diurnal simulations with and without the GR CUP scheme, in order to examine the role of GR scheme in regulating the rainfall diurnal cycle over the Central U.S. To investigate the contribution from the resolved precipitation to the model sensitivities of total rainfall diurnal variations, additional experiments are designed using the GR CUP scheme but with three different cloud microphysics parameterizations, including the Goddard Cumulus Ensemble (GCE) model (Tao et al. 2003), the New Thompson (Thompson et al. 2008), and the Morrison et al. (2009) scheme.

All of them are mixed-phased schemes and represent six classes of water substances: water vapor, cloud water, cloud rain, cloud ice, snow and graupel/hail. First, the GCE with three-class ice scheme is a one-moment bulk microphysics parameterization based on Lin et al. (1983) with several important modifications. They include the prognostic equations for mixing ratios of cloud hydrometers, the options to choose either graupel (low density and high number

concentration) or hail (high density and low number concentration), and the instantaneous adjustment for saturation computation to evaluate evaporation of rain and deposition or sublimation of snow/graupel/hail. Second, the New Thompson scheme is greatly improved compared to the one-moment parameterization by including a two-moment prognostic scheme for cloud ice. Differing from the GCE scheme, it assumes a generalized gamma distribution for all species instead of purely exponential distribution. Third, the Morrison scheme is a two-moment scheme. The prognostic variables are number concentrations and mixing ratios of six water species whose particle size distributions are represented as gamma distributions. Meanwhile, the size distribution intercept parameter of each hydrometer is specified as a function of predicted number concentration and mixing ratio.

Given that the ECP scheme includes five different cumulus closure assumptions (AS, W, MC, KF, and TD), the third group of experiments evaluates the effects of these five closure assumptions on the Central U.S. diurnal cycle simulation, emphasizing on the TD closure which the GR CUP scheme is also built upon.

Motivated by the study of Lee et al. (2008) in which the lifting depth trigger plays a key role on the realistic simulation of summer rainfall diurnal phase over the Central U.S., the fourth group of experiments examines the sensitivity of simulated diurnal cycle by the GR CUP scheme to different lifting depth triggers. The comparison between the latter two groups of experiments can help identify the relative importance of two main components in the GR CUP scheme such as the closure assumption and trigger function for the rainfall diurnal cycle simulation over the Central U.S.

5.3. Results

5.3.1. Summer mean precipitation amount and pattern

The following comparisons are made on the main flooding periods of 1993 JJA (June-August) and 2008MJJ (May-July). The outcome will systematically depict the model sensitivity to the convective parameterization. Figure 5.1 shows the geographic distributions of observed and simulated 1993 summer mean precipitation by CWRF using 12 different CUP schemes including the ECP, G3, BMJ, ZML, NKF, TDK, GR, MIT, GFDL, SAS, NSAS and CSU (references in Chapter 2). Several model deficiencies can be identified in major rainfall areas. First, all CUP schemes produce a heavy rainfall center over the Central U.S. but large discrepancies exist in the simulated rainfall amounts. The ECP, G3, and ZML show clear advantages over other schemes in reproducing the floods location and amount. However, several CUP schemes that are often used in major GCMs, such as the TDK, MIT, GFDL and CSU, systematically underestimate the summer rainfall amount over the Central U.S. This suggests that further refinements are required to account for the scale dependence of CUP in weather prediction and climate simulation.

Second, three schemes such as the G3, ZML, and NKF tend to produce widespread large wet biases along the U.S. Atlantic Coast. In particular, the ZML significantly overestimates the summer mean precipitation over the entire U.S. East plus South coastal oceans. The ECP scheme is developed from the G3 scheme, but more realistically simulates the rainfall pattern and intensity along the U.S. Atlantic Coast than the G3 scheme. The possible reason is that the ECP only adopts the cloud-base vertical velocity closure rather than ensemble closures in the G3 scheme discussed in Chapter 4. On the other hand, the ZML and NKF both based on the total instability adjustment closure assumption generally yield excessive coastal ocean rainfall, consistent with previous finding of Liang et al. (2004b) that the parameterization of Kain and Fritsch (1993) with the same closure generated large wet bias along the U.S. coastal oceans.

Figure 5.2 summarizes the CWRF simulated mean rainfall biases compared to the observations averaged over the Central U.S. (a) and the U.S. Atlantic Coast and Gulf of Mexico (b) for 1993 JJA and 2008 MJJ by using 12 different CUP schemes. Combined with the mean bias statistics in Table 5.2, it clearly shows that predictive skills of the CUP schemes with respect to the summer mean precipitation amount and pattern are strongly dependent upon climate regimes. For instance, three schemes including the ECP, G3 and ZML produce relatively smaller mean biases over the Central U.S. than other schemes. However, the ECP greatly reduces the wet biases in the G3 scheme over the U.S. coastal ocean. Although the ZML generates the most realistic rainfall amounts over the Central U.S., it has the worst performance in predicting the U.S. overall pattern distribution due to the large wet biases over the North American Monsoon region and Southeast U.S. along with the U.S. coastal oceans.

In contrast, the BMJ, GR, MIT and NSAS show advantages over others in simulating the general pattern of summer mean precipitation in the entire continental U.S. (shown in Table 5.2), but they tend to have large deficits over the Central U.S. Due to the complementary regime-dependences of these seven schemes (ECP, G3, ZML, BMJ, GR, MIT, NSAS), the following study will focus on the evaluation of their relative performances in predicting the daily rainfall frequency distribution and diurnal cycle over the Central U.S.

5.3.2. Daily precipitation variation and frequency distribution

Figure 5.3 compares the model simulated daily rainfall variations averaged over the Central U.S. with the observations for the 1993 and 2008 cases in Taylor diagrams by depicting three important statistics: temporal correlation, normalized standard deviation, and rms errors. The plotted values in the diagrams are also listed in Table 5.2. The ECP scheme produces the highest temporal correlations and smallest rms differences for both cases, indicating its superior

in reproducing the daily rainfall variations over the Central U.S. Although the G3 and NSAS schemes both well capture the temporal variation, the former generates relatively larger rms errors than the ECP scheme and the latter significantly underestimates the amplitude of daily variability. On the other hand, the ZML scheme poorly simulates the daily rainfall variation, albeit with the smallest mean biases over the Central U.S.

Figure 5.4 compares the frequency distributions of 1993 summer daily precipitation and relative contributions to the total amount over the Central U.S. between the observations, the ERI reanalysis, and CWRF simulations with the aforementioned seven CUP schemes. Here, we only show 1993 case because the 2008 case exhibits the similar characteristics of daily rainfall probability distributions. The ERI systematically overpredicts the frequency of light rainfall events less than 10 mm day^{-1}, but significantly underestimates the frequency and intensity of extreme events with daily rainfall exceeding 35 mm day^{-1}. The seven CUP schemes can be roughly divided into two categories according to their daily rainfall frequency prediction. One group includes the ECP, G3, and ZML schemes. These three more realistically reproduce the overall frequency distribution by greatly reducing the ERI deficiency in predicting the heavy rainfall occurrence. Among them, the ECP scheme accurately predicts the relative contribution of daily rainfall intensity within the medium range (10-30 mm day^{-1}) than the other two schemes. On the other hand, another group including the GR, MIT, NSAS and BMJ schemes generally underestimates the frequency of heavy rainfall events and overestimates the contributions from the light (GR and MIT) to medium (NSAS and BMJ) events.

5.3.3. Precipitation diurnal cycle

Figure 5.5 compares the summer mean precipitation diurnal cycles for both 1993 and 2008 cases averaged over the Central U.S. simulated by CWRF using the seven CUP schemes in

comparison with the NARR as observations. Following Liang et al. (2004b), the 3-hourly data from both the NARR and CWRF simulations are interpolated into hourly values by utilizing spline fit method. To enhance the compatibility between observations and model results regarding the amplitude and phase of diurnal variations, the hourly rainfall amounts at each grid are normalized by a division of its daily mean values. The observed diurnal cycles for both cases exhibit a daytime minimum and a nighttime maximum but slightly differ in amplitudes and phases. For instance, the 1993 observed summer mean diurnal cycle exhibits a larger amplitude compared to the 2008 case, and the nocturnal rainfall peak occurs in the early morning at around 3-6 AM LST which is several hours later than that in the 2008 case.

For the two groups classified by the prediction of daily rainfall frequency distributions, the diurnal cycle simulated by the seven CUP schemes are compared accordingly. The first group including the ECP, G3 and ZML schemes systematically generates a diurnal cycle with the peak locked at 15-18 PM LST, all failing to capture the observed nocturnal rainfall maxima. In the second group, the MIT and BMJ schemes unfaithfully simulate rainfall maxima at early to late afternoon, but the GR and NSAS schemes show capabilities of capturing the diurnal timing. This is in good agreement with previous findings by Liang et al. (2004a) and Lee et al. (2008). However, the NSAS scheme in CWRF largely underestimates the nocturnal rainfall peak amounts for both cases and has a tendency to rain slightly earlier than observations particularly in 1993 summer. The most encouraging finding is that the GR scheme most realistically reproduces the diurnal amplitude and phase among these popular schemes. As such, the following study attempts to explore the role of CUP in regulating the rainfall diurnal cycle simulations over the Central U.S. by focusing on the GR scheme.

Figure 5.6 compares the 1993 summer mean rainfall diurnal cycles over the Central U.S. from the NARR and the CWRF simulations using the GCE microphysical scheme with (GR-GCE) or without GR (NoCUP-GCE) scheme. To examine the sensitivity of diurnal cycle simulations to the large-scale resolved precipitation, two additional experiments are also conducted by using the cumulus parameterization of GR scheme but with different microphysics schemes including the New Thompson and Morrison scheme. When cumulus parameterization is excluded, the CWRF only with the GCE microphysics scheme tends to produce a much stronger rainfall peak in the late evening at around 21 PM LST which is 6 hours earlier than the observation. This earlier rainfall peak can be attributed to that microphysics scheme over the Central U.S. is more responsive to the large-scale dynamic forcing such as the Great Plain low-level jet whose strongest intensity generally leads the rainfall maxima for several hours (Liang et al. 2001; Lee et al. 2007a). By adding the GR cumulus scheme, the late evening peak amount in the NoCUP-GCE experiment is substantially reduced and the rainfall maximum is delayed to occur at the early morning around 03-06 AM LST in better agreement with the observation. This improvement indicates that the cumulus parameterization plays an essential role in regulating the simulation of the Central U.S. precipitation diurnal cycle.

Three experiments using the GR CUP scheme but with different microphysics schemes all well predict the diurnal timing, but differ in diurnal amplitudes and rainfall magnitudes. Compared to the GCE scheme, the New Thompson and Morrison schemes both produce weaker amplitudes and the latter scheme tends to predict a much smaller nocturnal rainfall peak. This clearly shows that the large-scale precipitation primarily contributes to the rainfall peak amount and diurnal amplitude but hardly affects the diurnal phase. On the other hand, the CWRF simulated diurnal timing using the GR cumulus scheme is insensitive to the choice of

microphysics schemes, implying that the GR scheme has intrinsic advantages over other CUP schemes in representing the physical mechanisms that control the Central U.S. precipitation diurnal variation.

Figure 5.7 shows the 1993 summer mean precipitation diurnal cycles averaged over the Central U.S. simulated by CWRF using the ECP scheme with five different closures (AS, W, MC, KF, TD) compared to the simulation without cumulus parameterization, as well as the NARR observation. Results show that the ECP with the AS, MC or KF closure assumption generally fails in capturing the nighttime rainfall peaks, but tends to produce a diurnal cycle with rainfall peak locked at 15PM LST over the Central U.S. These failures have been identified in the cumulus parameterization of BMJ, controlled version of ECP and ZML scheme which uses the above three closures respectively. However, when the TD closure is applied in the ECP scheme, it significantly improves the diurnal cycle simulation by generating a rainfall peak at the early morning with intensified intensity compared to other closures. Also, the ECP with the TD closure shifts the rainfall peak from the late evening in the simulation without CUP to around 03AM LST, albeit with 3-hour phase error. It corresponds well with the behavior of the GR scheme which uses the same instability tendency closure assumption (Liang et al. 2004a).

In addition to the cumulus closure assumption, certain trigger function has also been suggested to affect the realistic simulation of diurnal phase over the Central U.S. For instance, Lee et al. (2008) showed that the lifting depth trigger plays a key role in simulating the nocturnal rainfall peak in the SAS scheme by defining the distance between the cloud base and convective starting level must be less than 150 hPa. Figure 5.8 compares the 1993 summer mean diurnal cycles simulated by CWRF using the GR cumulus scheme but with three lifting depth triggers including 25, 50 (control) and 150 hPa. It shows that shallower depth (25 hPa) generally tends to

suppress the convection because the condition to active the convection is difficult to meet if the ambient air is quite dry and the level of free convection forms in much higher altitudes. In contrast, as the lifting depth trigger is increased to 150 hPa, daytime convection especially during the early afternoon is significantly enhanced because the threshold depth is so large that more deep convection can be triggered even at the presence of strong convective inhibition energy. As such, the lifting depth trigger in the GR scheme primarily suppresses the daytime convection, thereby affecting the Central U.S. diurnal cycle simulation.

5.4. Conclusions

The CUP schemes in this study include 6 original WRF schemes (BMJ, NKF, SAS, NSAS, TDK, G3) and 6 new schemes (ECP, ZML, CSU, GFDL, MIT, GR) that have been widely used in GCMs or RCMs. All of them are implemented as deep convection schemes and combined with the UW shallow convection in order to provide a consistent evaluation for the moist cumulus parameterization. Sensitivity experiments using the CWRF with these 12 CUP schemes are carried out for 1993 and 2008 summer when both record floods occurred over the Central U.S.

Results show that these widely-used CUP schemes have distinctive skills in predicting the U.S. summer mean precipitation characteristics, with strong regional dependence. The seven CUP schemes are identified with complementary regime dependences in the prediction of summer rainfall patterns and amounts. One group including the ECP, G3 and ZML schemes shows advantages over other schemes in reproducing the Central U.S. flood locations and amounts, but has large model disparities in other U.S. regions and the adjacent coastal oceans. Particularly, the ECP scheme well reproduces the Central U.S. floods and greatly reduces the wet biases in the G3 and ZML schemes along the U.S. coastal oceans. The second group including

the BMJ, GR, MIT and NSAS schemes is superior in simulating the general pattern of U.S. summer precipitation, but tends to produce large dry biases over the Central U.S.

Further comparison of daily rainfall statistics shows that the CUP schemes significantly affect the CWRF predictions of the Central U.S. summer daily precipitation variation and frequency distributions. The ECP scheme most realistically reproduces regional mean daily rainfall variation and the overall frequency distributions. It not only greatly reduces the deficiency of ERI reanalysis by better capturing the occurrence of heavy rainfall events, but also more accurately predicts the contributions from daily precipitation in medium intensity than the G3 and ZML schemes.

Most CUP schemes fail to reproduce the observed nocturnal rainfall maxima over the Central U.S. An encouraging finding is that the GR scheme is superior in reproducing the Central U.S. diurnal amplitude and phase, though it slightly underestimates the rainfall peak amount. When there is no CUP implemented in the CWRF, the large-scale microphysical schemes tend to have stronger but much earlier rainfall peaks, while the inclusion of GR scheme effectively regulates the diurnal phase by postponing the rainfall peak from late evening to early morning in a better agreement with observations. The diurnal timing simulated by the GR scheme is insensitive to the choice of microphysics schemes, implying that large-scale precipitation primarily contributes to the rainfall peak amount and the diurnal amplitude but hardly affects the diurnal phase.

Replacing the moisture convergence closure in the ECP scheme with the instability tendency closure used in the GR scheme greatly improves the ECP simulated diurnal cycle by generating a nocturnal rainfall peak. This suggests that the advantage of the GR scheme is primarily due to its closure assumption in which the convection is determined by the instability tendency. In addition, the lifting depth trigger in the GR cumulus scheme also affects the Central U.S. diurnal cycle

simulation by mainly suppressing the daytime convection, consistent with the study by Lee et al. (2008). Given the importance of instability tendency closure in reproducing the Central U.S. rainfall diurnal phase and amplitude, more efforts in the future will be made to incorporate the instability tendency assumption as a trigger function in the ECP scheme with the moisture convergence closure for improving its diurnal cycle simulation over the Central U.S.

5.5. Figures and Tables

Table 5.1 Summary of four groups of sensitivity experiments conducted by CWRF with different cumulus and microphysics configurations.

Run	Integration time	Deep CUP	Microphysics
CUP tests	1993 May 1- August 31 2008 May 1- August 31	12 CUPs [ECP, G3, BMJ, ZML, NKF, TDK, GR, MIT, GFDL, SAS, NSAS, CSU]	GCE
MP tests	1993 May 1- August 31	No CUP	GCE
		Grell	GCE New Thompson Morrison
Closure tests	1993 May 1- August 31	ECP [AS, W, MC, KF, TD closures]	GCE
Trigger tests	1993 May 1- August 31	Grell [three lifting depth triggers]	GCE

Table 5.2 CWRF simulated rainfall statistics for 1993 JJA (June-August) and 2008 MJJ (May-July) by using 12 different cumulus parameterization schemes.

CUPs	Bias (%) [Central U.S.]		Pattern correlation [U.S.]		RMS errors [U.S.]		Daily rainfall correlation [Central U.S.]		Normalized variances [Central U.S.]	
	1993	2008	1993	2008	1993	2008	1993	2008	1993	2008
ECP	**-2.4**	**13.7**	**0.69**	**0.74**	**1.70**	**1.77**	**0.65**	**0.65**	**1.11**	**1.16**
G3	**7.1**	**-11.3**	**0.71**	**0.72**	**1.57**	**1.28**	**0.65**	**0.60**	**1.29**	**1.01**
BMJ	-21.9	-43.5	**0.71**	**0.67**	**1.35**	**1.25**	0.58	0.52	0.89	0.51
ZML	**-1.6**	**-2.7**	0.41	0.54	2.91	2.45	0.59	0.50	1.23	0.82
NKF	-28.6	-18.1	0.59	0.67	1.96	1.42	0.50	0.54	0.99	1.00
TDK	-28.4	-49.0	0.64	0.60	1.64	1.45	0.44	0.48	1.25	0.74
GR	-8.1	-25.2	**0.72**	**0.71**	**1.38**	**1.17**	0.43	0.53	1.33	0.85
MIT	-5.8	-19.5	**0.68**	**0.69**	**1.46**	**1.28**	0.51	0.47	1.10	0.96
GFDL	-34.6	-47.6	0.61	0.62	1.76	1.43	0.39	0.48	1.06	0.66
SAS	-49.8	-49.1	0.61	0.65	1.63	1.33	0.39	0.48	0.56	0.68
NSAS	-30.7	-34.1	**0.69**	**0.69**	**1.31**	**1.15**	**0.62**	**0.61**	**0.73**	**0.58**
CSU	-43.8	-47.5	0.54	0.61	1.92	1.44	0.43	0.51	0.76	0.69

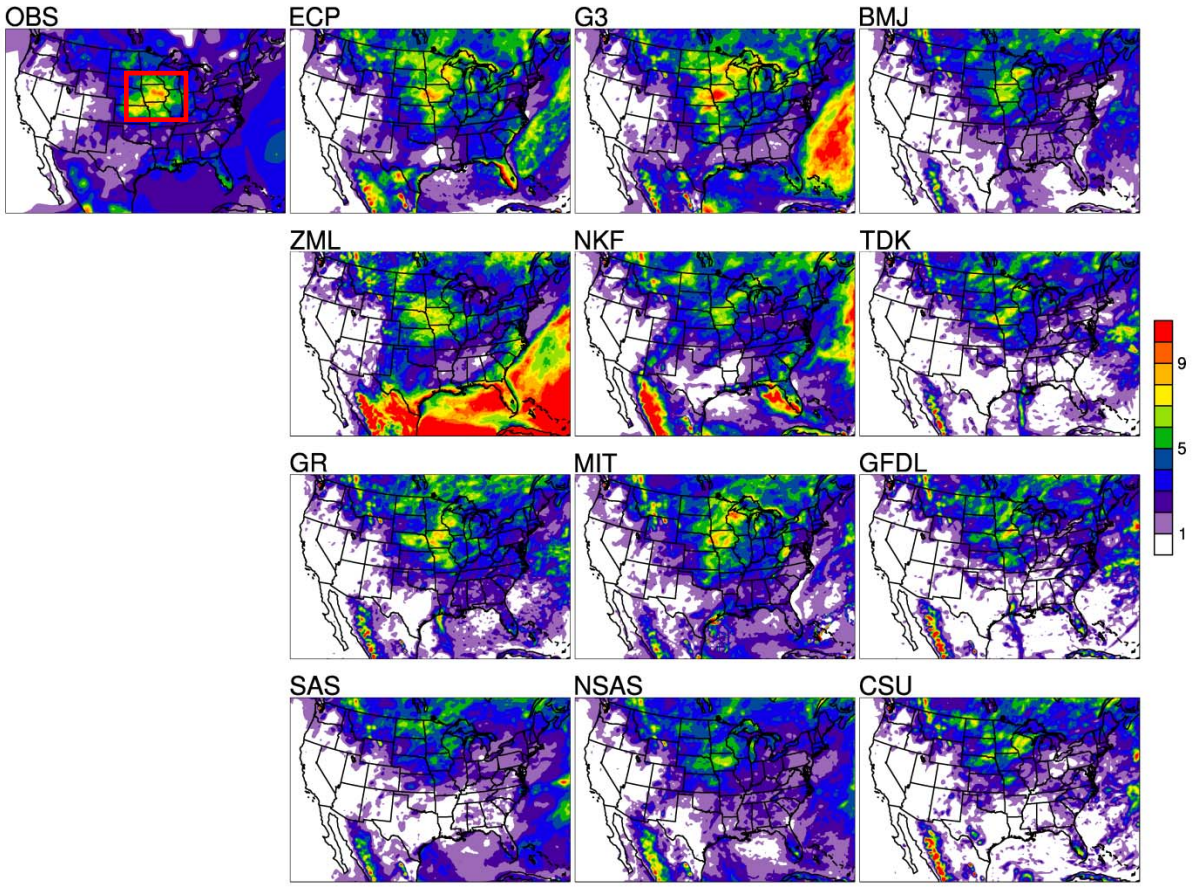

Figure 5.1 The geographic distributions of observed and simulated 1993 summer mean precipitation by the CWRF using 12 different cumulus parameterization schemes including the ECP, G3, BMJ, ZML, NKF, TDK, GR, MIT, GFDL, SAS, NSAS and CSU. Outlined in the first figure is the Central U.S. in focus (36º-43ºN, 100º - 87ºW).

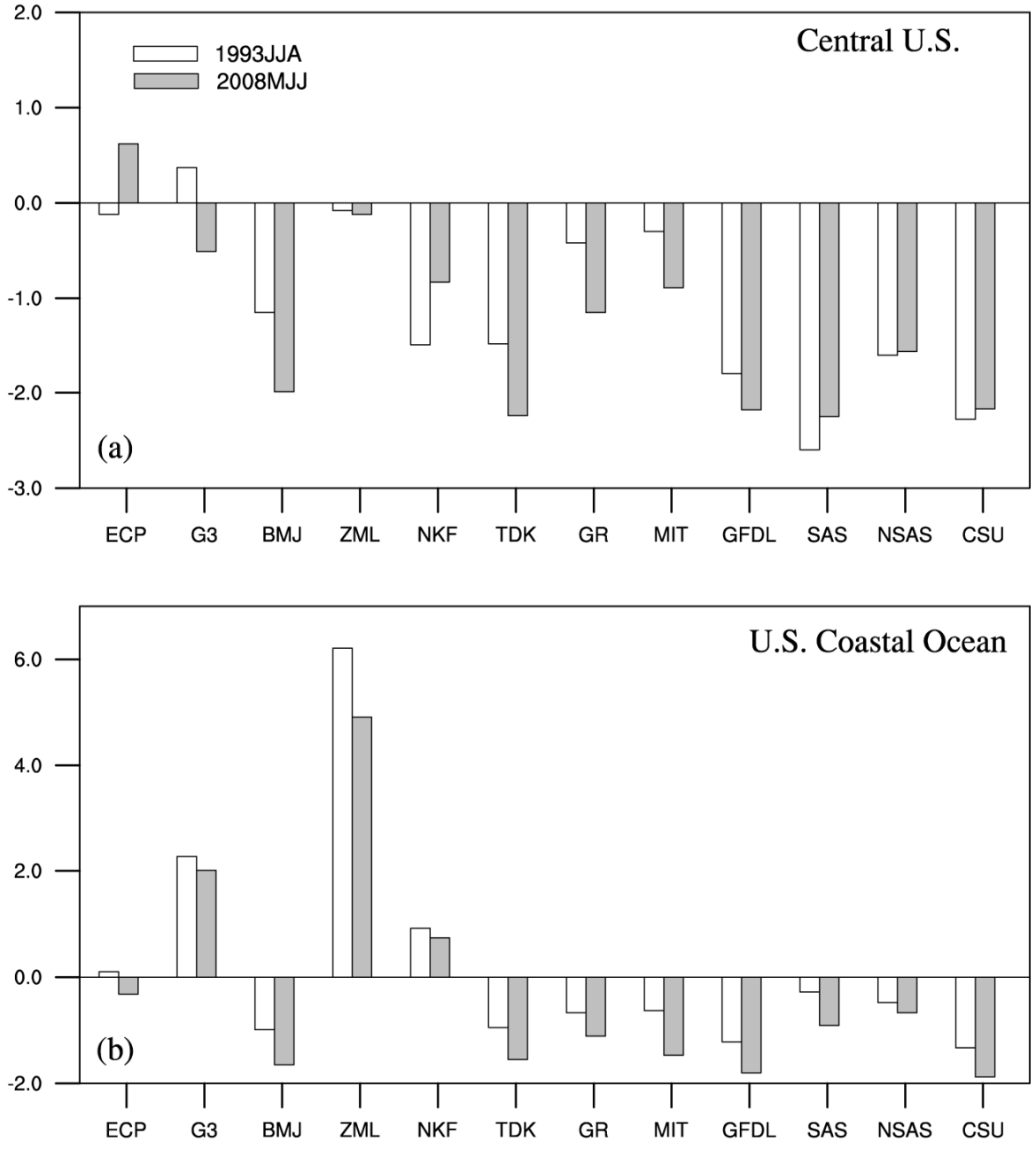

Figure 5.2 The mean precipitation biases simulated by the CWRF using the 12 different cumulus schemes from the observations averaged over the Central U.S. (a) and the U.S. Atlantic Coast and Gulf of Mexico (b) for 1993 June-August and 2008 May-July.

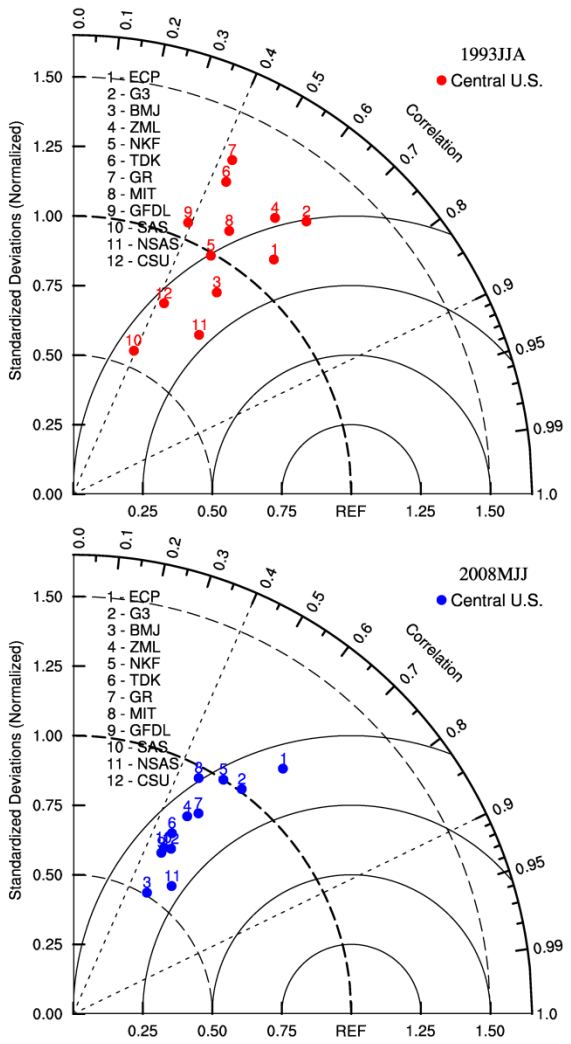

Figure 5.3 Taylor diagram showing the model performance of simulated 1993 JJA (June-August) and 2008 MJJ (May-July) daily precipitation variability averaged over the Central U.S. by using 12 different cumulus parameterization schemes, in terms of the normalized standard deviation of the modeled daily means (proportional to the distance from the origin), the rms difference between the simulated and observed daily means (proportional to the distance from the REF point), and the temporal correlation between the simulated and observed daily means (cosine values of the angle of model point from the horizontal axis).

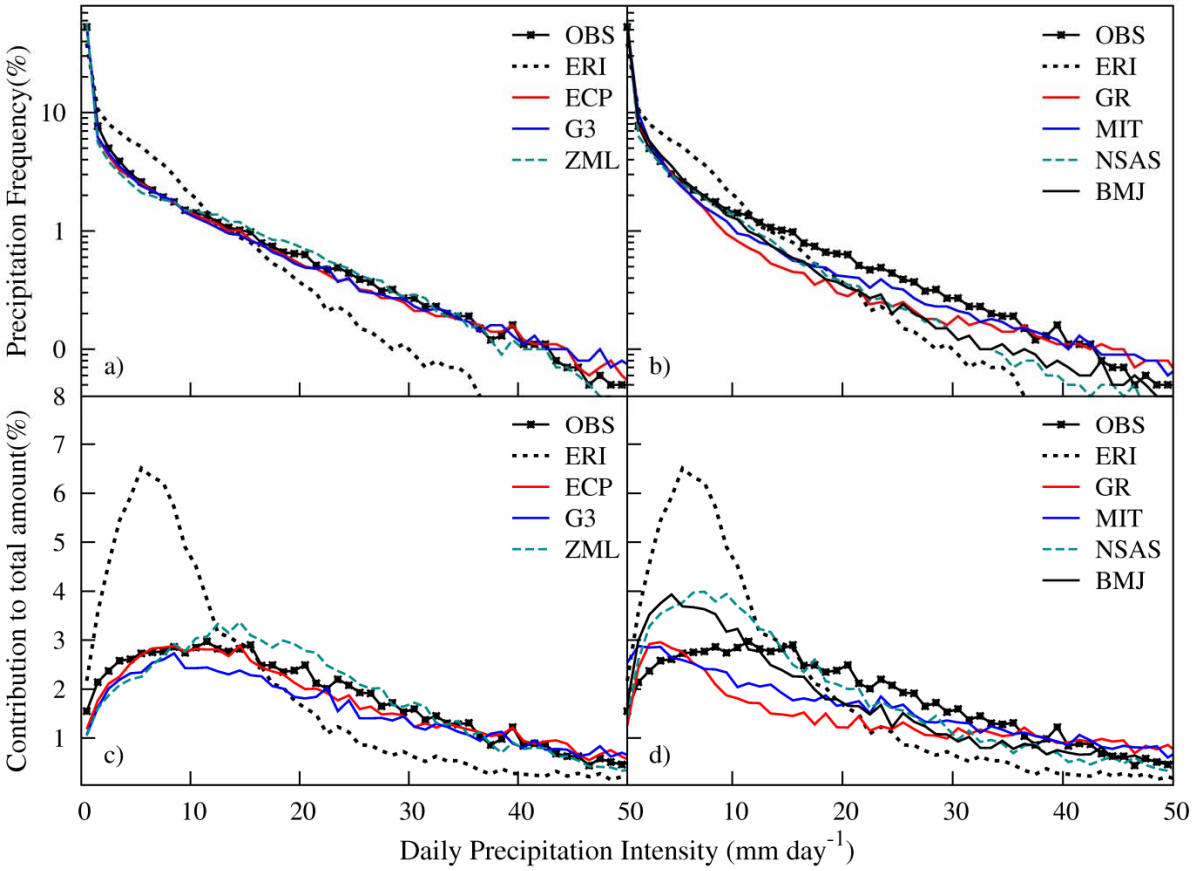

Figure 5.4 Frequency distributions (a, b, in logarithm scales) of 1993 summer daily precipitation and the relative contribution to total amount (c, d) from each unit binned precipitation (1mm day^{-1}) for all grids over the Central U.S. as observed (OBS), and simulated by the CWRF using seven different cumulus schemes (ECP, G3, ZML, GR, MIT, NSAS, BMJ).

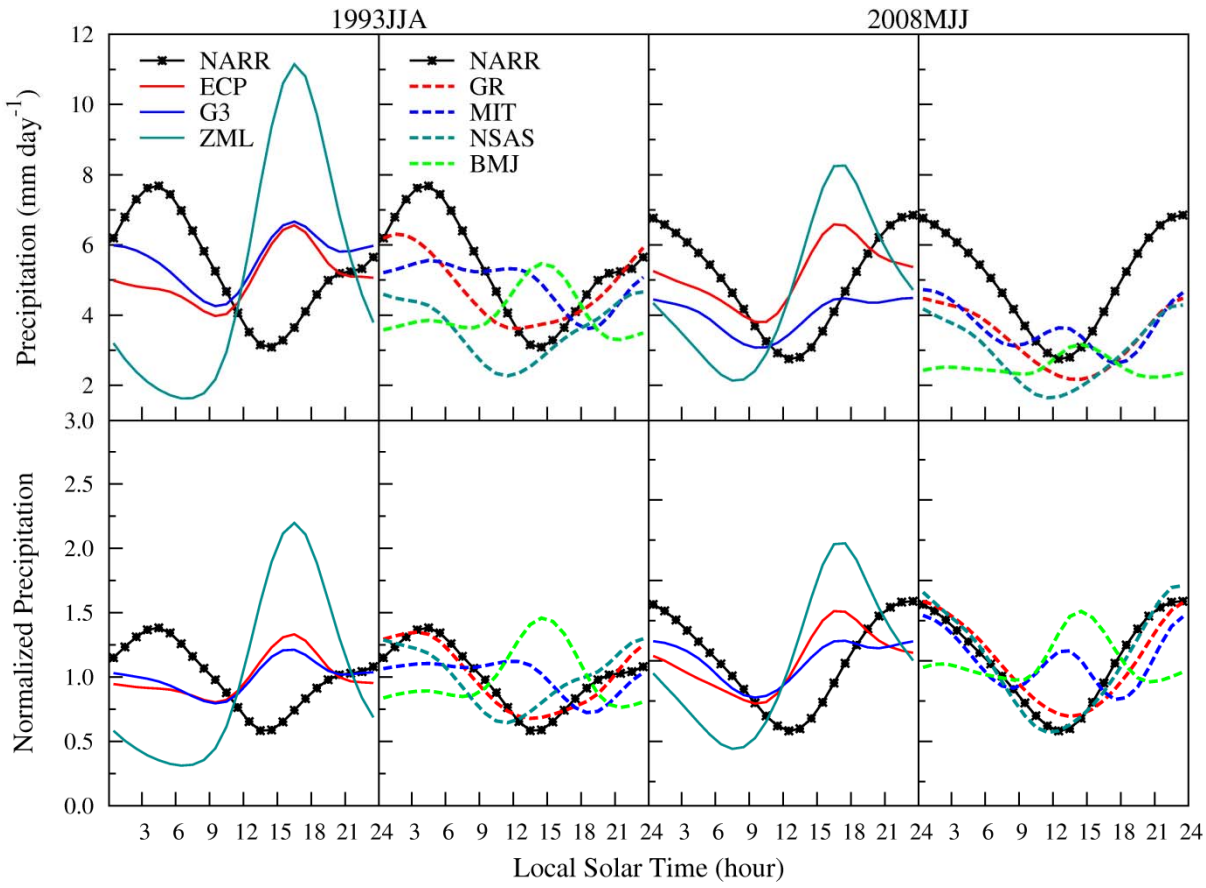

Figure 5.5 Mean diurnal evolution (relative to local solar time) of hourly (mm day^{-1}, *upper panels*) and normalized hourly rainfall (*bottom panels*) averaged over the Central U.S. for 1993 JJA (June-August) and 2008 MJJ (May- July) simulated by the CWRF using seven different cumulus schemes (ECP, G3, ZML, GR, MIT, NSAS, BMJ) compared with the NARR.

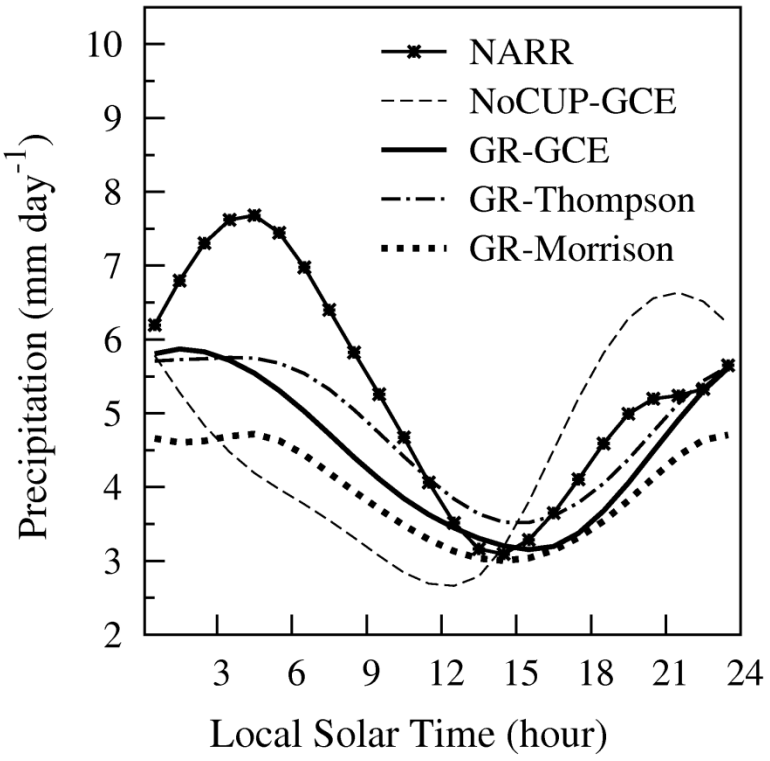

Figure 5.6 1993 summer mean diurnal evolution (relative to local solar time) of (mm day^{-1}) rainfall averaged over the Central U.S. simulated by the CWRF using the Grell cumulus scheme with three different microphysics including the Goddard Cumulus Ensemble (GR-GCE), the New Thompson (GR-Thompson) and the Morrison (GR-Morrison) schemes, as compared to the simulation without the Grell cumulus scheme (NoCUP-GCE) and the NARR as observation.

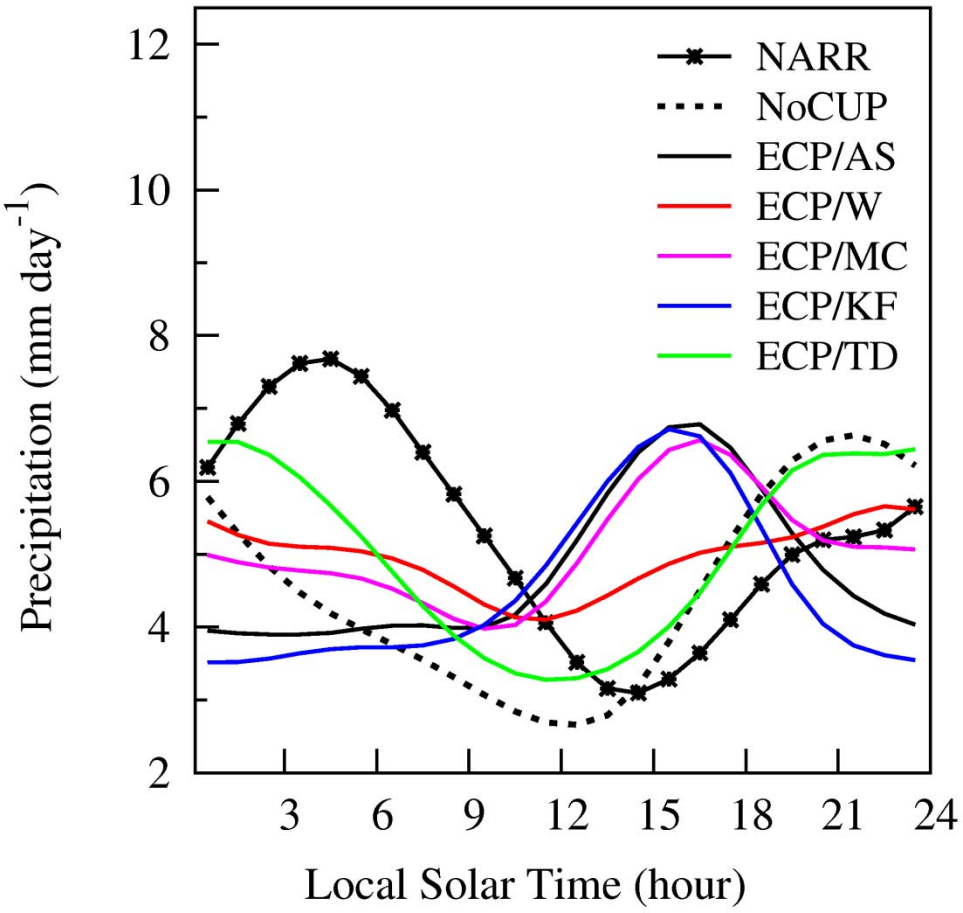

Figure 5.7 1993 summer mean precipitation diurnal cycle (mm day^{-1}, local solar time) averaged over the Central U.S. as observed (NARR) and simulated by the CWRF using the ECP scheme with five different closures (AS, W, MC, KF, TD) compared to the simulation without cumulus parameterization (NoCUP).

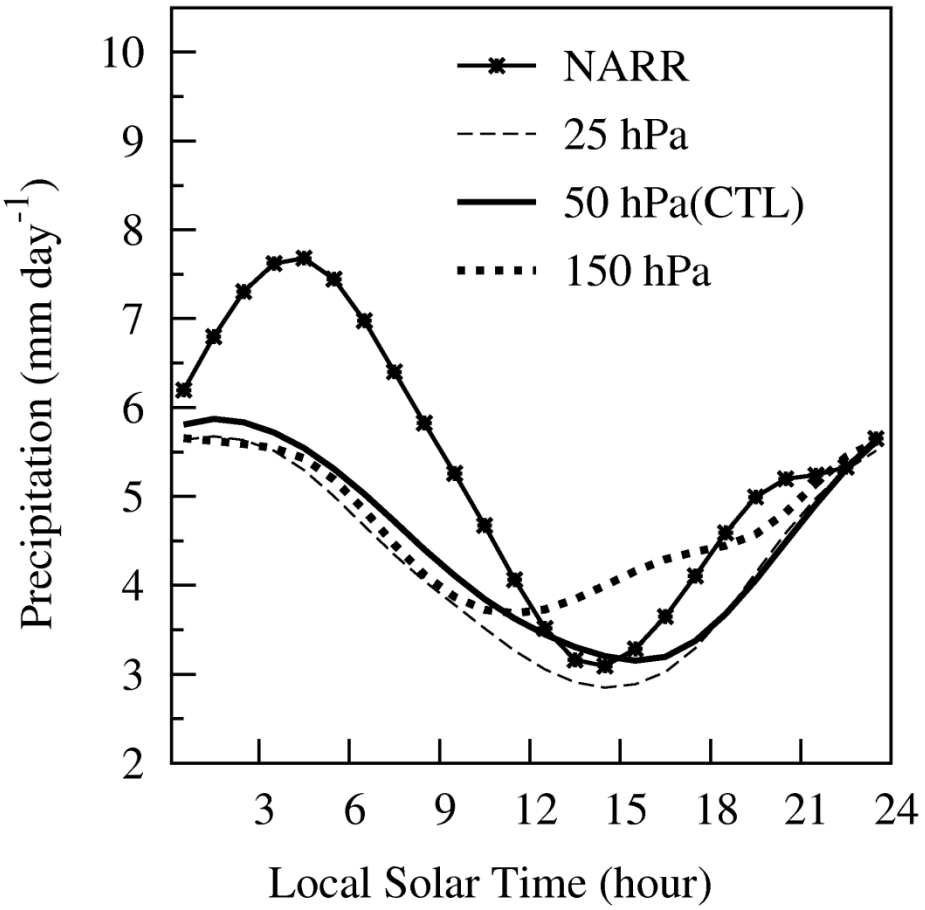

Figure 5.8 1993 summer mean precipitation diurnal cycle (mm day^{-1}, local solar time) averaged over the Central U.S. as observed (NARR) and simulated by the CWRF using the Grell cumulus scheme with three different lifting depth triggers including 25 hPa, 50 hPa (CTL, control) and 150 hPa.

CHAPTER 6: CONCLUSIONS AND FUTURE WORK

6.1. Conclusions

This research aims to improve the CWRF summer precipitation prediction over the continental U.S and adjacent coastal oceans that distinguishes three key characteristics: geographic variation of total/mean amount, precipitation frequency and intensity, and rainfall diurnal cycle. The focus is to systematically evaluate the effects of cumulus closure assumption, which is the core problem of current cumulus parameterizations.

This is facilitated by utilizing the ECP scheme incorporated in the CWRF. This scheme is built upon the parameterization framework of the G3 scheme but with numerous improvements. It includes five major cumulus closure assumptions with 16 different algorithms that consider the large-scale forcing perturbations from the surrounding nine grid points, while the G3 scheme contains four types of closures by removing the Quasi-Equilibrium assumption. Another important improvement is that the ECP scheme adds relative weights for those closures and considers regional dependence between land and oceans. Briefly, the five major closure assumptions are: 1) the AS closure assumes an instantaneous equilibrium between the large scale forcing and the convection by relaxing the cloud work function toward a climatological value, 2) the W closure assumes that net cloud base mass flux is determined by environmental mass flux averaged from the surrounding nine points at lower tropospheric levels, 3) the MC closure assumes convection develops to balance the column integrated moisture convergence, 4) the KF closure assumes the convection simply removes the total instability within a specified convective time scale, 5) the TD closure determines the convection by the increase rate of instability.

A series of CWRF simulations using the ECP scheme with these different cumulus closures are conducted over the continental U.S. and adjacent oceans separately. Results reveal the

characteristic behavior of individual closure assumptions over different regimes at various time scales (seasonal, daily and diurnal). The outcome of this study not only helps explain the major precipitation modeling deficiencies and uncertainties in parameterizing the effects of cumulus convection, but also establishes the basis for further optimization of the ECP scheme if appropriate localized weights can be derived for certain optimal closures that complementarily capture the observed signals.

This research further compares the performance of CWRF using the ECP scheme and the other 11 CUP schemes in predicting the Central U.S. summer floods. It will greatly benefit the further improvement of the ECP scheme by adopting the advantages of other schemes, such as the GR scheme in capturing the Central U.S. nocturnal rainfall maxima. The major conclusions of this thesis are summarized below with future work proposed.

6.1.1. Effects on summer precipitation prediction over the U.S. coastal oceans

This study evaluates CWRF's ability to simulate the summer precipitation variations over the U.S. coastal oceans, focusing on the effects of cumulus parameterization closure assumptions regarding three key precipitation characteristics. The CWRF integrations utilizing the ECP scheme with five ensemble closures (AS, W, MC, KF, and TD) are performed for three summers (2008, 2003, 1999) when abnormally heavy rainfall occurred over the key coastal ocean areas: the north and south portion of U.S. Atlantic Coast and the Gulf of Mexico.

Results show that none of the five ensemble closures can fully represent all the observed precipitation features. The AS, KF, and MC closures overpredict the occurrence of rainy days and more likely produce widespread large wet biases along the entire coastal oceans. The W closure better captures the major rainband along the U.S. Atlantic Coast, but overestimates the

rainy days and total amounts further east. On the other hand, the TD closure is most capable of capturing the diurnal phases but systematically underestimates the rainfall amount.

Further experiments using the ECP scheme with 16 subensemble closure algorithms show that the algorithms based on the average vertical velocity at cloud base (W_2) and moisture convergence (MC_3) complementarily reproduce the observed precipitation pattern and amount, and perform better than other closures in capturing the frequency of heavy rainfall events. For the diurnal cycle, the instability tendencies closures are superior in capturing the rainfall diurnal phase but with much larger deficits. All of these findings suggest that the vertical velocity at cloud base and the moisture convergence are the primary factors controlling precipitation seasonal mean and daily variation, while the instability tendency plays a more critical role in regulating the diurnal phase. Our findings are supported by previous studies that have suggested the large-scale ascent as an important dynamical control of precipitation occurrence in the Tropics (Barlow et al. 1998) and the moisture flux convergence as a significant contributor to U.S. daily precipitation variations (Becker et al. 2009).

The large disparities of model biases among various cumulus closures directly arise from their formulations in computing the cloud base mass flux. The ECP closures can be categorized as two major groups that differ in cloud base mass flux magnitude. One group with larger magnitude encompasses all the closure algorithms that generally produce excessive precipitation, while the other group that systematically has smaller cloud base mass flux tends to generate precipitation deficits.

Cumulus closures affect the coastal ocean precipitation simulation mainly through their impacts on the atmospheric instability and wind structures. In particular, the W_2 generates a narrow band of upward motion, CAPE tongue and convective precipitation, but the MC_3

produces a widespread distribution of stronger upward motion and convective precipitation associated with a wide CAPE tongue. It explains why the W_2 most realistically captures the spatial distribution of major rainband but with insufficient amount, while the MC_3 improves the precipitation amount but with unrealistically widespread pattern.

6.1.2. Effects on summer precipitation prediction over the continental U.S.

This study utilizes the ECP scheme incorporated in the CWRF model to evaluate the effects of cumulus closure assumptions on the continental U.S. summer precipitation prediction. The evaluation is concentrated on three key regions including the Central U.S., the NAM, and the Southeast U.S. where the summer rainfall exhibits large interannual variability and is highly sensitive to the cumulus parameterization. Three summers (1993, 2003, 2006) are chosen because they represent distinguished hydrological climate conditions over the above three key regions. By implementing the CWRF integrations using the ECP scheme with five different ensemble closures separately to these summer cases, several important model deficiencies and typical characteristics associated with these cumulus closures are identified.

First, cumulus closure effects alone could largely explain the model sensitivity to certain CUPs in summer mean precipitation simulations over the continental U.S. For instance, the KF closure consistently produces large wet biases over the NAM and Southeast U.S. and strong deficit over the Central U.S., explaining the systematic errors suggested by Liang et al. (2004) related to the Kain-Fritsch scheme using the same closure. Conversely, the TD closure systematically has large deficits over the Southeast U.S., but small biases over the Central U.S. and NAM. This is also consistent with the biases in the CMM5 simulation using the Grell cumulus scheme that is based on a similar closure with the instability tendency assumption.

Second, cumulus closures have different impacts on the summer mean precipitation and daily variation over the continental U.S., depending upon the climate regimes. The MC closure most realistically reproduces the summer precipitation mean and daily variability over the Central U.S., but overestimates the rainfall amount over the NAM and Southeast U.S. However, these wet biases over the latter two regions can be significantly reduced by using the W closure. These results suggest that the moisture convergence primarily controls the Central U.S. summer precipitation pattern and daily variability, but the low-level wind convergence and associated upward velocity is a good candidate depicting the major physical process which organizes the mesoscale deep convection and precipitation over the NAM and Southeast U.S.

Third, cumulus closures significantly affect the combination of daily rainfall frequency and intensity, depending upon the region. Both the W and MC closures have advantages over others in capturing the frequency distribution of heavy rain events over the continental U.S. and Northern Mexico, but mainly differ in their predictions from the light and medium rainfall events. A robust signal is that the MC closure shows clear superiority in reproducing the Central U.S. daily rainfall frequency distributions.

Fourth, cumulus closures fundamentally differ in representing the interactions between the subgrid convection and the large-scale forcing, leading to distinct predictive skills in capturing the key regional diurnal variations. The AS, KF, and MC closures all fail to produce the nocturnal maxima over the Central U.S. and produce locked diurnal precipitation peaks at around 15 PM LST over the three key regions. However, the TD closure more likely depicts the observed nocturnal rainfall maximum over the Central U.S., but poorly simulates the diurnal phase over the NAM and strongly underestimates the rainfall peak amount over the Southeast U.S., while the KF closure qualitatively captures the diurnal timing but overestimates the peak

magnitude over the NAM. All the cumulus closures did not accurately predict the diurnal phase over the Southeast U.S. Further improvements in the simulation of diurnal cycle may require refining critical triggers functions such as the convective initiation level and the relaxation time scale.

Detailed comparison of the 16 subensemble algorithms with their corresponding ensemble closures shows that the W ensemble closure has overall superior in reproducing the U.S. summer mean status, although the averaged moisture convergence (MC_3) greatly reduces the biases in the MC ensemble. The MC_3 subensemble complements the W ensemble on the daily variation prediction for the dry and wet events over the Southeast U.S. This implies that in future work, enhanced predictive skills for daily variability over different climate regimes can be achieved if specific localized weights for these closures are derived.

6.1.3. Sensitivity of Central U.S. summer floods prediction to cumulus parameterization

This study comprehensively evaluates the CWRF performance using 12 popular CUP schemes in predicting the summer precipitation over the Central U.S. In particular, the moisture convergence and the averaged cloud-base vertical velocity closure assumptions are separately applied in the ECP over land and oceans. Those two closures are identified with advantages over other closures by previous sensitivity experiments in predicting the Central U.S. summer rainfall and coastal oceans, respectively.

Results show that these CUP schemes have distinctive skills in predicting the U.S. summer mean precipitation distribution, with strong regional dependence. The seven CUP schemes are identified with complementary regime dependences in the prediction of summer rainfall pattern and amount. One group including the ECP, G3, and ZML schemes tends to have advantages over others in reproducing the Central U.S. floods location and amount, but with large model

disparities in other U.S. regions and adjacent coastal oceans. Particularly, the ECP scheme most realistically reproduces the Central U.S. floods and greatly reduces the wet biases in the G3 and ZML schemes along the U.S. coastal oceans. The second group including the BMJ, GR, MIT and NSAS schemes shows superiority in simulating the general pattern of U.S. summer precipitation, but tends to produce large dry biases over the Central U.S. Further comparison of daily rainfall statistics shows that the CUP schemes significantly affect the CWRF prediction of the Central U.S. summer daily precipitation variation and frequency distributions. The ECP most realistically reproduces the regional mean daily variation and the overall frequency distribution of daily precipitation.

Most CUP schemes fail to reproduce the observed nocturnal rainfall maxima over the Central U.S. An encouraging finding is that the GR scheme is superior in reproducing the Central U.S. diurnal amplitudes and phases. The large-scale precipitation tends to have stronger but much earlier rainfall peaks, while the inclusion of GR scheme effectively regulates the diurnal phase by postponing the rainfall peak from late evening to early morning in a better alignment with observations. The diurnal timing simulated by the GR scheme is insensitive to the choice of microphysics schemes, implying that large-scale resolved precipitation primarily contributes to the rainfall peak amount and the diurnal amplitude but hardly affects the diurnal phase.

Replacing the moisture convergence closure in the ECP scheme with the instability tendency closure that is also used in the GR scheme greatly improves the ECP simulated diurnal cycle by generating a nocturnal rainfall peak. This suggests that the advantage of the GR scheme is primarily due to its closure assumption in which the convection is determined by the instability tendency. In addition, the lifting depth trigger in the GR cumulus scheme also affects the Central

U.S. diurnal cycle simulation by mainly suppressing the daytime convection, consistent with the study by Lee et al. (2008).

6.2. Future work

This research explicitly illustrates the regime dependence of the ECP cumulus closure assumptions in predicting summer precipitation variations at different time scales over the U.S. land and coastal oceans. Although several closures have been identified to have advantages or complementary effects over others in realistically predicting certain observed precipitation feature(s) in specific region(s), it is still a challenge for CWRF with the ECP scheme to fully capture all the observed precipitation features. Future work will attempt to enhance the predictive skills of the ECP scheme by developing an optimized ensemble method for closures or by refining other physical processes such as convective triggers, entrainment/detrainment, and shallow cumulus convection.

First, the ECP scheme can be further optimized by deriving specific weights for the optimal closures that have been identified from this research for a more realistic prediction of overall summer mean rainfall distribution. For instance, the closures based on the average vertical velocity at cloud-base (W_2) and moisture convergence (MC_3) complementarily capture the U.S. coastal ocean rainfall patterns and amounts. On the other hand, the moisture convergence (MC) closure realistically reproduces the Central U.S. summer rainfall pattern and amount, but generates wet biases over the NAM and Southeast U.S., which can be greatly reduced by using the ensemble cloud-base vertical velocity (W) closure. In Liang et al. (2007), an optimal ensemble based on two CUP schemes that are strongly complementary in simulating certain observed signals can produce a more skillful result overall regarding the interannual anomaly

and climate mean precipitation. Therefore, the complementary advantages of these four closures provide an opportunity to develop an optimized ensemble method that incorporates varying weights to account for their regional differences.

Second, the instability tendency assumption can be added as an additional trigger function in the ECP scheme to improve the prediction of daily precipitation frequency distribution and diurnal phase over the U.S. coastal oceans. The W_2 and MC_3 closures both overpredict the total number of rainy days and produce earlier rainfall peaks compared to TRMM observations, despite the fairly realistic pattern and amount of summer mean precipitation. However, the averaged instability tendency closure generates much fewer rainy days and better reproduces the diurnal phase. By including this assumption, it is likely to inhibit the convection occurrence, leading to improvements in precipitation predictions in terms of frequency distributions and diurnal cycles.

Third, the ECP simulation of summer rainfall diurnal cycle over several key regions in the continental U.S. warrants further investigation. This research has suggested that the instability tendency closure in the GR scheme plays a dominant role in regulating the Central U.S. rainfall diurnal variation. Xie et al. (2004) also implemented a convective trigger function that utilizes this assumption to effectively reduce the frequent occurrence of daytime convection. As such, more efforts in the future will be made to incorporate the instability tendency assumption as trigger function in the ECP scheme over the land in order to improve its diurnal cycle simulation. But all the cumulus closures could not accurately predict the diurnal phase over the Southeast U.S. Future studies will examine whether other CUP schemes are superior in realistically reproducing the afternoon rainfall peaks over this region, and thereby improve the ECP scheme by including the corresponding mechanisms.

Fourth, this research focuses on examining the deep cumulus closure effects. However, it is also imperative to examine the effects of entrainment/detrainment rate or shallow convection on the precipitation prediction. Previous studies have suggested that the enhanced entrainment rate tends to increase convective plume dilution and prolongs the development of deep convection, resulting in reduced convective precipitation and delayed rainfall maxima (Tiedtke 1989; Bechtold et al. 2004; Wang et al. 2007). Such effects can be studied by conducting sensitivity experiments using the ECP scheme with various entrainment rates. Furthermore, the shallow convection can regulate the morning development of PBL and thus may act as a precondition that prevents deep cumulus from occurring too often or too early (Wang et al. 2007). This may affect either precipitation frequency or diurnal cycle over the land or oceans.

It is notable that the difficulties in accurately predicting the precipitation diurnal cycle regarding both the phase and magnitude could also be caused by the deficiencies in other related physical processes, such as land or ocean surface, the planetary boundary layer, and microphysics. Dai and Trenberth (2004) have suggested that many of the diurnal variations associated with the above processes could not be realistically captured by current GCMs, implying that improvements of diurnal cycle simulation also require a better understanding and representation of the interactions between these physical processes.

REFERENCES

Arakawa, A., 2004: The cumulus parameterization problem: Past, present, and future. *J. Climate*, **17**, 2493–2525.

Arakawa, A., and W. H. Schubert, 1974: Interaction of a Cumulus Cloud Ensemble with the Large-Scale Environment, Part I. *J. Atmos. Sci.*, **31**, 674–701.

Barlow, M., S. Nigam, and E. H. Berbery, 1998: Evolution of the North American Monsoon System. *J. Climate*, **11**, 2238–2257.

Bechtold, P., J.-P. Chaboureau, A. beljaars, A.K. Betts, M. Köhler, M. Miller, and J.-L. Redelsperger, 2004: The simulation of the diurnal cycle of convective precipitation over land in a global model. *Quart. J. Roy. Meteor. Soc.*, **130**, 3119–3137.

Becker, E. J., E. H. Berbery, and R. W. Higgins, 2009: Understanding the characteristics of daily precipitation over the United States Using the North American Regional Reanalysis. *J. Climate*, **22**, 6268–6286.

Beljaars, A. C. M., P. Viterbo, M. J. Miller, and A. K. Betts, 1996: The Anomalous Rainfall over the United States during July 1993: Sensitivity to Land Surface Parameterization and Soil Moisture Anomalies. *Mon. Wea. Rev.*, **124**, 362–383.

Bell, G. D., and J. E. Janowiak, 1995: Atmospheric Circulation Associated with the Midwest Floods of 1993. *Bull. Amer. Meteor. Soc.*, **76**, 681–695.

Betts, A. K., and M. J. Miller, 1986: A new convective adjustment scheme. Part II: Single column tests using GATE wave, BOMEX, and arctic air-mass data sets. *Quart. J. Roy. Meteor. Soc.*, **112**, 693–709.

Betts, A.K., 1986: A new convective adjustment scheme. Part I: Observational and theoretical basis. *Quart. J. Roy. Meteor. Soc.*, **112**, 677–691.

Bosilovich, M. G., and W. Sun, 1999: Numerical Simulation of the 1993 Midwestern Flood: Land–Atmosphere Interactions. *J. Climate*, **12**, 1490–1505.

Bretherton, Christopher S., Sungsu Park, 2009: A New Moist Turbulence Parameterization in the Community Atmosphere Model. *J. Climate*, **22**, 3422–3448.

Brown, J. M., 1979: Mesoscale unsaturated downdrafts driven by rainfall evaporation: A Numerical Study. *J. Atmos. Sci.*, **36**, 313–338.

Chen, M., W. Shi, P. Xie, V. B. S. Silva, V. E. Kousky, R. W. Higgins, and J. E. Janowiak, 2008: Assessing objective techniques for gauge-based analyses of global daily precipitation. *J. Geophys. Res.*, **113**, 13 PP.

Choi, H.I., and X.-Z. Liang, 2010: Improved terrestrial hydrologic representation in mesoscale land surface models. *J. Hydrometeorology*, **11**, 797–809.

Choi, H.I., P. Kumar, and X.-Z. Liang, 2007: Three-dimensional volume-averaged soil moisture transport model with a scalable parameterization of subgrid topographic variability. *Water Resour. Res.*, **43**, W04414, doi:10.1029/2006WR005134, 15pp.

Chou, M.-D., and M.J. Suarez, 1999: A solar radiation parameterization for atmospheric studies. [Last revision on March 2002] *Technical Report Series on Global Modeling and Data Assimilation*, M.J. Suarez (Ed.), NASA/TM-1999-104606, Vol. 15, Goddard Space Flight Center, Greenbelt, MD, 42 pp.

Chou, M.-D., M.J. Suarez, X.-Z. Liang, and M.M.-H. Yan, 2001: A thermal infrared radiation parameterization for atmospheric studies. [Last revision on July 2002] *Technical Report*

Series on Global Modeling and Data Assimilation, M.J. Suarez (Ed.), NASA/TM-2001-104606, Vol. 19, Goddard Space Flight Center, Greenbelt, MD, 56 pp.

Covey, C., K. M. AchutaRao, U. Cubasch, P. Jones, S. J. Lambert, M. E. Mann, T. J. Phillips, and K. E. Taylor, 2003: An overview of results from the Coupled Model Intercomparison Project. *Global Planet. Change*, **37**, 103–133.

Dai, A., 1999: Recent changes in the diurnal cycle of precipitation over the United States. *Geophys. Res. Lett.*, **26**, 341–344.

Dai, A., 2006: Precipitation Characteristics in Eighteen Coupled Climate Models. *J. Climate*, **19**, 4605–4630, doi:10.1175/JCLI3884.1.

Dai, A., and K. E. Trenberth, 2004: The Diurnal cycle and its depiction in the Community Climate System Model. *J. Climate*, **17**, 930–951.

Dai, F., R. Yu, X. Zhang, Y. Yu, and J. Li, 2003: The impact of low-level cloud over the eastern subtropical Pacific on the "double ITCZ" in LASG FGCM-0, *Adv. Atmos. Sci.*, **20**(3), 461-467.

Daly, C., M. Halbleib, J.I. Smith, W.P. Gibson, M.K. Doggett, G.H. Taylor, J. Curtis, and P.A. Pasteris, 2008: Physiographically-sensitive mapping of temperature and precipitation across the conterminous United States. *Int. J. Climatol.*, **28**, 2031–2064.

Davis, C. A., K. W. Manning, R. E. Carbone, S. B. Trier, and J. D. Tuttle, 2003: Coherence of Warm-Season Continental Rainfall in Numerical Weather Prediction Models. *Mon. Wea. Rev.*, **131**, 2667–2679.

Delworth, T., R. Stouffer, K. Dixon, M. Spelman, T. Knutson, A. Broccoli, P. Kushner, and R. Wetherald, 2002: Review of simulations of climate variability and change with the GFDL R30 coupled climate model. *Climate Dyn.*, **19**, 555–574.

Dirmeyer, P. A., and J. L. Kinter, 2010: Floods over the U.S. Midwest: A Regional Water Cycle Perspective. *J. Hydrometeorology*, **11**, 1172–1181.

Donner, L., C. J. Seman, R. S. Hemler, and S. Fan, 2001: A cumulus parameterization including mass fluxes, convective vertical velocities, and mesoscale effects: Thermodynamic and hydrological aspects in a general circulation model. *J. Climate*, **14**, 3444–3463.

Donner, L.J., 1993: A cumulus parameterization including mass fluxes, vertical momentum dynamics, and mesoscale effects. *J. Atmos. Sci.*, **50**, 889–906.

Emanuel, K.A., 1991: A scheme for representing cumulus convection in Large-Scale models. *J. Atmos. Sci.*, **48**, 2313–2335.

Emanuel, K.A., and M. Živković-Rothman, 1999: Development and evaluation of a convection scheme for use in climate models. *J. Atmos. Sci.*, **56**, 1766–1782.

Fletcher, Jennifer K., Christopher S. Bretherton, 2010: Evaluating boundary layer–based mass flux closures using cloud-resolving model simulations of deep convection. *J. Atmos. Sci.*, **67**, 2212–2225.

Fowler, L.D., and D.A. Randall, 2002: Interactions between cloud microphysics and cumulus convection in the CSU general circulation model. *J. Atmos. Sci.*, **59**, 3074–3098.

Frank, W. M., and C. Cohen, 1987: Simulation of Tropical Convective Systems. Part I: A Cumulus Parameterization. *J. Atmos. Sci.*, **44**, 3787–3799.

Fu, Rong, Anthony D. Del Genio, William B. Rossow, 1994: Influence of ocean surface conditions on atmospheric vertical thermodynamic structure and deep convection. *J. Climate*, **7**, 1092–1108.

Giorgi, F., and C. Shields, 1999: Tests of precipitation parameterizations available in latest version of NCAR regional climate model (RegCM) over continental United States. *J. Geophys. Res.*, **104**, 6353–6375.

Gochis, D. J., W. J. Shuttleworth, and Z.-L. Yang, 2002: Sensitivity of the Modeled North American Monsoon Regional Climate to Convective Parameterization. *Mon. Wea. Rev.*, **130**, 1282–1298.

Groisman, P. Y., R. W. Knight, and T. R. Karl, 2012: Changes in Intense Precipitation over the Central United States. *J. Hydrometeor.*, **13**, 47–66.

Grell, G. A., 1993: Prognostic evaluation of assumptions used by cumulus parameterizations. *Mon. Wea. Rev.*, **121**, 764–787.

Grell, G. A., and D. Dévényi, 2002: A generalized approach to parameterizing convection combining ensemble and data assimilation techniques. *Geophys. Res. Lett.*, **29**, 4 PP., doi:200210.1029/2002GL015311.

Grell, Georg A., Ying-Hwa Kuo, Richard J. Pasch, 1991: Semiprognostic Tests of Cumulus Parameterization Schemes in the Middle Latitudes. *Mon. Wea. Rev.*, **119**, 5–31.

Han, Jongil, Hua-Lu Pan, 2011: Revision of Convection and Vertical Diffusion Schemes in the NCEP Global Forecast System. *Wea. Forecasting*, **26**, 520–533.

Henderson, K.G. and A.J. Vega, 1996: Regional Precipitation Variability in the Southern United States. *Physical Geography* **17**, 93-112.

Hennessy, K. J., J. M. Gregory, and J. F. B. Mitchell, 1997: Changes in daily precipitation under enhanced greenhouse conditions. *Climate Dyn.*, **13**, 667–680.

Higgins, R. W., J. E. Janowiak, and Y.-P. Yao, 1996: A gridded hourly precipitation data base for the United States (1963-1993). NCEP/Climate Prediction Center Atlas 1, National Centers for Environmental Prediction, 46pp.

Higgins, R. W., K. C. Mo, and Y. Yao, 1998: Interannual Variability of the U.S. Summer Precipitation Regime with Emphasis on the Southwestern Monsoon. *J. Climate*, **11**, 2582–2606.

Iguchi, T., T. Kozu, R. Meneghine, J. Awaka, and K. Okamoto, 2000: Rain-profiling algorithm for the TRMM precipitation radar. *J. Appl. Meteor.*, **39**, 2038-2052.

Janjic, Z.I., 1994: The step-mountain eta coordinate model: further developments of the convection, viscous sublayer and turbulence closure schemes, *Mon. Wea. Rev.*, **122**, 927–945.

Janowiak, John E., Phillip A. Arkin, Mark Morrissey, 1994: An examination of the diurnal cycle in oceanic tropical rainfall using satellite and in situ data. *Mon. Wea. Rev.*, **122**, 2296–2311.

Kahn, R.A., B.J. Gaitley, J.V. Martonchik, D.J. Diner, K.A. Crean, and B. Holben, 2005: Multiangle Imaging Spectroradiometer (MISR) global aerosol optical depth validation based on 2 years of coincident Aerosol Robotic Network (AERONET) observations. *J. Geophys. Res.*, **110**, D10S04, doi:10:1029/2004JD004706.

Kain, J. S., 2004: The Kain–Fritsch Convective Parameterization: An Update. *J. Appl. Meteor.*, **43**, 170–181.

Kain, J. S., and J. M. Fritsch, 1993: Convective parameterization for mesoscale models: The Kain-Fritcsh scheme. In *The Representation of Cumulus Convection in Numerical Models*, K.A. Emanuel and D.J. Raymond (eds.), *Amer. Meteor. Soc.*, 246pp.

Karl, T. R., and R. W. Knight, 1998: Secular Trends of Precipitation Amount, Frequency, and Intensity in the United States. *Bull. Amer. Meteor. Soc.*, **79**, 231–241.

Koster, R. D., and M. J. Suarez, 1995: Relative contributions of land and ocean processes to precipitation variability. *J. Geophys. Res.*: Atmospheres, **100**, 13775–13790.

Krishnamurti, T. N., S. Low-Nam, and R. Pasch, 1983: Cumulus parameterization and rainfall rates II. *Mon. Wea. Rev.*, **111**, 815–828.

Kunkel, K. E., S. A. Changnon, and J. R. Angel, 1994: Climatic Aspects of the 1993 Upper Mississippi River Basin Flood. *Bull. Amer. Meteor. Soc.*, **75**, 811–822.

Kunkel, K. E., D. R. Easterling, K. Redmond, and K. Hubbard, 2003: Temporal variations of extreme precipitation events in the United States: 1895–2000. *Geophys. Res. Lett.*, **30**, doi:10.1029/2003GL018052.

Kuo, H. L., 1974: Further Studies of the Parameterization of the Influence of Cumulus Convection on Large-Scale Flow. *J. Atmos. Sci.*, **31**, 1232–1240.

Kuo, Ying-Hwa, Richard A. Anthes, 1984: Semiprognostic Tests of Kuo–Type Cumulus Parameterization Schemes in an Extratropical Convective System. *Mon. Wea. Rev.*, **112**, 1498–1509.

Kuwano-Yoshida, A., S. Minobe, and S.-P. Xie, 2010: Precipitation Response to the Gulf Stream in an Atmospheric GCM. *J. Climate*, **23**, 3676–3698.

Lee, M.-I. and Coauthors, 2007a: Sensitivity to Horizontal Resolution in the AGCM Simulations of Warm Season Diurnal Cycle of Precipitation over the United States and Northern Mexico. *J. Climate*, **20**, 1862–1881.

Lee, M.-I., S. D. Schubert, M. J. Suarez, T. L. Bell, and K.-M. Kim, 2007b: Diurnal cycle of precipitation in the NASA Seasonal to Interannual Prediction Project atmospheric general circulation model. *J. Geophys. Res.*, **112**, doi:10.1029/2006JD008346.

Lee, M.-I., S. D. Schubert, M. J. Suarez, J.-K. E. Schemm, H.-L. Pan, J. Han, and S.-H. Yoo, 2008: Role of convection triggers in the simulation of the diurnal cycle of precipitation over the United States Great Plains in a general circulation model. *J. Geophys. Res.*, **113**, 10 PP., doi:200810.1029/2007JD008984.

Leung, L. R., L. O. Mearns, F. Giorgi, and R. L. Wilby, 2003: Regional Climate Research. *Bull. Amer. Meteor. Soc.*, **84**, 89–95.

Liang, Xin-Zhong, Kenneth E. Kunkel, Arthur N. Samel, 2001: Development of a Regional Climate Model for U.S. Midwest Applications. Part I: Sensitivity to Buffer Zone Treatment. *J. Climate*, **14**, 4363–4378.

Liang, X.-Z., L. Li, A. Dai, and K.E. Kunkel, 2004a: Regional climate model simulation of summer precipitation diurnal cycle over the United States. *Geophys. Res. Lett.*, **31**, L24208, doi:10.1029/2004GL021054.

Liang, X.-Z., L. Li, K.E. Kunkel, M. Ting, and J.X.L. Wang, 2004b: Regional climate model simulation of U.S. precipitation during 1982-2002. Part 1: Annual cycle. *J. Climate*, **17**, 3510–3528.

Liang, X.-Z., M. Xu, W. Gao, K.E. Kunkel, J. Slusser, Y. Dai, Q. Min, P.R. Houser, M. Rodell, C.B. Schaaf, and F. Gao, 2005: Development of land surface albedo parameterization bases on Moderate Resolution Imaging Spectroradiometer (MODIS) data. *J. Geophys. Res.*, **110**, D11107, doi:10.1029/2004JD005579.

Liang, X.-Z., J. Pan, J. Zhu, K. E. Kunkel, J. X. L. Wang, and A. Dai, 2006: Regional climate model downscaling of the U.S. summer climate and future change. *J. Geophys. Res.*, **111**, D10108, doi:10.1029/2005JD006685.

Liang, X.-Z., M. Xu, K. E. Kunkel, G. A. Grell, and J. S. Kain, 2007: Regional climate model simulation of U.S.–Mexico summer precipitation using the optimal ensemble of two cumulus parameterizations. *J. Climate*, **20**, 5201–5207.

Liang, X.-Z., M. Xu, X. Yuan, T. Ling, H.I. Choi, F. Zhang, L. Chen, S. Liu, S. Su, F. Qiao, Y. He, J.X.L. Wang, K.E. Kunkel, W.Gao, E. Joseph, V. Morris, T.-W. Yu, J. Dudhia, and J. Michalakes, 2012: Regional Climate-Weather Research and Forecasting Model (CWRF). *Bull. Amer. Meteor. Soc.*, 120404072510007, doi:10.1175/BAMS-D-11-00180.1.

Lin, Chichung, Akio Arakawa, 1997: The Macroscopic Entrainment Processes of Simulated Cumulus Ensemble. Part II: Testing the Entraining-Plume Model. *J. Atmos. Sci.*, **54**, 1044–1053.

Lin, Jia-Lin, 2007: The Double-ITCZ Problem in IPCC AR4 Coupled GCMs: Ocean–Atmosphere Feedback Analysis. *J. Climate*, **20**, 4497–4525.

Lin, J.-T., D. Youn, X.-Z. Liang, and D. J. Wuebbles, 2008: Global model simulation of summertime U.S. ozone diurnal cycle and its sensitivity to PBL mixing, spatial resolution, and emissions. *Atmospheric Environment*, **42**, 8470–8483.

Lin, Y.-L., R. D. Farley, and H. D. Orville, 1983: Bulk Parameterization of the Snow Field in a Cloud Model. *J. Climate Appl. Meteor.*, **22**, 1065–1092.

Ling, T.-J., X.-Z. Liang，M. Xu，Z. Wang，and B. Wang, 2010: A multilevel ocean mixed-layer model for 2-dimension applications. Acta Oceanologica Sinica (submitted).

Lord, S. J., W. C. Chao, and A. Arakawa, 1982: Interaction of a Cumulus Cloud Ensemble with the Large-Scale Environment. Part IV: The Discrete Model. *J. Atmos. Sci.*, **39**, 104–113.

Ma, Chung-Chun, Carlos R. Mechoso, Andrew W. Robertson, Akio Arakawa, 1996: Peruvian Stratus Clouds and the Tropical Pacific Circulation: A Coupled Ocean-Atmosphere GCM Study. *J. Climate*, **9**, 1635–1645.

Maloney, E. D., and D. L. Hartmann, 2001: The sensitivity of intraseasonal variability in the NCAR CCM3 to changes in convective parameterization. *J. Climate*, **14**, 2015–2034.

Manabe, S., J. Smagorinsky, R. F. Strickler, 1965: Simulated climatology of a general circulation model with a hydrological cycle. *Mon. Wea. Rev.*, **93**, 769–798.

Mesinger, F. and Coauthors, 2006: North American Regional Reanalysis. *Bull. Amer. Meteor. Soc.*, **87**, 343–360.

Minobe, S., A. Kuwano-Yoshida, N. Komori, S.-P. Xie, and R. J. Small, 2008: Influence of the Gulf Stream on the troposphere. *Nature*, **452**, 206–209.

Mo, K. C., J. N. Paegle, and R. W. Higgins, 1997: Atmospheric Processes Associated with Summer Floods and Droughts in the Central United States. *J. Climate*, **10**, 3028–3046.

Molinari, John, Michael Dudek, 1992: Parameterization of Convective Precipitation in Mesoscale Numerical Models: A Critical Review. *Mon. Wea. Rev.*, **120**, 326–344.

Morrison, H., G. Thompson, and V. Tatarskii, 2009: Impact of Cloud Microphysics on the Development of Trailing Stratiform Precipitation in a Simulated Squall Line: Comparison of One- and Two-Moment Schemes. *Mon. Wea. Rev.*, **137**, 991–1007.

Murphy, J. M., D. M. H. Sexton, D.N. Barnett, G. S. Jones, M. J. Webb, M. Collins, and D. A. Stainforth, 2004: Quantification of modeling uncertainties in a large ensemble of climate change simulations. *Nature*, **430**, 768-772.

Neggers, R. A. J., A. P. Siebesma, G. Lenderink, and A. A. M. Holtslag, 2004: An Evaluation of Mass Flux Closures for Diurnal Cycles of Shallow Cumulus. *Mon. Wea. Rev.*, **132**, 2525–2538.

Nesbitt, S. W., and E. J. Zipser, 2003: The diurnal cycle of rainfall and convective intensity according to three years of TRMM measurements. *J. Climate*, **16**, 1456–1475.

Nordeng, T. E., 1995: Extended version of the convective parameterization scheme at ECMWF and their impact on the mean and transient activity of the model in the Tropics. ECMWF Research Department Tech. Memo. 2006, 41 pp.

Paegle, J., K. C. Mo, and J. Nogués-Paegle, 1996: Dependence of Simulated Precipitation on Surface Evaporation during the 1993 United States Summer Floods. *Mon. Wea. Rev.*, **124**, 345–361.

Paluch, Ilga R., 1979: The Entrainment Mechanism in Colorado Cumuli. *J. Atmos. Sci.*, **36**, 2467–2478.

Pan, D.-M., and D. A. Randall, 1998: A cumulus parameterization with a prognostic closure. *Quart. J. Roy. Meteor. Soc.*, **124**, 949–981.

Pan, H.-L., and W.-S. Wu, 1995: Implementing a mass flux convection parameterization package for the NMC Medium-Range Forecast Model, *NMC Office Note*, 409, 40 pp., Natl. Cent. for Environ. Predict., CampSprings, Md.

Park, S., and C.S. Bretherton, 2009: The University of Washington shallow convection and moist turbulence schemes and their impact on climate simulations with the Community Atmosphere Model. *J. Climate*, **22**, 3449–3469.

Randall, David, Marat Khairoutdinov, Akio Arakawa, Wojciech Grabowski, 2003: Breaking the Cloud Parameterization Deadlock. *Bull. Amer. Meteor. Soc.*, **84**, 1547–1564.

Raymond, David J., 1979: A Two-Scale Model of Moist, Non-Precipitating Convection. *J. Atmos. Sci.*, **36**, 816–831.

Raymond, David J., 1995: Regulation of Moist Convection over the West Pacific Warm Pool. *J. Atmos. Sci.*, **52**, 3945–3959.

Raymond, David J., Alan M. Blyth, 1986: A Stochastic Mixing Model for Nonprecipitating Cumulus Clouds. *J. Atmos. Sci.*, **43**, 2708–2718.

Reynolds, R. W., N. A. Rayner, T. M. Smith, D. C. Stokes, and W. Wang, 2002: An Improved In Situ and Satellite SST Analysis for Climate. *J. Climate*, **15**, 1609–1625.

Riehl, H., and J. S. Malkus, 1958: On the heat balance of the equatorial trough zone. *Geophysica*, **6**, 503-538.

Rontu, L., 2006: A study on parameterization of orography-related momentum fluxes in a synoptic-scale NWP model. *Tellus*, **58A**, 69–81.

Sato, T., H. Miura, M. Satoh, Y.N. Takayabu, and Y. Wang, 2009: Diurnal cycle of precipitation in the tropics simulated in aglobal cloud-resolving model. *J. Climate*, 22, 4809–4826.

Simpson, Joanne, 1971: On Cumulus Entrainment and One-Dimensional Models. *J. Atmos. Sci.*, **28**, 449–455.

Skamarock, W.C., J.B. Klemp, J. Dudhia, D.O. Gill, D.M. Barker, M.G. Duda, X.-Y. Huang, W. Wang, and J.G. Powers, 2008: *A Description of the Advanced Research WRF Version 3*. NCAR Technical Note, NCAR/TN-475+STR, 113 pp.

Sun, Y., S. Solomon, A. Dai, and R. W. Portmann, 2006: How Often Does It Rain? *J. Climate*, **19**, 916–934.

Takayabu, Yukari N., Shoichi Shige, Wei-Kuo Tao, Nagio Hirota, 2010: Shallow and deep latent heating modes over Tropical Oceans observed with TRMM PR spectral latent heating data. *J. Climate*, **23**, 2030–2046.

Takle, E.S., W.J. Gutowski Jr., R.W. Arritt, Z. Pan, C.J. Anderson, R.R. da Silva, D. Caya, S.-C. Chen, F. Giorgi, J.H. Christensen, S.-Y. Hong, H.-M.H. Juang, J. Katzfey, W.M. Lapenta, R. Laprise, G.E. Listen, P. Lopez, J. McGregor, R.A. Pielke Sr., and J.O. Roads, 1999: Project to intercompare regional climate simulations (PIRCS): Description and initial results. *J. Geophys. Res.*, **104**, 19443-19461.

Tao, W.-K, J. Simpson, D. Baker, S. Braun, M.-D. Chou, B. Ferrier, D. Johnson, A. Khain, S. Lang, B. Lynn, C.-L. Shie, D. Starr, C.-H. Sui, Y. Wang, and P. Wetzel, 2003: Microphysics, radiation and surface processes in the Goddard Cumulus Ensemble (GCE) model. *Meteor. Atmos. Phys.*, **82**, 97–137.

Taylor, Gregory R., Marcia B. Baker, 1991: Entrainment and Detrainment in Cumulus Clouds. *J. Atmos. Sci.*, **48**, 112–121.

Thompson, G., P. R. Field, R. M. Rasmussen, and W. D. Hall, 2008: Explicit Forecasts of Winter Precipitation Using an Improved Bulk Microphysics Scheme. Part II: Implementation of a New Snow Parameterization. *Mon. Wea. Rev.*, **136**, 5095–5115.

Tiedtke, M., 1989: A Comprehensive Mass Flux Scheme for Cumulus Parameterization in Large-Scale Models. *Mon. Wea. Rev.*, **117**, 1779–1800.

Ting, M., and H. Wang, 2006: The Role of the North American Topography on the Maintenance of the Great Plains Summer Low-Level Jet. *J. Atmos. Sci.*, **63**, 1056–1068.

Trenberth, K. E., A. Dai, R. M. Rasmussen, and D. B. Parsons, 2003: The Changing Character of Precipitation. *Bull. Amer. Meteor. Soc.*, **84**, 1205–1217.

Uppala, S.M., D.P. Dee, S. Kobayashi, P. Berrisford, and A.J. Simmons, 2008: Towards a climate data assimilation system: Status update of ERA-Interim. *ECMWF Newsletter,* **115**, 12–18.

Vellinga, M., and R. A. Wood, 2002: Global Climatic Impacts of a Collapse of the Atlantic Thermohaline Circulation. *Climatic Change*, **54**, 251–267.

Wagner, Till M., Hans-F. Graf, 2010: An Ensemble Cumulus Convection Parameterization with Explicit Cloud Treatment. *J. Atmos. Sci.*, **67**, 3854–3869.

Wang, Yuqing, Li Zhou, Kevin Hamilton, 2007: Effect of Convective Entrainment/Detrainment on the Simulation of the Tropical Precipitation Diurnal Cycle. *Mon. Wea. Rev.*, **135**, 567–585.

Wehner, M., R. Smith, G. Bala, and P. Duffy, 2010: The effect of horizontal resolution on simulation of very extreme US precipitation events in a global atmosphere model. *Climate Dyn.*, **34**, 241–247.

Wilcox, E. M., and L. J. Donner, 2007: The Frequency of Extreme Rain Events in Satellite Rain-Rate Estimates and an Atmospheric General Circulation Model. *J. Climate*, **20**, 53–69.

Wu, X., X.-Z. Liang, and G.J. Zhang, 2003: Seasonal migration of ITCZ precipitation across the equator: Why can't GCMs simulate it? *Geophys. Res. Lett.*, **30**, 1824, doi:10.1029/2003GL017198.

Xie, S., K.-M. Xu, R. T. Cederwall, P. Bechtold, A. D. D. Genio, S. A. Klein, D. G. Cripe, S. J. Ghan, D. Gregory, S. F. Iacobellis, S. K. Krueger, U. Lohmann, J. C. Petch, D. A. Randall, L. D. Rotstayn, R. C. J. Somerville, Y. C. Sud, K. V. Salzen, G. K. Walker, A. Wolf, J. J. Yio, G. J. Zhang, and M. Zhang, 2002: Intercomparison and evaluation of cumulus parametrizations under summertime midlatitude continental conditions. *Q. J. R. Meteorol. Soc.*, **128**, 1095–1135.

Xie, S., M. Zhang, J. S. Boyle, R. T. Cederwall, G. L. Potter, and W. Lin, 2004: Impact of a revised convective triggering mechanism on Community Atmosphere Model, Version 2, simulations: Results from short-range weather forecasts. *J. Geophys. Res.*, **109**, D14102, doi:10.1029/2004JD004692.

Xu, J., and E. E. Small, 2002: Simulating summertime rainfall variability in the North American monsoon region: The influence of convection and radiation parameterizations. *J. Geophys. Res.*, **107**, 4727, doi:10.1029/2001JD002047.

Xu, Kuan-Man, David A. Randall, 2000: Explicit Simulation of Midlatitude Cumulus Ensembles: Comparison with ARM Data. *J. Atmos. Sci.*, **57**, 2839–2858.

Yang, G.-Y., and J. Slingo, 2001: The Diurnal Cycle in the Tropics. *Mon. Wea. Rev.*, **129**, 784–801.

Zhang, G. J., 2003: Roles of tropospheric and boundary layer forcing in the diurnal cycle of convection in the U.S. southern great plains. *Geophys. Res. Lett.*, VOL. **30**, NO. 24, 2281, doi:10.1029/2003GL018554.

Zhang, G. J., and H. Wang, 2006: Toward mitigating the double ITCZ problem in NCAR CCSM3. *Geophys. Res. Lett.*, **33**, L06709, doi:10.1029/2005GL025229.

Zhang, G. J., and M. Mu, 2005: Effects of modifications to the Zhang-McFarlane convection parameterization on the simulation of the tropical precipitation in the National Center for Atmospheric Research Community Climate Model, version 3. *J. Geophys. Res.*, **110**, 12 PP., doi:200510.1029/2004JD005617.

Zhang, G.J., and N.A. McFarlane, 1995: Sensitivity of climate simulations to the parameterization of cumulus convection in the Canadian Climate Centre general circulation model. *Atmos.–Ocean,* **33,** 407–446.

Zhou, L., and Y. Wang, 2006: Tropical Rainfall Measuring Mission observation and regional model study of precipitation diurnal cycle in the New Guinean region. *J. Geophys. Res.*, **111**, D17104, doi:10.1029/2006JD007243.